2-2012

Engineering Surface Functionality of Gold Nanoparticles for Therapeutic Applications

Chaekyu Kim
University of Massachusetts Amherst, chaekyu@chem.umass.edu

ENGINEERING SURFACE FUNCTIONALITY OF GOLD NANOPARTICLES FOR THERAPEUTIC APPLICATIONS

A Dissertation Presented

by

CHAEKYU KIM

Submitted to the Graduate School of the
University of Massachusetts Amherst in partial fulfillment
of the requirements for the degree of

DOCTOR OF PHILOSOPHY

FEBRUARY 2012

CHEMISTRY

ENGINEERING SURFACE FUNCTIONALITY OF GOLD NANOPARTICLES FOR THERAPEUTIC APPLICATIONS

A Dissertation Presented

by

CHAEKYU KIM

Approved as to style and content by:

_____
Vincent M. Rotello, Chair

_____
Craig T. Martin, Member

_____
Richard W. Vachet, Member

_____
Gregory N. Tew, Member

_____
Craig T. Martin, Department Head
Chemistry

DEDICATION

To my family and friends

ACKNOWLEDGMENTS

First, I would like to thank to my research adviser, Professor Vincent M. Rotello for his support and guidance for these past five years. As a mentor and teacher, he educated me to have a scientific view and skill. I learned how to approach and solve a scientific issue, deal with a project, and manage time and relationships with collaborators. Under his guidance, I was able to have a productive PhD life. I appreciate the opportunity he gave me to work on wonderful projects along with all his precious advice. I will remember it fondly and it is my honor that we were able to share part of our lives working on science together.

I would like to thank my committee, Prof. Craig Martin, Prof. Richard Vachet, and Prof. Gregory Tew for their valuable comments on my research. I also would like to thank all the past and present research group members including all the visiting students for sharing their thoughts, cultures, and scientific advice. They were all my friends, colleagues, and teachers. Especially, I would like to mention some of them here, Sarit, Gang, Partha, Chiara, Zhengjiang, Gulen, Myounghwan, Youngdo, Yi-Cheun, Bo, Sungtae, Yu, Rui, Krish, Brad, Brian, David, Changsu, Oscar, Carol, and Dale.

Lastly, I would like to express my gratitude to my family and friends. With their support and love, I successfully complete PhD here away from my country.

ABSTRACT

ENGINEERING SURFACE FUNCTIONALITY OF GOLD NANOPARTICLES FOR THERAPEUTIC APPLICATIONS

FEBRUARY 2012

CHAE KYU, B.A., INHA UNIVERSITY

M.A., INHA UNIVERSITY

Ph.D., UNIVERSITY OF MASSACHUSETTS AMHERST

Directed by: Professor Vincent M. Rotello

Over the past few decades, tremendous efforts have been made to develop nanomaterials for biotechnological applications such as therapeutics. Understanding and engineering interfaces between biomacromolecules and nanomaterials is a key to the creation of successful therapeutic systems. My research has been oriented toward developing therapeutic systems using gold nanoparticles (AuNPs) incorporating material science, organic synthesis, and biology. For this purpose, mixed monolayer-protected AuNPs (~2 nm core size) with various functional groups have been employed for triggering therapeutic effects. Several strategies have been accomplished using anticancer drugs that non-covalently and covalently incorporate onto AuNPs as a drug delivery carrier. Alternatively, AuNPs were developed by regulating host-guest complexation processes inside the cell, allowing control of the therapeutic effect of the AuNP. In addition, by using host-guest chemical events on the AuNPs, exocytosis of the AuNPs was controlled, enabling their prolonged retention inside of the cells, providing new strategies for improving conventional drug delivery systems. Therefore,

engineering of the AuNP surface can afford new pathways for designing and improving therapeutics.

TABLE OF CONTENTS

Page

LIST OF TABLES

Table Page

LIST OF FIGURES

Figure Page

CHAPTER 1

GOLD NANOPARTICLES IN THERAPEUTICS

1.1 Introduction

Nanoparticles provide a useful platform, demonstrating unique properties gleaning a wide range of therapeutic applications. [1] Monolayer protected metal nanoparticles particularly have proven to be the most versatile and widely used constituents in biotechnology.[2, 3, 4, 5] Nanoparticles represent hybrid systems of nano-scale metal cores covered by a self-assembled monolayers of organic ligands. The use of nanoparticles in therapeutic applications takes advantage of both the dimensions and the physical properties of the inorganic core, as well as the functions of the organic surface periphery.

Nanoparticles exhibit a number of unique physical and chemical properties relative to bulk material. The novel properties of nanoparticles arise from a variety of attributes, including their enormous surface area. In addition, the versatile and tunable properties of nanoparticles are based on their component, size, shape, functionalized surface, and chemical surroundings. The unique properties of nanoparticles have attracted great interest in the scientific community and have been utilized in various chemical and biological applications, including electronic and optical studies, chemical and biological sensing, cell labeling and imaging, and cancer therapy.[6, 7, 8, 9, 10] Table 1.1 list some well known core materials with their corresponding surface ligands and their various biological applications.

Table 1.1 Characteristics, ligands, and representative applications for various metal and semiconductor materials.

Core material	Characteristics	Ligand(s)	Applications
Au	Optical absorption, fluorescence and fluorescence quenching, stability	Thiol, disulfide, phosphine, amine	Biomolecular recognition, delivery, sensing, therapeutics
Ag	Surface-enhanced fluorescence	Thiol	Sensing
Pt	Catalytic property	Thiol, phosphine, amine, isocyanide	Bio-catalyst, sensing
CdSe	Luminescence, photo-stability	Thiol, phosphine, pyridine	Imaging, sensing
Fe_2O_3	Magnetic property	Diol, dopamine derivative, amine	MR imaging and biomolecule purification
SiO_2	biocompatibility	Alkoxysilane	Biocompatible by surface coating

Of these metal nanoparticles, the utility of gold nanoparticles (AuNPs) in biology has attracted attention due to its biocompatibility,[11] controlled fabrication, and functional versatility.[12, 13, 14] Stimulated by the pioneering work of Brust *et al.* in 1994,[15] thiol-protected AuNPs have evolved to one of the most widely studied particle-ligand systems.[16] The optical, electronic and bioinert properties of the gold core combined with the versatile surface functionalization facilitate the applications of these materials in both fundamental research and industrial development.[17, 18, 19, 20] These functional nanomaterials have shown promising potential in electronics,[21] catalysis,[22] biosensing,[23] and nanomedicine.[24]

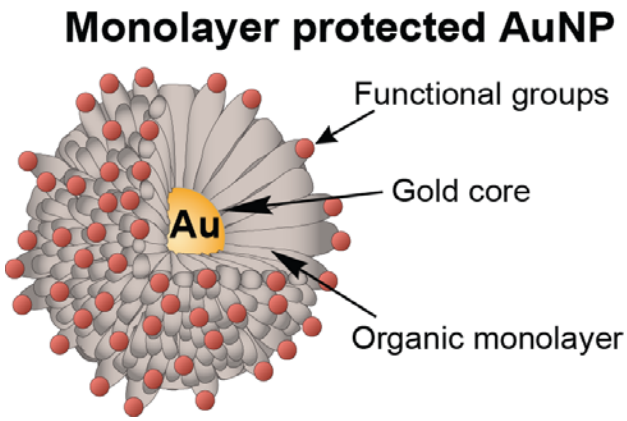

Figure 1.1 Schematic illustration of monolayer-protected gold nanoparticles: the inorganic gold core protected by an organic monolayer that can feature chemically different end group for a myriad of biomedical applications.

The functionalization of gold clusters is achieved through Brust-Schriffrin reduction followed by Murray place-exchange reaction [25] with appropriate functional ligands. The incorporation of multiple functionality within the scaffold of a single cluster coupled with a scale comparable with biomacromolecules (*e.g.* proteins and DNA) provides multiple applications at the interface of biotechnology and nanomaterials. For instance, some recent studies have shown that proper surface functionalization holds great promise in disrupting protein-protein interaction,[26] regulating DNA transcription,[27] gene transfection,[28] etc. This thesis work utilized AuNP as a scaffold for designing systems for therapeutic applications. Therefore, as a background to this work, synthesis and functionalization, properties, and some therapeutic applications of AuNPs will be discussed in this chapter.

1.2 Synthesis and surface functionalization of gold nanoparticles

AuNPs can be synthesized either through chemical reduction of gold salts or through the physical treatment of bulk gold. The synthesis of AuNPs has been widely explored during the past few decades. Concurrently various strategies have been applied to control their size, shape, stability, solubility, and surface functionality. AuNPs of various sizes can be prepared by using appropriate stabilizing agents during the chemical reduction of gold salts. These stabilizing agents provide the necessary barrier to avoid particle coalescence. Some common synthetic methods of AuNPs are summarized in Table 1.2.

Table 1.2 Synthetic methods for AuNPs of diverse core size.

Core size (*d*)	Synthetic methods	Capping agents	References
1-2 nm	Reduction of AuCl(PPh3) with diborane or sodium borohydride	Phosphine	29,30,31
1.5-5 nm	Biphasic reduction of HAuCl4 by sodium borohydride in the presence of thiol capping agents	Alkanethiol	32,33,34
5-8 nm	Reduction of HAuCl4 by sodium borohydride in the presence of TOAB	Quaternary ammonium salt (TOAB)	35
8-20 nm	Reduction of HAuCl4 by oleyl amine in water under heating	Oleyl amine	36, 37
10-40 nm	Reduction of HAuCl4 with sodium citrate in water	citrate	38,39,40

In 1994, the breakthrough in AuNP synthesis was achieved by Brust and Schriffin.[15] AuNPs soluble in organic solvents were synthesized by using the surfactant tetraoctylammonium bromide (TOAB) to transfer hydrogen tetrachloroaurate from aqueous phase to toluene phase. In this method, Sodium borohydride was used as reducing agent in the presence of alkanethiols. This methodology produces relatively monodisperse AuNPs protected by thiol ligands and with diameters ranging from 1.5 to 5 nm. The nanoparticle size is controllable by varying the reaction conditions such as gold-

to-thiol ratio, reduction rate, and reaction temperature. Thiol-protected AuNPs possess higher stability compared to most other AuNPs due to the synergic effect of strong thiol-gold interactions and van der Waals attractions between the ligands. These nanoparticles can be thoroughly dried and redispersed in solution without any aggregation. In the biphasic reduction protocol, slightly larger nanoparticles can be achieved by using quaternary ammonium instead of a thiol ligand and show considerable stability in solution. These particles serve as excellent precursors for further functionalization of nanoparticles.

Various capping agents (e.g. amino acid,[41] oelyl amine, and aliphatic and aromatic amines[42, 43]) have been introduced to reduce gold salts into nanoparticles with different core sizes. The size and shape of AuNPs can be further manipulated by physicochemical treatments such as light-irradiation and thermolysis. For example, conventional ripening[44, 45, 46] and digestive ripening[47, 48] treatments have been conducted to control the nanoparticle size. UV and laser irradiation provides another powerful approach to improve quality of the nanoparticle.[49, 50]

The capping agents used for synthesizing AuNPs are generally lacking in chemical functionality, thus restricting their applications in therapeutics. Place-exchange process introduced by Murray is an efficient approach for functionalizing surface of AuNPs (Figure 1.2).[25] During a place-exchange reaction, the thiol ligands initially anchored on the nanoparticle surface are replaced by the external thiol ligands in an equilibrium process.[51] The loading of functional ligands can be controlled by modulating the reaction time and/or the amount of incoming ligand. Mixed monolayer-protected gold

clusters can also be obtained by using a mixture of two or more ligands as the incoming thiol agents.

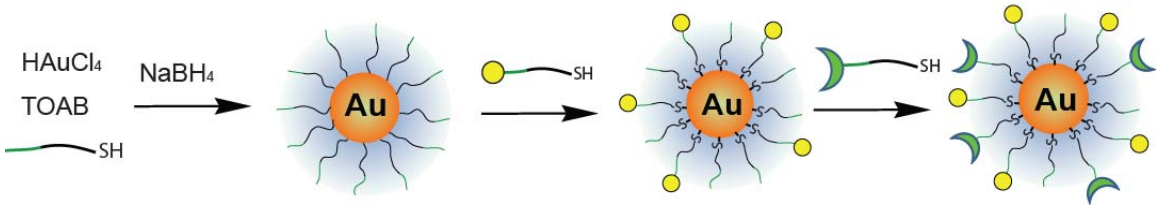

Figure 1.2 Synthesis of AuNP and its surface functionalization through place exchange reaction.

Labile capping agents, such as citrate, [52] triphenylphosphine, [53] and dimethylaminopyridine,[54] can be displaced by thiols under mild reaction conditions with no residual capping agent. Citrate-stabilized AuNPs are important precursors for large functionalized colloidal ensembles such as those carrying oligonucleotide, protein, or antibody functionalities.[55, 56] However, chemisorption of thiol ligands onto the citrate-stabilized nanoparticles leads to their irreversible aggregation.[57] Therefore, to prevent aggregation, nonionic surfactant such as Tween 20 is usually used during the place-exchange. The thiol ligands on gold surface possess a certain level of mobility and consequently they can undergo repositioning on the surface to optimize interaction with analytes.[58]

1.3 Cellular interaction of gold nanoparticles

For developing a therapeutic system with AuNPs, an understanding of the interaction of AuNPs with cells is important. Cellular uptake and intracellular fate of AuNPs depend on surface functionality and size.[59] Charge is an important determinant,[60]

Rotello and Vachet have demonstrated that cellular uptake of functionalized AuNPs is dependent on both charge and hydrophobicity.[61] Stellacci *et al*. have reported that cell membrane penetration of nanoparticle is also dependent on ligand shell morphology,[62] with "striped" (structured ligand shell) nanoparticles apparently capable of directly passing through the plasma membrane of the cells without creating pores on cell membrane that can cause cytotoxicity (Figure 1.3).

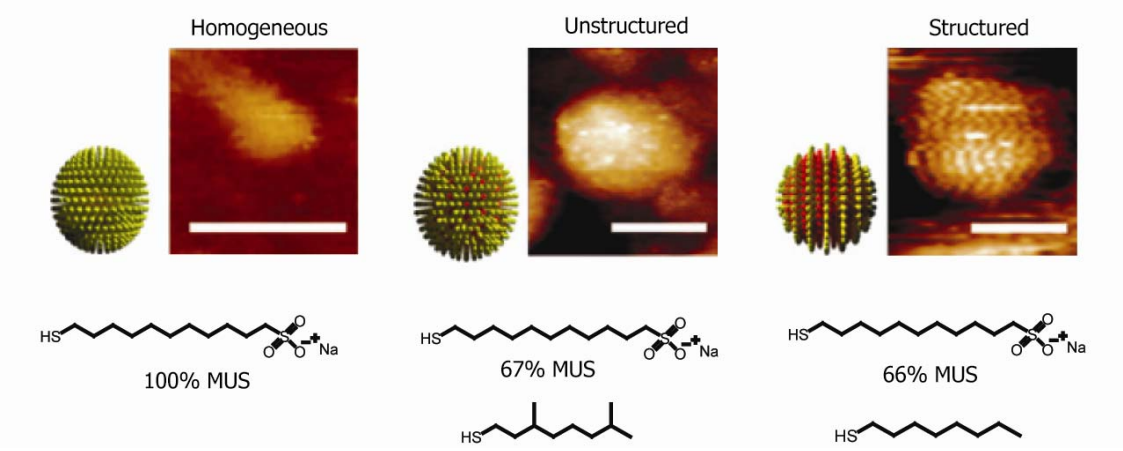

Figure 1.3 Schematic diagrams of the ligand shell structure of the nanoparticles and representative STM images (scale bars 5 nm).

Furthermore, organelle-specific localization of particles can be easily achieved by decorating the surface with a targeting moiety. For example, Feldheim et al. have demonstrated nuclear targeting of particles modified with nuclear localization sequence (NLS).[63] Recently, Brust *et al.* have used transmission electron microscopy[64] to show that specific cellular targets such as the nucleus and other organelles can be targeted by modifying the particle surface with cell penetrating peptides (CPPs) (e.g. the

oligopeptides TAT (AGRKKRRQRRR) and Pntn (GRQIKIWFQNRRMKWKK)) and the nuclear localization sequence (NLS: GGFSTSLRARKA) (Figure 1.4).

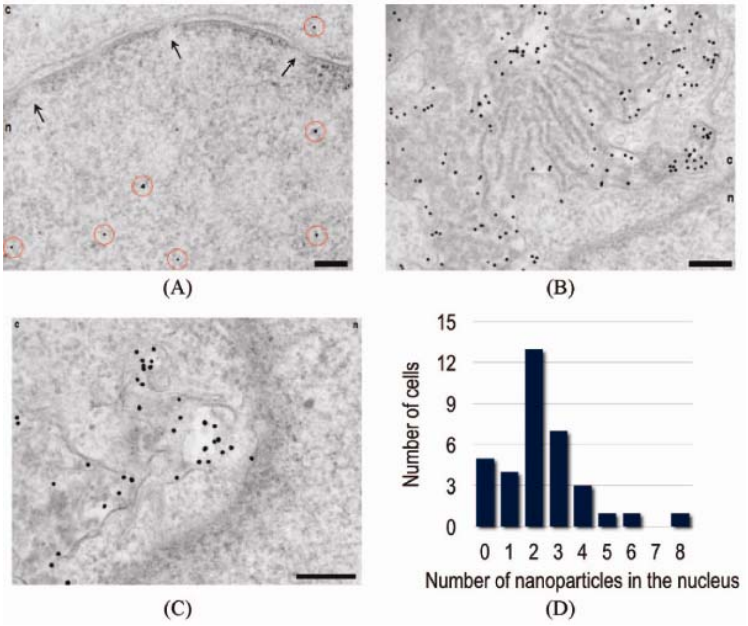

Figure 1.4 Nuclear targeting (A) by PEG-modified nanoparticles functionalized with a combination of CPPs (2% TAT and 2% Pntn) and 2% NLS. Nanoparticles are highlighted by red circles. The nuclear envelope with nuclear pores (arrows) is clearly shown in this image. The nucleus is denoted n, and the cytosol c. Unusual perinuclear membranous structures (B and C) that are highly loaded with nanoparticles are typically also observed under these conditions. Nuclear targeting is enhanced in comparison with experiments in the absence of CPPs (D). Scale bars are 200 nm.

Particle size provides the second key determinant of particle uptake. Chan et al. have demonstrated that cellular uptake depends on the size of nanoparticles.[65] AuNPs (2-100 nm) coated with Herceptin were fabricated and tested for ErbB2 receptor-mediated internalization in breast cells. They found that most efficient cellular uptake occurred with the 20~50 nm particles and programmed cell death (apoptosis) was enhanced by

particles the 40–50 nm range. The authors also have investigated the effect of AuNP size (10-100 nm) on passive targeting of tumors in vivo.[66] The larger nanoparticles remained near the vasculature, whereas smaller nanoparticles rapidly diffused from blood vessels to tumor matrix (Figure 1.5).

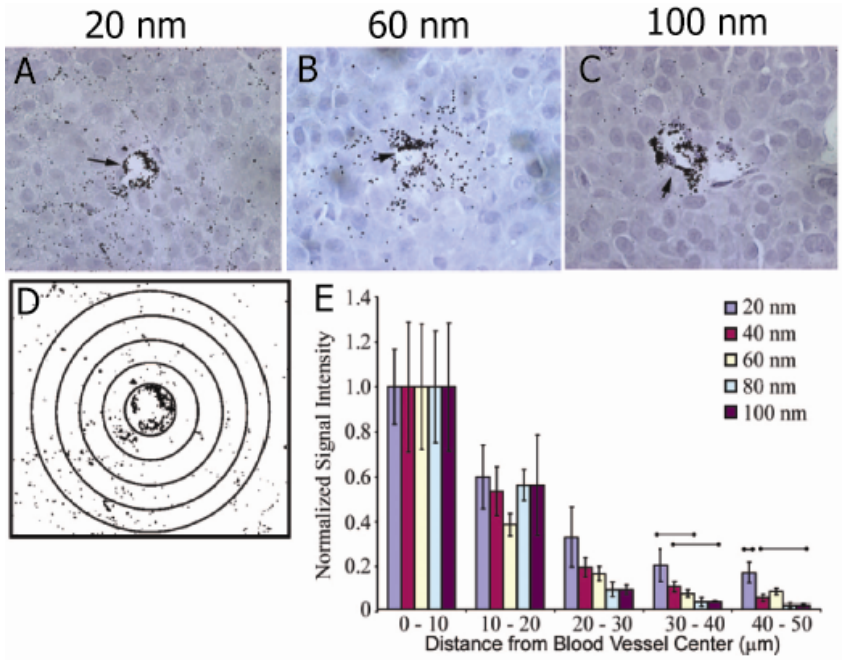

Figure 1.5 Particle size-dependent permeation of the tumor interstitial space. (A-C) Histological samples were obtained for 20, 60, and 100 nm particle sizes at 8 h postinjection (HPI). (D) ImageJ software was used to generate contrast-enhanced images for densitometry analysis. (E) Densitometry signal was quantified at 10 μm distances away from blood vessel centers 8 HPI and was normalized to the signal at 0-10 μm66.

1.4 Gold nanoparticles in drug delivery

Considerable effort has been focused on the creation of drug delivery systems (DDS) for improving efficacy of cancer chemotherapy, with the goals of enhancing therapeutic selectivity and efficacy.[67] One area where DDSs have proved highly

beneficial is in targeted delivery, where marked improvements in chemotherapy have been achieved through passive and/or active targeting approaches with nanocarriers including liposomes,[68] polymer micelles and vesicles,[69] dendrimers,[70] and metal nanoparticles.[71]

AuNPs have recently emerged as highly promising DDSs.[72] AuNPs have multiple aspects that make them well-suited for use in delivery applications over other nanocarriers. First, AuNPs of many different sizes (1-150 nm) can be fabricated in a controlled fashion with control over size dispersity,[73] while polymer based carriers have the issue caused by the intrinsic heterogeneous structure of polymers due to a high polydispersity index indices. Furthermore, due to their high surface area to volume ratio, a high density of ligands can be archived on the surface of AuNPs for targeting or drug loading purpose. For example, 2-nm core sized AuNP has around 100 lignads on particles.[34] Second, functional diversity can be readily achieved by creation of multifunctional monolayers using techniques such as the ligand place-exchange reaction, allowing multiple functional moieties such as anticancer drugs and targeting agents to be placed onto the particle surface. In terms of the mitifunctionalization, dendrimers are a promising nanocarrier with a well defined structure. However, many repetitive steps for synthesis and expensive production are major challenges. Lastly, the gold core is essentially inert, non-toxic, and biocompatible.[74]

The facile functionalization of AuNP surface has enabled their use in a variety of delivery strategies. In one approach, prodrugs can be covalently conjugated to AuNPs via cleavable linkers. Alternatively, hydrophobic drugs can be non-covalently loaded onto AuNPs, allowing conjugation without structural modification of the drug payload. Once

loaded, AuNP payloads can be released by either internal (e.g. glutathione)[12] or external (e.g. light)[75] stimuli. The versatility of the AuNP monolayer is central to release mechanisms, providing tunability for endogenous release mechanisms and a functional platform for external release strategies.

1.4.1 Drug attachment and release strategies using gold nanoparticles

Both the transport and release of drugs play critical roles in providing effective delivery systems. In general drugs can be loaded onto nanocarriers by either covalent conjugation or non-covalent interactions.[76] The non-covalent approach employs active drugs while the covalent attachment generally requires intercellular processing of a prodrug.[77] The ease of controlling the functionality and structure of AuNP monolayers makes them excellent platforms for DDS creation.

DDS systems based on glutathione (GSH)-mediated payload release exploit the dramatically higher intracellular GSH concentration (1–10 mM)[78] relative to extracellular thiol levels (GSH 2 μM, cysteine 8 μM).[79] The high levels of intracellular GSH can be used to release prodrugs (payloads) on AuNPs through either place-exchange reactions at the core or via disulfide exchange. Importantly, the monolayer of nanoparticles can provide steric shielding against exchange with surface cysteines of proteins in the bloodstream,[80] enabling their potential use *in vivo.*

In early studies, Rotello *et al*. developed a nanoparticle-based delivery system featuring glutathione release. The particles (core diameter: ~ 2 nm) featured a mixed monolayer composed of cationic ligands (TTMA) and fluorogenic ligands (HSBDP) (Figure 1.6). The cationic surface of the nanoparticles facilitated the penetration through

cell membrane, and the payload release was triggered by intracellular glutathione (GSH). In this delivery system, the BODIPY moiety of the HSDBP ligand was non-fluorescent when attached to the particle due to fluorescence quenching by the Au core.[81] The fluorescence was recovered upon GSH treatment in cuvette, or with intracellular thiols in human liver cells (Hep G2). GSH-controlled release of the dye was verified by treating mouse embryonic fibroblast cells (MEF, having >50% lower intracellular GSH levels than HepG2) with varying concentration of glutathione monoester (GSH-OEt), transiently increasing glutathione level inside the cells. In these studies, a dose-dependent increase in fluorescence was observed with increasing GSH-OEt concentration. In a similar fashion, AuNP-mediated DNA transfection efficiency was regulated by controlling the intracellular glutathione level.[82]

The ligand-displacement rate by intracellular thiols (e.g. DHLA and GSH) depends strongly on the monolayer structure and surface charge,[83] allowing controlled release of payload. As an example, Kotov *et al*. have demonstrated that AuNPs bearing 6-mercaptopurine-9- -D-ribofuranoside significantly enhanced the anti-proliferative effect against K-562 leukemia cells compared to the same drug in free form.[84] This improvement was attributed to enhanced intracellular transport followed by the subsequent GSH-mediated release in cytoplasm and lysosomes.

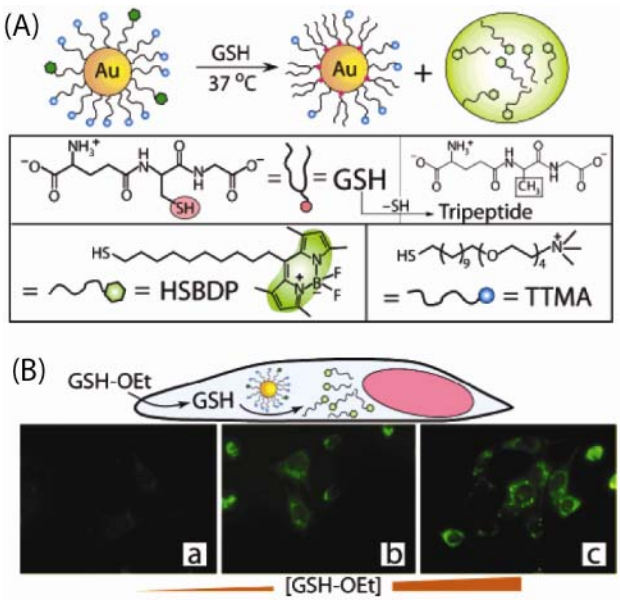

Figure 1.6 (A) Schematic illustration of GSH-mediated surface monolayer exchange reaction/payload release. (B) Fluorescence images of MEF cells displaying GSH-controlled release of the fluorophore after incubation with 0, 5, and 20 mM GSH-OEt.

In a strategy that combines glutathione-mediated release with non-covalent loading of drugs (*vide infra*), Kim *et al*. reported cyclodextrin-functionalized AuNPs as carriers of anti-cancer drugs.[85] The AuNPs used the cyclodextrin moieties to encapsulate drugs, anti-epidermal growth factor receptor (anti-EGFR) antibody as a targeting moiety, and poly(ethyleneglycol) (PEG) as an anti-fouling shell (Figure 1.7). The anticancer drug -Lapachone, was efficiently encapsulated into the hydrophobic cavity of cyclodextrin onto AuNPs and then released by intracellular GSH. The introduction of an anti-EGFR antibody onto the AuNPs was shown to both enhance the uptake of AuNPs and increase the degree of apoptosis.

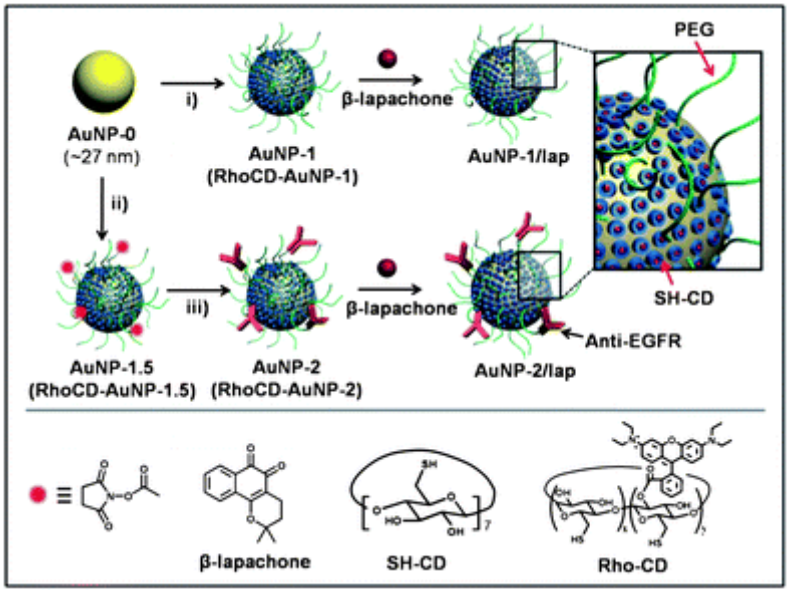

Figure 1.7 Schematic illustration of the functionalization of AuNP with β-lapachone, using: i) SH-CD and mPEG-SH for AuNP-1 (RhoCD and mPEG-SH for RhoCD-AuNP-1); ii) SH-CD, mPEG-SH, and NHS-PEG-SH for AuNP-1.5 (RhoCD, mPEG-SH, NHS-PEG-SH for RhoCD-AuNP-1.5) and iii) anti-EGFR.

1.4.2 Encapsulation of therapeutics in monolayer of gold nanoparticles

Non-covalent incorporation of drugs into AuNP monolayers provides an alternative delivery strategy that allows direct use of unmodified drugs, thus avoiding prodrug processing issues. Drug encapsulation with AuNPs relies on the use of ligands that generate a hydrophobic interior to the monolayer. Structurally, the radial nature of the monolayer results in a decrease in ligand density as one goes further from the core of small AuNP cores (< ~6 nm).[86] Consequently "hydrophobic pockets" are created inside the monolayer of the AuNP into which hydrophobic materials can be partitioned. Pasquato *et al*. demonstrated the encapsulation of radical probes in AuNP monolayers, using EPR spectroscopy to monitor the partition of the lipophilic probe between

monolayer of AuNP and bulk water.[87] As expected, smaller particles featuring more strongly radial monolayers favor guest encapsulation (Figure 1.8).

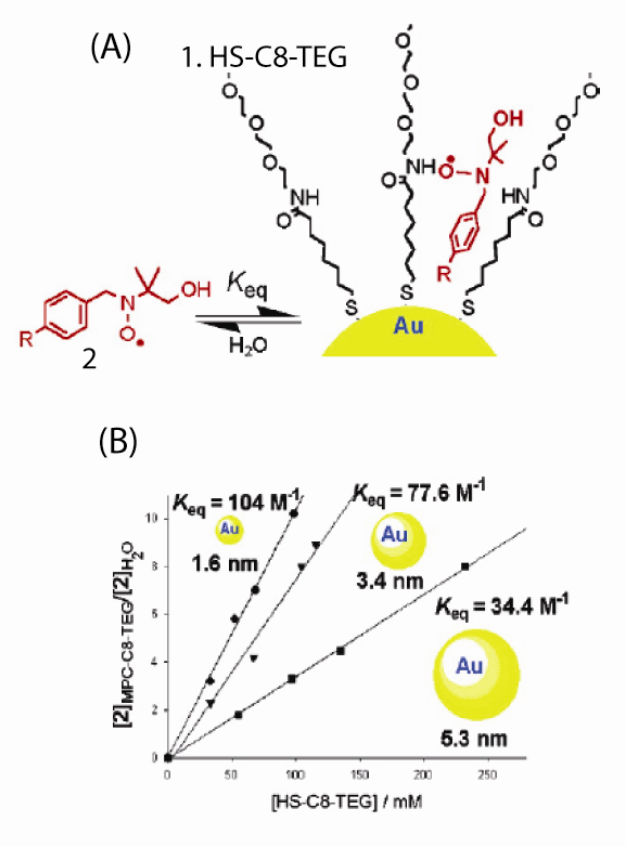

Figure 1.8 (A) Schematic representation of AuNP and the nitroxide probe inclusion. (B) Plot of the ratio between the concentration of **2** partitioned in the monolayer and that of the free species (● 16 nm; ▼ 3.4 nm; ■ 5.3 nm) as a function of [HS-C8-TEG] bound to the gold.

The concept of monolayer encapsulation has recently been applied to drug delivery. Rotello *et al.* have developed a biocompatible AuNP carrier that employs hydrophobic pockets to encapsulate drugs and deliver them into cancer cells.[88] The particles (~ 2.5 nm core) featured a hydrophobic alkanethiol interior and a hydrophilic

shell composed of a tetra(ethylene glycol) (TEG) unit terminated with a zwitterionic headgroup designed to minimize nonspecific binding with biomacromolecules[89] and other cell surface functionality (Figure 1.9). Hydrophobic payloads were kinetically entrapped in the monolayer, with the resulting host-guest materials stable in buffer and serum. The entrapped payloads were released into cells by membrane-mediated diffusion, as demonstrated by both fluorescence microscopy (using a fluorophore payload) and through drug efficacy with therapeutic guests. No particle uptake was observed with these systems using ICP-MS, making these systems excellent candidates for passive targeting using the enhanced permeability and retention (EPR) effect.[90]

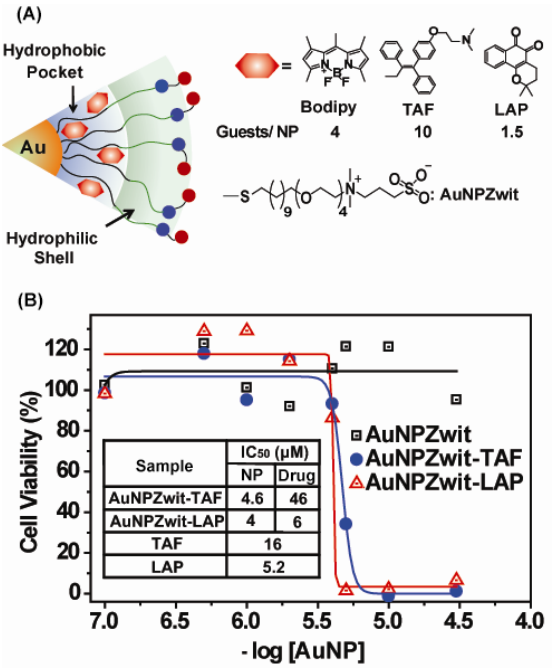

Figure 1.9 (A) Structure of particles and guest compounds: Bodipy, TAF, and LAP, the number of encapsulated guests per particle (B) Cytotoxicity of AuNPZwit complexes measured by Alamar blue assay after 24 h incubation with MCF-7 cells. IC_{50} of AuNP (NP), equivalent drugs (Drug), and free drugs are shown in table.

Photodynamic therapy (PDT) is a promising strategy that uses reactive oxygen species (ROS) to induce apoptosis or necrosis. Burda *et al*. reported the use of PEGylated AuNP-Pc4 (Si-phthalocyanine) conjugates as efficient platforms for PDT (Figure 1.10 (a)).[91] The phthalocyanine photosensitizing agent was encapsulated by the PEG ligands through van der Waals interaction, with the PEG ligand inhibiting colloid aggregation and providing significant resistance to non-specific binding with biomacromolecules. The release of Pc4 from AuNP *in vitro* in a two-phase solution system and *in vivo* in cancer-bearing mice (Figure 1.10 (b)) indicated that the delivery process was highly efficient, with Pc4 preferentially accumulated in tumor sites. With the Au NP-Pc 4 conjugates, the drug delivery time required for PDT was reduced from 2 days using the free drug to 2 h, using the conjugate (Figure 1.10).

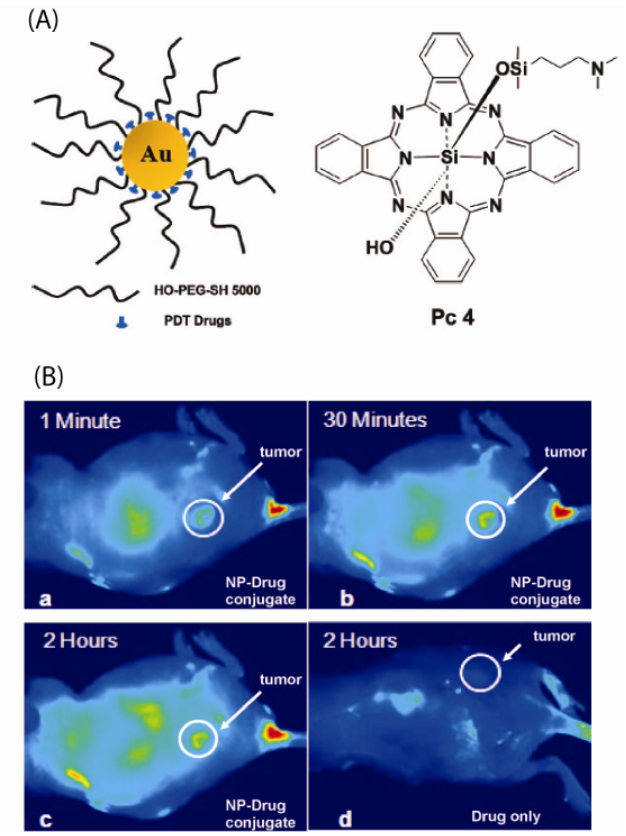

Figure 1.10 (A) Sturcture of the water-soluble AuNPs as a PDT drug delivery agent, Pc 4 structure (B) Fluorescence images of a tumor-bearing mouse after being injected with Au NP-Pc 4 conjugates in normal saline (0.9% NaCl, pH 7.2), (a) 1 min, (b) 30 min, and (c) 120 min after intravenous tail injection. Any bright signal is due to Pc 4 fluorescence. For comparison, a mouse that got only a Pc 4 formulation without the AuNP vector injected is shown in panel (d). No circulation of the drug in the body or into the tumor was detectable 2 h after injection without the AuNP as a drug vector.

1.4.3 Light-regulated release of payload

The ability to regulate drug release is an important property for drug delivery systems. While endogenous approaches such as GSH-mediated release provide very useful strategies for delivery, externally controlled release provides a complementary tool

for site- and time-specific control of payload release.[92] Recently, caged drugs have been developed where the activity of the drug was suppressed by attaching it to a blocking element through a photoremovable protecting group.[93] Rotello et al. have applied this strategy to AuNP delivery vehicles, utilizing a photo-cleavable *o*-nitrobenzyl ester moiety that dissociates upon light irradiation to alter the surface potential from positive to negative, thereby releasing adsorbed DNA. In more recent studies, the authors demonstrated light-controlled release of anticancer drug (5-fluorouracil) from nanoparticles (Figure 1.11).[94] The AuNPs (Au_PCFU, Au core: ~2 nm) featured a mixed monolayer of zwitterionic and photocleavable ligands. The zwitterionic ligand provided solubility and prevented cellular uptake. The photocleavable ligand linked the fluorouracil to the particle through an orthonitrobenzyl group that could be effectively cleaved using near-UV irradiation (365 nm). An IC_{50} value of 0.7 μM observed upon irradiation for Au_PCFU on a per particle basis, whereas no significant cell death was observed in cells treated with only light or only Au_PCFU.

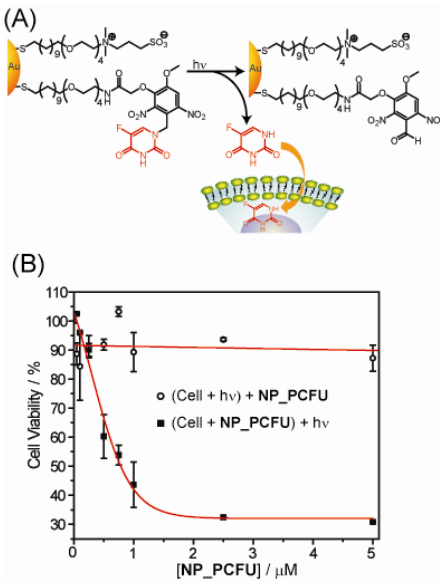

Figure 1.11 (A) Photochemical reaction (365 nm) of Au_PCFU and delivery of payload to cell. (B) Cytotoxicity of different concentrations of Au_PCFU under uncaging conditions. The IC_{50} value was 0.7 μM per particle, 11.9 μM per drug.

In related research, Nakanishi *et al*. have reported a photoresponsive nanocarrier of amines, including cell signaling agents. (Figure 1.12).[95] In this approach a carbamate linkage could be dissociated via the photocleavage reaction of the 2-nitrobenzyl group upon near-UV irradiation. The caging process was very effective: histamine had no biological activity while it was attached to AuNPs but became active when it was released from the particles upon photo-irradiation.

1.4.4 Other attachment/release strategies

A variety of additional delivery strategies have been developed using AuNP platforms. Schoenfisch et al. have demonstrated that nitric oxide (NO) can be efficiently released at acidic pH from gold nanoparticles,[96] providing a potential means of controlling multiple cellular processes including angiogenesis, vasodilation, and the

immune response.[97] Hwu *et al*. have used a phosphate linker to conjugate paclitaxel to AuNP and Fe_3O_4 particles.[98] The drug could be released from the particles using phosphodiesterase.

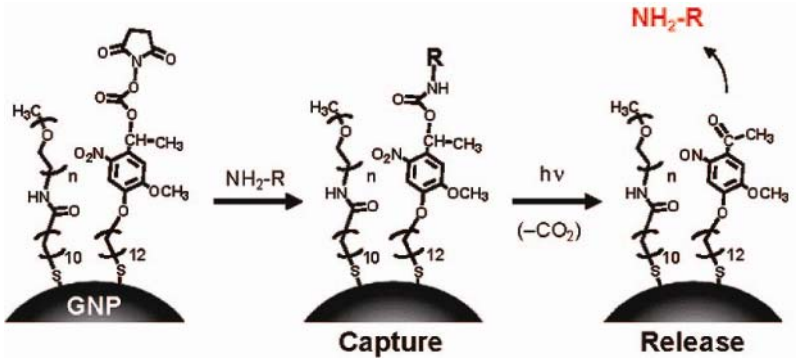

Figure 1.12 Capture and release of amines on GNPs having a photocleavable succinimidyl ester.

1.5 Dissertation overview

Engineering the interfaces between biomolecules and nanomaterials is important for the creation of systems with potential applications in therapeutics. My research has been oriented toward biotechnological applications in cancer therapy via engineering the interface between biomacromolecules and nanomaterials. For the purpose, I have employed a synergistic approach, combining materials, surface science, organic synthesis, and biology to develop surface functionalized AuNPs with a tailored monolayer. In the following chapters, details of designing functionalized AuNPs and their use in therapeutic applications are described.

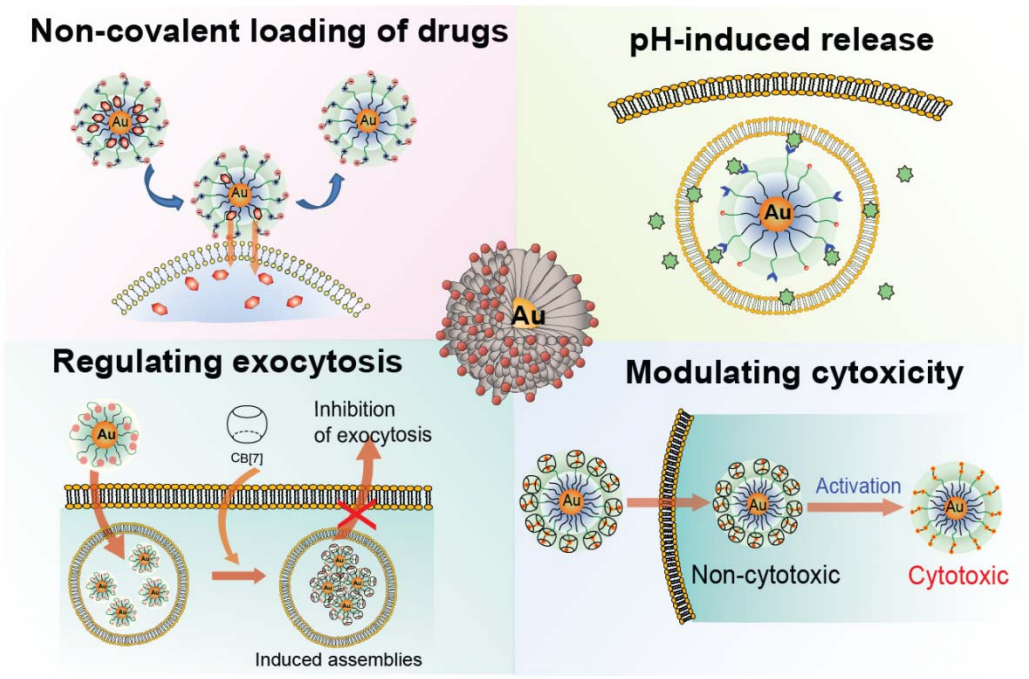

Figure 1.13 Dissertation overview. Schematic illustration of therapeutic applications of AuNPs described in this thesis.

In Chapter 2, AuNPs with non-covalent loading of drugs on the monolayer will be discussed. Non-covalent incorporation of drugs into AuNP monolayers provides an alternative delivery strategy that allows direct use of unmodified drugs, thus avoiding prodrug processing issues. Hydrophobic payloads were kinetically entrapped in the monolayer with the resulting host–guest materials stable in buffer and serum. Upon incubation with cancer cells, the entrapped payloads were efficiently released into cells by membrane-mediated diffusion without cellular uptake of the particles, showing therapeutic efficiency. This system is an excellent candidate for passive targeting using the enhanced permeability and retention effect.

Chapter 3 will discuss about pH-labile prodrugs incorporated AuNPs with positive or negative surface charges to study diffusion of the payloads and their carrier in

cylindroids tumor model. Anticancer drugs are attached on the AuNP surface through acid-cleavable linkers, allowing pH induced drug release. Positively charged nanoparticles improved delivery of payloads to the majority of cells in tumours, whereas negatively charged particles would perform better when delivering drugs deep into tissues. The ability to tune surface charge to control tissue penetration and drug release makes gold nanoparticles a flexible and powerful drug delivery vehicle.

Chapter 4 will illustrate the recognition mediated activation of therapeutic AuNPs through regulation of synthetic host-guest complexation process inside the living cell. We will describe a supramolecular synthetic host-guest system featuring diaminohexane terminated AuNPs (AuNP-NH_2) and cucurbit[7]uril (CB[7]). In this system, threading of CB[7] on the particle surface reduces the cytotoxicity of the AuNP-NH_2 by sheathing the lethal diaminohexane ligand. Intracellular triggering of the therapeutic effect of AuNP-NH_2 was achieved via the administration of 1-adamantylamine (ADA). ADA binds to CB[7] with higher affinity than the diaminohexane ligand and thus removes CB[7] from the nanoparticle surface. This intracellular disassembly of AuNP-NH_2 and CB[7] complex activates the *in situ* cytotoxicity of AuNP-NH_2 and hence induced cell death. This result presents a new strategy for triggering therapeutic systems through the use of competitive interactions of orthogonally presented guest molecules.

In Chapter 5, regulating exocytosis of AuNPs by using host-guest chemistry will be discussed. AuNPs featuring quaternary amine head groups were internalized into the cells by endocytosis. Subsequent in situ treatment of a complementary cucurbit[7]uril (CB[7]) to the amine head groups induced the particles-CB[7] complexation inside of the cells, rendering the particles assembled each other. The larger induced particle assemblies

remained sequestered in the endosomes, inhibiting exocytosis of the particles without any observed cytotoxicity. This approach would provide a potential strategy for prolonged retention of drug carriers within endosome, enabling sustained release of the loaded therapeutics in the carriers.

1.6 References

1. De, M.; Ghosh, P. S.; Rotello, V. M., Applications of Nanoparticles in Biology. *Adv. Mater*. **2008,** *20* (22), 4225-4241.
2. Alivisatos, A. P.; Gu, W. W.; Larabell, C., Quantum dots as cellular probes. *Annu. Rev. Biomed. Eng.* **2005,** *7*, 55-76.
3. Verma, A.; Rotello, V. M., Surface recognition of biomacromolecules using nanoparticle receptors. *Chem. Commun.* **2005,** (3), 303-312.
4. Medintz, I. L.; Uyeda, H. T.; Goldman, E. R.; Mattoussi, H., Quantum dot bioconjugates for imaging, labelling and sensing. *Nat. Mater.* **2005,** *4* (6), 435-446.
5. Geissbuehler, I.; Hovius, R.; Martinez, K. L.; Adrian, M.; Thampi, K. R.; Vogel, H., Lipid-coated nanocrystals as multifunctionalized luminescent scaffolds for supramolecular biological assemblies. *Angew. Chem. Int. Edit.* **2005,** *44* (9), 1388-1392.
6. Alivisatos, P., The use of nanocrystals in biological detection. *Nat. Biotechnol.* **2004,** *22* (1), 47-52.
7. Niemeyer, C. M., Nanoparticles, proteins, and nucleic acids: Biotechnology meets materials science. *Angew. Chem. Int. Edit.* **2001,** *40* (22), 4128-4158.
8. West, J. L.; Halas, N. J., Applications of nanotechnology to biotechnology - Commentary. *Curr. Opin. Biotech.* **2000,** *11* (2), 215-217.

9. Parak, W. J.; Gerion, D.; Pellegrino, T.; Zanchet, D.; Micheel, C.; Williams, S. C.; Boudreau, R.; Le Gros, M. A.; Larabell, C. A.; Alivisatos, A. P., Biological applications of colloidal nanocrystals. *Nanotechnology* **2003,** *14* (7), R15-R27.

10. Rosi, N. L.; Mirkin, C. A., Nanostructures in biodiagnostics. *Chem. Rev.* **2005,** *105* (4), 1547-1562.

11 . Bhattacharya, R.; Mukherjee, P., Biological properties of "naked" metal nanoparticles. *Adv. Drug Deliv. Rev.* **2008,** *60* (11), 1289-1306

12. Hong, R.; Han, G.; Fernandez, J. M.; Kim, B. J.; Forbes, N. S.; Rotello, V. M., Glutathione-mediated delivery and release using monolayer protected nanoparticle carriers. *J. Am. Chem. Soc.* **2006,** *128* (4), 1078-1079.

13. Paciotti, G. F.; Kingston, D. G. I.; Tamarkin, L., Colloidal gold nanoparticles: A novel nanoparticle platform for developing multifunctional tumor-targeted drug delivery vectors. *Drug Develop. Res.* **2006,** *67* (1), 47-54.

14. Ghosh, P.; Han, G.; De, M.; Kim, C. K.; Rotello, V. M., Gold nanoparticles in delivery applications. *Adv. Drug Deliv. Rev.* **2008,** *60* (11), 1307-1315.

15. Brust, M.; Walker, M.; Bethell, D.; Schiffrin, D. J.; Whyman, R., Synthesis of Thiol-Derivatized Gold Nanoparticles in a 2-Phase Liquid-Liquid System. *J. Chem. Soc. Chem. Comm.* **1994,** (7), 801-802.

16. Daniel, M. C.; Astruc, D., Gold nanoparticles: Assembly, supramolecular chemistry, quantum-size-related properties, and applications toward biology, catalysis, and nanotechnology. *Chem. Rev.* **2004,** *104* (1), 293-346.

17. Thomas, K. G.; Kamat, P. V., Chromophore-functionalized gold nanoparticles. *Acc. Chem. Res.***2003,** *36* (12), 888-898.

18. Pasquato, L.; Pengo, P.; Scrimin, P., Nanozymes: Functional nanoparticle-based catalysts. *Supramol. Chem.* **2005,** *17* (1-2), 163-171.

19. Eustis, S.; El-Sayed, M. A., Why gold nanoparticles are more precious than pretty gold: Noble metal surface plasmon resonance and its enhancement of the radiative and nonradiative properties of nanocrystals of different shapes. *Chem. Soc. Rev.* **2006,** *35* (3), 209-217.

20. You, C. C.; Verma, A.; Rotello, V. M., Engineering the nanoparticle-biomacromolecule interface. *Soft Matter* **2006,** *2* (3), 190-204.

21. Gittins, D. I.; Bethell, D.; Schiffrin, D. J.; Nichols, R. J., A nanometre-scale electronic switch consisting of a metal cluster and redox-addressable groups. *Nature* **2000,** *408* (6808), 67-69.

22. Li, H.; Luk, Y. Y.; Mrksich, M., Catalytic asymmetric dihydroxylation by gold colloids functionalized with self-assembled monolayers. *Langmuir* **1999,** *15* (15), 4957-4959.

23. You, C. C.; Miranda, O. R.; Gider, B.; Ghosh, P. S.; Kim, I. B.; Erdogan, B.; Krovi, S. A.; Bunz, U. H. F.; Rotello, V. M., Detection and identification of proteins using nanoparticle-fluorescent polymer 'chemical nose' sensors. *Nat. Nanotechnol.* **2007,** *2* (5), 318-323.

24. Jain, P. K.; El-Sayed, I. H.; El-Sayed, M. A., Au nanoparticles target cancer. *Nano Today* **2007,** *2* (1), 18-29.

25. Templeton, A. C.; Wuelfing, M. P.; Murray, R. W., Monolayer protected cluster molecules. *Acc. Chem. Res.* **2000,** *33* (1), 27-36.

26. Bayraktar, H.; Ghosh, P. S.; Rotello, V. M.; Knapp, M. J., Disruption of protein-protein interactions using nanoparticles: inhibition of cytochrome c peroxidase. *Chem. Commun.* **2006,** (13), 1390-1392.

27. Han, G.; You, C. C.; Kim, B. J.; Turingan, R. S.; Forbes, N. S.; Martin, C. T.; Rotello, V. M., Light-regulated release of DNA and its delivery to nuclei by means of photolabile gold nanoparticles. *Angew. Chem. Int. Edit.* **2006,** *45* (19), 3165-3169

28. Rosi, N. L.; Giljohann, D. A.; Thaxton, C. S.; Lytton-Jean, A. K. R.; Han, M. S.; Mirkin, C. A., Oligonucleotide-modified gold nanoparticles for intracellular gene regulation. *Science* **2006,** *312* (5776), 1027-1030.

29. Schmid, G.; Pfeil, R.; Boese, R.; Bandermann, F.; Meyer, S.; Calis, G. H. M.; Vandervelden, W. A., Au55[P(C6h5)3]12cl6 - a Gold Cluster of an Exceptional Size. *Chem. Ber. Recl.* **1981,** *114* (11), 3634-3642.

30. Schmid, G., Large Clusters and Colloids - Metals in the Embryonic State. *Chem. Rev.* **1992,** *92* (8), 1709-1727.

31. Weare, W. W.; Reed, S. M.; Warner, M. G.; Hutchison, J. E., Improved synthesis of small (d(CORE) approximate to 1.5 nm) phosphine-stabilized gold nanoparticles. *J. Am. Chem. Soc.* **2000,** *122* (51), 12890-12891.

32. Brust, M.; Walker, M.; Bethell, D.; Schiffrin, D. J.; Whyman, R., Synthesis of Thiol-Derivatized Gold Nanoparticles in a 2-Phase Liquid-Liquid System. *J. Chem. Soc. Chem. Comm.* **1994,** (7), 801-802.

33. Leff, D. V.; Ohara, P. C.; Heath, J. R.; Gelbart, W. M., Thermodynamic Control of Gold Nanocrystal Size - Experiment and Theory. *J. Phys. Chem.-Us* **1995,** *99* (18), 7036-7041.

34. Hostetler, M. J.; Wingate, J. E.; Zhong, C. J.; Harris, J. E.; Vachet, R. W.; Clark, M. R.; Londono, J. D.; Green, S. J.; Stokes, J. J.; Wignall, G. D.; Glish, G. L.; Porter, M. D.; Evans, N. D.; Murray, R. W., Alkanethiolate gold cluster molecules with core diameters from 1.5 to 5.2 nm: Core and monolayer properties as a function of core size. *Langmuir* **1998,** *14* (1), 17-30.

35. Fink, J.; Kiely, C. J.; Bethell, D.; Schiffrin, D. J., Self-organization of nanosized gold particles. *Chem. Mater.* **1998,** *10* (3), 922-926.

36. Aslam, M.; Fu, L.; Su, M.; Vijayamohanan, K.; Dravid, V. P., Novel one-step synthesis of amine-stabilized aqueous colloidal gold nanoparticles. *J. Mater. Chem.* **2004,** *14* (12), 1795-1797.

37. Hiramatsu, H.; Osterloh, F. E., A simple large-scale synthesis of nearly monodisperse gold and silver nanoparticles with adjustable sizes and with exchangeable surfactants. *Chem. Mater.* **2004,** *16* (13), 2509-2511.

38. Turkevich, J.; Stevenson, P. C.; Hillier, J., A Study of the Nucleation and Growth Processes in the Synthesis of Colloidal Gold. *Discuss. Farad. Soc.* **1951,** (11), 55 -75.

39. Grabar, K. C.; Freeman, R. G.; Hommer, M. B.; Natan, M. J., Preparation and Characterization of Au Colloid Monolayers. *Anal. Chem.* **1995,** *67* (4), 735-743.

40. Schmid, G.; Simon, U., Gold nanoparticles: assembly and electrical properties in 1-3 dimensions. *Chem. Commun.* **2005,** (6), 697-710.

41. Bhargava, S. K.; Booth, J. M.; Agrawal, S.; Coloe, P.; Kar, G., Gold nanoparticle formation during bromoaurate reduction by amino acids. *Langmuir* **2005,** *21* (13), 5949-5956.

42. Leff, D. V.; Brandt, L.; Heath, J. R., Synthesis and characterization of hydrophobic, organically-soluble gold nanocrystals functionalized with primary amines. *Langmuir* **1996,** *12* (20), 4723-4730.

43. Newman, J. D. S.; Blanchard, G. J., Formation of gold nanoparticles using amine reducing agents. *Langmuir* **2006,** *22* (13), 5882-5887.

44. Zhong, C. J.; Zhang, W. X.; Leibowitz, F. L.; Eichelberger, H. H., Size and shape evolution of core-shell nanocrystals. *Chem. Commun.* **1999,** (13), 1211-1212.

45. Maye, M. M.; Zheng, W. X.; Leibowitz, F. L.; Ly, N. K.; Zhong, C. J., Heating-induced evolution of thiolate-encapsulated gold nanoparticles: A strategy for size and shape manipulations. *Langmuir* **2000,** *16* (2), 490-497.

46. Carroll, J. B.; Frankamp, B. L.; Srivastava, S.; Rotello, V. M., Electrostatic self-assembly of structured gold nanoparticle/polyhedral oligomeric silsesquioxane (POSS) nanocomposites. *J. Mater. Chem.* **2004,** *14* (4), 690-694.

47. Prasad, B. L. V.; Stoeva, S. I.; Sorensen, C. M.; Klabunde, K. J., Digestive ripening of thiolated gold nanoparticles: The effect of alkyl chain length. *Langmuir* **2002,** *18* (20), 7515-7520.

48. Prasad, B. L. V.; Stoeva, S. I.; Sorensen, C. M.; Klabunde, K. J., Digestive-ripening agents for gold nanoparticles: Alternatives to thiols. *Chem. Mater.* **2003,** *15* (4), 935-942.

49. Kurita, H.; Takami, A.; Koda, S., Size reduction of gold particles in aqueous solution by pulsed laser irradiation. *Appl. Phys. Lett.* **1998,** *72* (7), 789-791.

50. Sau, T. K.; Pal, A.; Jana, N. R.; Wang, Z. L.; Pal, T., Size controlled synthesis of gold nanoparticles using photochemically prepared seed particles. *J. Nanopart. Res.* **2001,** *3* (4), 257-261.

51. Hong, R.; Fernandez, J. M.; Nakade, H.; Arvizo, R.; Emrick, T.; Rotello, V. M., In situ observation of place exchange reactions of gold nanoparticles. Correlation of monolayer structure and stability. *Chem. Commun.* **2006,** (22), 2347-2349.

52. Levy, R.; Thanh, N. T. K.; Doty, R. C.; Hussain, I.; Nichols, R. J.; Schiffrin, D. J.; Brust, M.; Fernig, D. G., Rational and combinatorial design of peptide capping Ligands for gold nanoparticles. *J. Am. Chem. Soc.* **2004,** *126* (32), 10076-10084.

53. Woehrle, G. H.; Brown, L. O.; Hutchison, J. E., Thiol-functionalized, 1.5-nm gold nanoparticles through ligand exchange reactions: Scope and mechanism of ligand exchange. *J. Am. Chem. Soc.* **2005,** *127* (7), 2172-2183.

54. Rucareanu, S.; Gandubert, V. J.; Lennox, R. B., 4-(N,N-dimethylamino)pyridine-protected Au nanoparticles: Versatile precursors for water- and organic-soluble gold nanoparticles. *Chem. Mater.* **2006,** *18* (19), 4674-4680.

55. Tkachenko, A. G.; Xie, H.; Coleman, D.; Glomm, W.; Ryan, J.; Anderson, M. F.; Franzen, S.; Feldheim, D. L., Multifunctional gold nanoparticle-peptide complexes for nuclear targeting. *J. Am. Chem. Soc.* **2003,** *125* (16), 4700-4701.

56. El-Sayed, I. H.; Huang, X. H.; El-Sayed, M. A., Selective laser photo-thermal therapy of epithelial carcinoma using anti-EGFR antibody conjugated gold nanoparticles. *Cancer Lett.* **2006,** *239* (1), 129-135.

57. Lin, S. Y.; Tsai, Y. T.; Chen, C. C.; Lin, C. M.; Chen, C. H., Two-step functionalization of neutral and positively charged thiols onto citrate-stabilized Au nanoparticles. *J. Phys. Chem. B* **2004,** *108* (7), 2134-2139.

58. Boal, A. K.; Rotello, V. M., Fabrication and self-optimization of multivalent receptors on nanoparticle scaffolds. *J. Am. Chem. Soc.* **2000,** *122* (4), 734-735..

59. Ferrari, M., Beyond drug delivery. *Nat. Nanotechnol.* **2008,** *3* (3), 131-132.

60. Cho, E. C.; Xie, J. W.; Wurm, P. A.; Xia, Y. N., Understanding the Role of Surface Charges in Cellular Adsorption versus Internalization by Selectively Removing Gold Nanoparticles on the Cell Surface with a I-2/KI Etchant. *Nano Lett.* **2009,** *9* (3), 1080-1084.

61. Zhu, Z.-J.; Ghosh, P. S.; Miranda, O. R.; Vachet, R. W.; Rotello, V. M., Multiplexed Screening of Cellular Uptake of Gold Nanoparticles Using Laser Desorption/Ionization Mass Spectrometry. *J. Am. Chem. Soc.* **2008,** *130* (43), 14139–14143.

62. Verma, A.; Uzun, O.; Hu, Y.; Hu, Y.; Han, H.-S.; Watson, N.; Chen, S.; Irvine, D. J.; Stellacci, F., Surface-structure-regulated cell-membrane penetration by monolayer-protected nanoparticles. *Nat. Mater.* **2008,** *7*, 588 - 595.

63. Tkachenko, A. G.; Xie, H.; Coleman, D.; Glomm, W.; Ryan, J.; Anderson, M. F.; Franzen, S.; Feldheim, D. L., Multifunctional gold nanoparticle-peptide complexes for nuclear targeting. *J. Am. Chem. Soc.* **2003,** *125* (16), 4700-4701

64. Nativo, P.; Prior, I. A.; Brust, M., Uptake and intracellular fate of surface-modified gold nanoparticles. *Acs Nano* **2008,** *2* (8), 1639-1644

65. Jiang, W.; Kim, B. Y. S.; Rutka, J. T.; Chan, W. C. W., Nanoparticle-mediated cellular response is size-dependent. *Nat. Nanotechnol.* **2008,** *3* (3), 145-150.

66. Perrault, S. D.; Walkey, C.; Jennings, T.; Fischer, H. C.; Chan, W. C. W., Mediating Tumor Targeting Efficiency of Nanoparticles Through Design. *Nano Lett.* **2009,** *9* (5), 1909-1915.

67. Allen, T. M.; Cullis, P. R., Drug Delivery Systems: Entering the Mainstream. *Science* **2004,** *303*, 1818-1822.

68. Torchilin, V. P., Recent advances with liposomes as pharmaceutical carriers. *Nat. Rev. Drug Discov.* **2005,** *4* (2), 145-160.

69. Davis, M. E.; Chen, Z.; Shin, D. M., Nanoparticle therapeutics: an emerging treatment modality for cancer. *Nat. Rev. Drug Discov.* **2008,** *7* (9), 771-782.

70. Lee, C. C.; MacKay, J. A.; Frechet, J. M. J.; Szoka, F. C., Designing dendrimers for biological applications. *Nat. Biotechnol.* **2005,** *23* (12), 1517-1526.

71. Peer, D.; Karp, J. M.; Hong, S.; Farokhzad, O. C.; Margalit, R.; Langer, R., Nanocarriers as an emerging platform for cancer therapy. *Nat. Nanotechnol.* **2007,** *2* (12), 751-760.

72 . Gibson, J. D.; Khanal, B. P.; Zubarev, E. R., Paclitaxel-functionalized gold nanoparticles. *J. Am. Chem. Soc.* **2007,** *129* (37), 11653-11661.

73. Schmid, G., Large Clusters and Colloids - Metals in the Embryonic State. *Chem. Rev.* **1992,** *92* (8), 1709-1727.

74 . Bhattacharya, R.; Mukherjee, P., Biological properties of "naked" metal nanoparticles. *Adv. Drug Deliver. Rev.* **2008,** *60* (11), 1289-1306.

75. Han, G.; You, C. C.; Kim, B. J.; Turingan, R. S.; Forbes, N. S.; Martin, C. T.; Rotello, V. M., Light-regulated release of DNA and its delivery to nuclei by means of photolabile gold nanoparticles. *Angew. Chem. Int. Edit.* **2006,** *45* (19), 3165-3169.

76. Torchilin, V. P., Structure and design of polymeric surfactant-based drug delivery systems. *J. Control. Release* **2001,** *73* (2-3), 137-172.

77. Morgan, M. T.; Nakanishi, Y.; Kroll, D. J.; Griset, A. P.; Carnahan, M. A.; Wathier, M.; Oberlies, N. H.; Manikumar, G.; Wani, M. C.; Grinstaff, M. W., Dendrimer-encapsulated camptothecins: Increased solubility, cellular uptake, and cellular retention affords enhanced anticancer activity in vitro. *Cancer Res.* **2006,** *66* (24), 11913-11921.

78. Anderson, M. E., Glutathione: an overview of biosynthesis and modulation. *Chem-Biol. Interact.* **1998,** *112*, 1-14.

79. Jones, D. P.; Carlson, J. L.; Mody, V. C.; Cai, J. Y.; Lynn, M. J.; Sternberg, P., Redox state of glutathione in human plasma. *Free Radical Bio. Med.* **2000,** *28* (4), 625-635.

80. Ghosh, P.; Han, G.; De, M.; Kim, C. K.; Rotello, V. M., Gold nanoparticles in delivery applications. *Adv. Drug Deliver. Rev.* **2008,** *60* (11), 1307-1315.

81. Sapsford, K. E.; Berti, L.; Medintz, I. L., Materials for fluorescence resonance energy transfer analysis: Beyond traditional donor-acceptor combinations. *Angew. Chem. Int. Edit.* **2006,** *45* (28), 4562-4588.

82. Ghosh, P. S.; Kim, C. K.; Han, G.; Forbes, N. S.; Rotello, V. M., Efficient Gene Delivery Vectors by Tuning the Surface Charge Density of Amino Acid-Functionalized Gold Nanoparticles. *Acs Nano* **2008,** *2* (11), 2213-2218.

83. Chompoosor, A.; Han, G.; Rotello, V. M., Charge dependence of ligand release and monolayer stability of gold nanoparticles by biogenic thiols. *Bioconjugate Chem* .**2008,** *19* (7), 1342-1345.

84. Podsiadlo, P.; Sinani, V. A.; Bahng, J. H.; Kam, N. W. S.; Lee, J.; Kotov, N. A., Gold Nanoparticles Enhance the Anti-Leukemia Action of a 6-Mercaptopurine Chemotherapeutic Agent. *Langmuir* **2008,** *24*, 568-574.

85. Park, C.; Youn, H.; Kim, H.; Noh, T.; Kook, Y. H.; Oh, E. T.; Park, H. J.; Kim, C., Cyclodextrin-covered gold nanoparticles for targeted delivery of an anti-cancer drug. *J. Mater. Chem.* **2009,** *19* (16), 2310-2315.

86. Love, J. C.; Estroff, L. A.; Kriebel, J. K.; Nuzzo, R. G.; Whitesides, G. M., Self-assembled monolayers of thiolates on metals as a form of nanotechnology. *Chem. Rev.* **2005,** *105* (4), 1103-1169.

87. Lucarini, M.; Franchi, P.; Pedulli, G. F.; Gentilini, C.; Polizzi, S.; Pengo, P.; Scrimin, P.; Pasquato, L., Effect of core size on the partition of organic solutes in the monolayer of water-soluble nanoparticles: An ESR investigation. *J. Am. Chem. Soc.* **2005,** *127* (47), 16384-16385.

88. Kim, C. K.; Ghosh, P.; Pagliuca, C.; Zhu, Z.-J.; Menichetti, S.; Rotello, V. M., Entrapment of Hydrophobic Drugs in Nanoparticle Monolayers with Efficient Release into Cancer Cells. *J. Am. Chem. Soc.* **2009,** *131*, 1360-1361

89. Rouhana, L. L.; Jaber, J. A.; Schlenoff, J. B., Aggregation-resistant water-soluble gold nanoparticles. *Langmuir* **2007,** *23* (26), 12799-12801.

90. D'Emanuele, A.; Attwood, D., Dendrimer-drug interactions. *Adv. Drug Deliver. Rev.* **2005,** *57* (15), 2147-2162.

91. Cheng, Y.; Samia, A. C.; Meyers, J. D.; Panagopoulos, I.; Fei, B. W.; Burda, C., Highly efficient drug delivery with gold nanoparticle vectors for in vivo photodynamic therapy of cancer. *J. Am. Chem. Soc.* **2008,** *130* (32), 10643-10647.

92. Kwon, I. C.; Bae, Y. H.; Kim, S. W., Electrically Erodible Polymer Gel for Controlled Release of Drugs. *Nature* **1991,** *354* (6351), 291-293.

93. Mccoy, C. P.; Rooney, C.; Edwards, C. R.; Jones, D. S.; Gorman, S. P., Light-triggered molecule-scale drug dosing devices. *J. Am. Chem. Soc.* **2007,** *129* (31), 9572-9573

94. Agasti, S. S.; Chompoosor, A.; You, C. C.; Ghosh, P.; Kim, C. K.; Rotello, V. M., Photoregulated Release of Caged Anticancer Drugs from Gold Nanoparticles. *J. Am. Chem. Soc.* **2009,** *131* (16), 5728-5729.

95. Nakanishi, J.; Nakayama, H.; Shimizu, T.; Ishida, H.; Kikuchi, Y.; Yamaguchi, K.; Horiike, Y., Light-Regulated Activation of Cellular Signaling by Gold Nanoparticles That Capture and Release Amines. *J. Am. Chem. Soc.* **2009,** *131* (11), 3822-3823

96. Polizzi, M. A.; Stasko, N. A.; Schoenfisch, M. H., Water-soluble nitric oxide-releasing gold nanoparticles. *Langmuir* **2007,** *23* (9), 4938-4943.

97. Yang, Q.; Wang, S. H.; Fan, P. W.; Wang, L. F.; Di, Y.; Lin, K. F.; Xiao, F. S., pH-responsive carrier system based on carboxylic acid modified mesoporous silica and polyelectrolyte for drug delivery. *Chem. Mater.* **2005,** *17* (24), 5999-6003.

98. Hwu, J. R.; Lin, Y. S.; Josephrajan, T.; Hsu, M. H.; Cheng, F. Y.; Yeh, C. S.; Su, W. C.; Shieh, D. B., Targeted Paclitaxel by Conjugation to Iron Oxide and Gold Nanoparticles. *J. Am. Chem. Soc.* **2009,** *131* (1), 66 -67.

CHAPTER 2

ENTRAPMENT OF HYDROPHOBIC DRUGS IN GOLD NANOPARTICLE MONOLAYERS WITH EFFICIENT RELEASE INTO CANCER CELLS

2.1 Introduction

Drug delivery systems (DDSs) provide an important tool for increasing efficacy of pharmaceuticals through improved pharmacokinetics and biodistribution.[1] A wide variety of nanoscale materials such as liposomes, polymeric micelles, and dendrimers, have been employed as drug carriers.[2] Both covalent and non-covalent approaches can be applied to the conjugation of drugs into these DDSs.[3,4] Non-covalent approaches have the capability of employing active drugs, whereas covalent attachment generally requires chemical modification which can cause reduced efficiency of drug release or incomplete intracellular processing of a prodrug.[5]

Recently, gold nanoparticle (AuNP) based drug/gene delivery systems have attracted attention due to their functional versatility,[6] biocompatibility,[7] and low toxicity,[8] Recent studies have demonstrated controlled release of payload by intracellular thiols.[9, 10, 11, 12, 13] However, controlled dissociation of drugs in active form from covalent AuNP-drug conjugates remains a challenge for clinical applications.[2]

2.1.1 Non-covalent loading of the drugs on gold nanoparticles

Non-covalent incorporation of drugs into AuNP monolayers provides an alternative delivery strategy with the potential for avoiding drug release and prodrug processing issues. The structure of commonly used water-soluble AuNPs is similar to that of unimolecular micelles such as dendrimers, featuring a hydrophobic interior and a hydrophilic exterior (Figure 2.1).[14] The alkanethiol monolayer of the nanoparticle coupled with the radial nature of the ligands[15] creates "hydrophobic pockets" inside monolayer of AuNP where organic solutes can be partitioned, as demonstrated by Lucarini and Pasquato.[16] We report here the use of these pockets to encapsulate drugs and deliver them with high efficiency to cells. This work has been reported as a communication in the *Journal of the American Chemical Society*.[17]

The biocompatible AuNPs used in this study feature two functional domains: a hydrophobic alkanethiol interior and a hydrophilic shell composed of a tetraethylene glycol (TEG) unit terminated with a zwitterionic headgroup. Particles with this general structure have been shown to minimize non-specific binding with biomacromolecules.[18, 19]

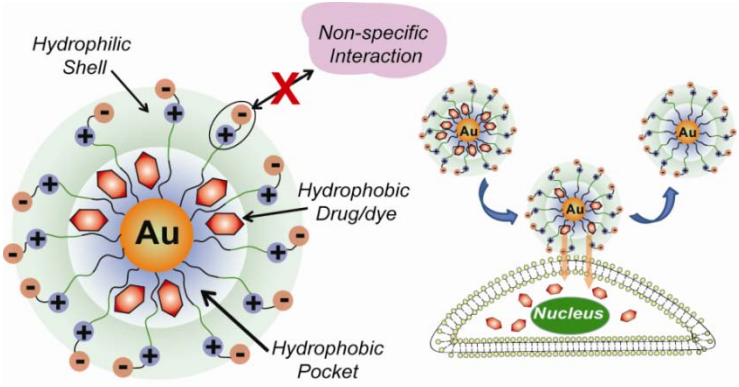

Figure 2.1 Delivery of payload to cell through monolayer-membrane interactions.

2.2 Results and discussion

2.2.1 Loading of drugs/dyes in the monolayer of gold nanoparticles

We chose three different hydrophobic guest compounds: 4,4-difluoro-4-bora-3a,4a-diaza-s-indacene (Bodipy) as a fluorescent probe,[20] and the highly hydrophobic therapeutics tamoxifen (TAF) and β-lapachone (LAP) as drugs (Figure 1). The nanoparticle-payload conjugates (AuNPZwit-Bodipy, TAF, and LAP) were prepared by the solvent displacement method.[21] First, AuNPZwit (Au core: 2.5 ± 0.4 nm) and guest were dissolved in an acetone/water mixture and the solvent slowly evaporated. The bulk of the excess guest precipitated out and was removed by filtration; the particles were further purified by multiple filtrations through a molecular weight cutoff filter until no free guest was observed, followed by dialysis against buffer. The number of entrapped guest molecules per particle was determined from ^{1}H NMR spectrum and NaCN-induced decomposition experiments and varied depending on size, hydrophobicity (logP), and molecular structure of hydrophobic molecules (Figure 2.2). The particle/guest complexes are stable in buffer for >1 month and to extended dialysis, a level of kinetic entrapment greater than that observed with dendrimers.

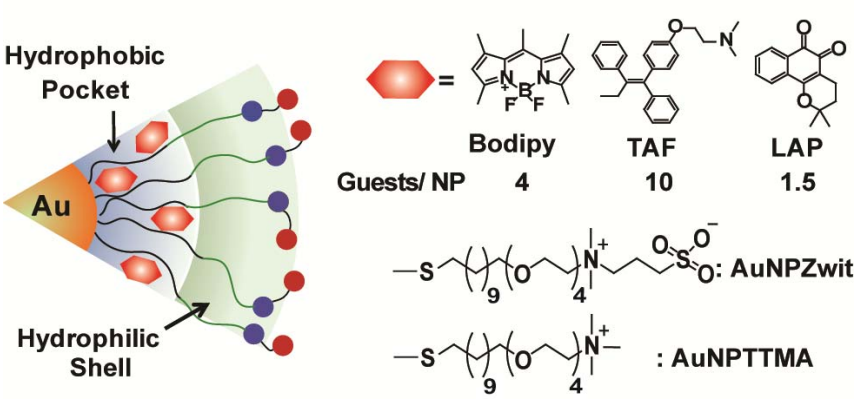

Figure 2.2 Structure of particles and guest compounds: Bodipy, TAF, and LAP, and the number of encapsulated guests per particle.

2.2.2 Stability of gold nanoparticles-payloads

The ability of the delivery systems to release their payload was first explored using AuNPZwit-Bodipy in a two-phase dichloromethane (DCM)-water system. In this system the dye is quenched by the AuNP, and photoluminescence (PL) only observed upon dye release. In these studies a rapid increase in PL intensity is observed along with transfer of Bodipy into the DCM layer (Figure 2.3 (a)). Significantly, since no release is observed in monophasic aqueous conditions and no particle was observed in the DCM layer, payload release presumably occurs via a particle-interface process.

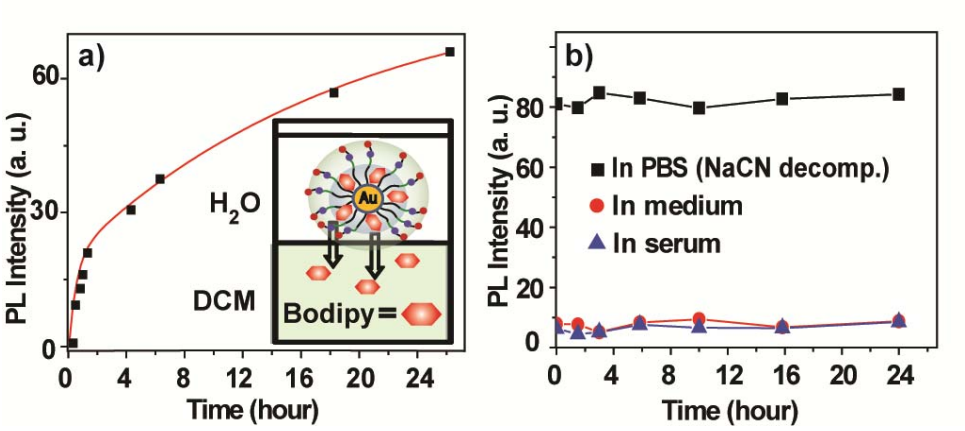

Figure 2.3 a) Release of Bodipy from AuNPZwit-Bodipy in DCM-aqueous solution two-phase systems (λ_{ex}= 499 nm, λ_{em}= 517 nm) b) PL intensity AuNPZwit-Bodipy in cell culture medium and 100 % serum, indicating little or no release relative to AuNPZwit-Bodipy in PBS after NaCN-induced release of guest molecules (λ_{ex}= 499 nm, λ_{em}= 510 nm).

2.2.3 Cellular uptake of the gold nanoparticles and their payloads

Payload delivery to cells using AuNPZwit-Bodipy was determined by confocal laser scanning microscopy (CLSM) using human breast cancer (MCF-7) cells. Efficient delivery of the dye to the cytosol is observed after 2 h incubation with AuNPZwit-Bodipy (Figure 2.4 (a)-(c)). Cellular uptake of nanoparticle was studied using transmission electron microscopy (TEM), and inductively coupled plasma mass spectrometry (ICP-MS), using the analogous cationic particle/dye conjugate AuNPTTMA-Bodipy as a positive control. Little or no cellular uptake of AuNPZwit was observed by either TEM (Figure 2.4 (d) and (e)) or ICP-MS (Figure 2.4 (f)) for AuNPZwit-Bodipy, whereas substantial particle uptake was observed with AuNPTTMA-Bodipy Since no free dye was observed during the 24 h incubation of AuNPZwit-Bodipy in medium and serum

solution at 37 ºC (Figure 2.3 (b)), Bodipy delivery presumably occurs via a monolayer-membrane transfer process, consistent with our in vitro studies. [22]

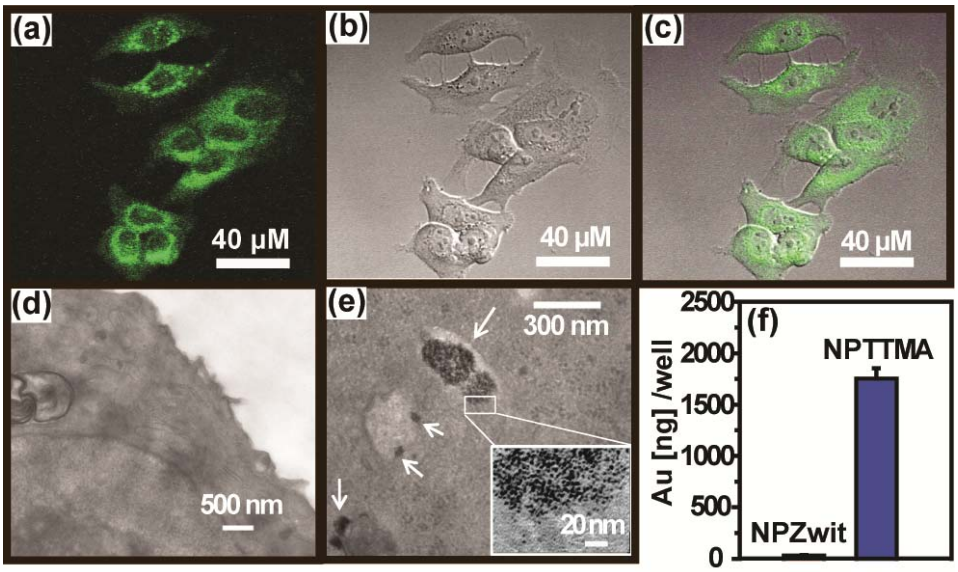

Figure 2.4 CLSM images of MCF-7 cell treated with AuNPZwit-Bodipy for 2h: (a) green channel (b) bright field, and (c) overlap. TEM images of fixed cell treated with (d) AuNPZwit-Bodipy and (e) AuNPTTMA as a positive control, Endosomally trapped AuNPs are marked by arrow. (f) ICP-MS measurement. (200,000 cells/well), NPZwit: AuNPZwit-Bodipy and NPTTMA: AuNPTTMA-Bodipy) indicating little cellular uptake of nanoparticle with AuNPZwit-Bodipy.

2.2.4 Delivery of the anticancer drugs into the cancer cells

Demonstration of drug delivery to MCF-7 cells was determined through cytotoxicity studies of free and encapsulated drugs using an Alamar blue assay (Figure 2.5). Notably, AuNPZwit itself was non-toxic at 30 μM. In contrast, IC_{50} values of 4 μM and 4.6 μM were observed using AuNPZwit-LAP and AuNPZwit-TAF, respectively. The delivery process was quite efficient, with the per drug molecule IC_{50} of AuNPZwit-TAF (46 μM) only three-fold higher than that of TAF (16 μM), and that of AuNPZwit-LAP (6.0 μM) essentially identical to that of LAP (5.2 μM).

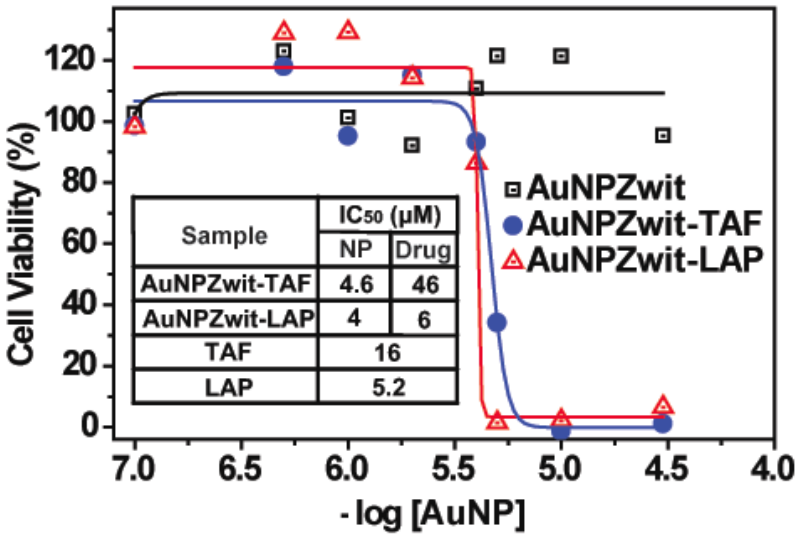

Figure 2.5 Cytotoxicity of AuNPZwit complexes measured by Alamar blue assay after 24h incubation with MCF-7 cells. IC_{50} of AuNP (NP), equivalent drugs (Drug), and free drugs are shown in table.

2.3 Summary and future outlook

In conclusion, we have demonstrated that hydrophobic dyes/drugs can be stably entrapped in the hydrophobic pocket of AuNPs and released into cell by membrane-mediated diffusion without uptake of the carrier nanoparticle. Importantly, the small size of these nanocarriers coupled with their biocompatible surface functionality should provide long circulation lifetimes and preferential accumulation in tumor tissues by the enhanced permeability and retention (EPR) effect.[23] Additionally, the non-interacting nature of their monolayer should make these systems highly amenable to targeting strategies.

2.4 Synthesis of materials and experimental methods

General

Dichloromethane (DCM) used after distillation under $CaCl_2$ and other chemicals from Aldrich were used as received. Dimethylamine, 1,3-Propanesulfone, trifluroacetic acid (TFA), triisopropylsilane (TIPS), and tamoxifen (TAF) were purchased from Aldrich. 4,4-difluoro-4-bora-3a,4a-diaza-*s*-indacene (Bodipy), β-lapachone (LAP), and AuNPTTMA were prepared by the literature procedures.[24, 25, 26] Theramanox® coverslips, uranyl acetate, osmium tetroxide, glutaraldehyde, lead citrate, epoxy embedding kit (Low Viscosity, as reported by Dr. Spurr) and 300 mesh copper grids with carbon film were purchased from Electron Microscopy Sciences.

^{1}H and ^{13}C NMR spectra were recorded on a Bruker AVANCE 400 at 400 and 100 MHz, respectively. ESI-MS spectra were obtained using JEOL MStation JMS700. UV-vis spectra were recorded on Hewlett-Packard 8452A spectrophotometer. Photoluminescence

spectrum was measured using Photon Technology International fluorescence spectrometer. Dynamic light scattering (DLS) was measured by Zetasizer Nano ZS. Fixed cell sections for TEM were cut by using Reichert Ultracut E Ultramicrotome and imaged using JEOL 100S electron microscopy. Cell viability using Alarmar blue assay was assessed by SpectraMax M5 microplate spectrophotometer and plotted by Origin 8. Fluorescence images was obtained using Zeiss LSM510 meta confocal microscope.

2.4.1 Synthesis of ligand and fabrication of nanoparticle

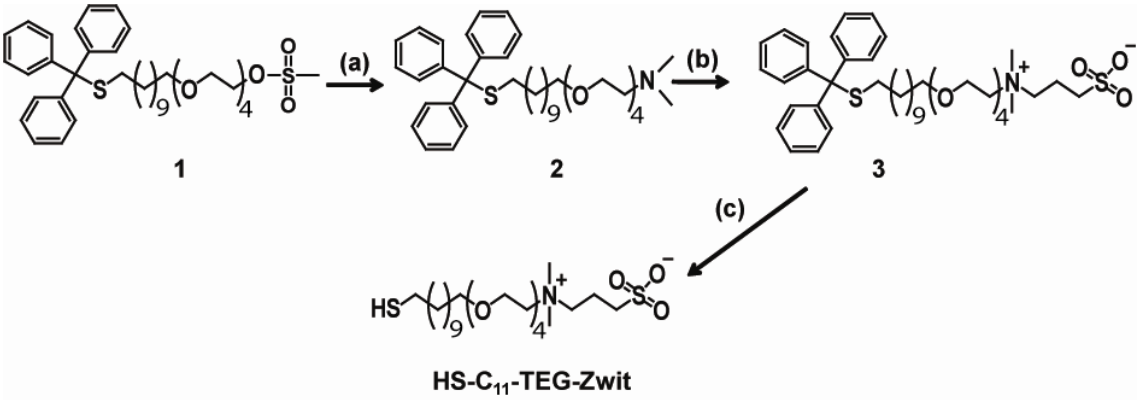

Figure 2.6 Synthesis of HS-C11-TEG-Zwit. (a) Dimethylamine, DCM, RT, overnight (b) 1,3-Propanesulfone, acetone, RT, overnight, (c) TFA, TIPS, RT, 4h

Compound **2**

Compound **1** (1 g, 1.4 mmol) was added to a solution of dimethylamine (0.6 g, 14 mmol in dichloromethane (20 mL) and the reaction mixture was stirred at room temperature for overnight. The reaction mixture was poured into a mixture of dichloromethane and distilled water. Organic layer was separated and concentrated at reduced pressure. The crud product was purified by column chromatography over silica gel using hexane/ethyl acetate (1:4, v/v) as an eluent. Solvent was removed in vacuo to afford compound **2** as

colorless oil (Yield 0.6 g, 65 %). ^{1}H NMR (400 MHz, $CDCl_3$) δ 7.41 (m, 6H, *Ph*-), 7.27 (m, 6H, *Ph*-), 7.20 (m, 3H, *Ph*-), 3.65-3.56 (m, 14H, -C*H*$_2$-*TEG*-), 3.44 (t, J = 6.8 Hz, 2H -OC*H*$_2$-CH_2-$N(CH_3)_2$), 2.53 (t, J = 5.8 Hz, 2H, -OCH_2-C*H*$_2$-$N(CH_3)_2$), 2.84 (s, 6H, -$N(CH_3)_2$), 2.14 (t, J = 7.3 Hz, 2H, -S-C*H*$_2$-), 1.40 (m, 18H, -S-CH_2-$(CH_2)_9$-); ^{13}C NMR (100.64 MHz, $CDCl_3$) δ 26.10, 28.60, 29.02, 29.19, 29.41, 29.48, 29.56, 29.65, 32.04, 45.81, 58.77, 66.36, 69.23, 70.07, 70.40, 70.61, 71.55, 126.49, 127.79, 129.62, 145.10.

Compound **3**

A anhydrous acetone solution (20 mL) of compound **2** (0.5 g, 0.77 mmol) and 1,3-propanesultone (0.14 g, 1.15 mmol) in anhydrous acetone was stirred at room temperature for overnight. The reaction mixture was filtered, and the resulting solid was washed with ethyl acetate/hexane (1:4, v/v) and dried in vacuum to afford compound **3** as a white solid (Yield 0.5 g, 84 %). ^{1}H NMR (400 MHz, $CDCl_3$) δ 7.41 (m, 6H, *Ph*-), 7.27 (m, 6H, *Ph*-), 7.20 (m, 3H, *Ph*-), 3.94 (m, 2H, -OC*H*$_2$-CH_2-$N(CH_3)_2$-), 3.78 (m, 2H, -OCH_2-C*H*$_2$-$N(CH_3)_2$-), 3.71-3.56 (m, 14H, -C*H*$_2$-*TEG*- and -CH_2-CH_2-C*H*$_2$-sulfonate), 3.42 (t, J = 6.8 Hz, 2H, -OC*H*$_2$-CH_2-$N(CH_3)_2$-), 3.23 (s, 6H, -$N(CH_3)_2$-), 2.88 (t, J = 6.7 Hz, 2H, -C*H*$_2$-CH_2-CH_2-sulfonate), 2.26 (m, 2H, -CH_2-C*H*$_2$-CH_2-sulfonate), 2.12 (t, J = 7.3 Hz, 2H, -S-C*H*$_2$-), 1.40 (m, 18H, -S-CH_2-$(CH_2)_9$-); MS (ESI-MS) calcd for $C_{43}H_{66}NO_7S_2$ 773.12, found 794.6 $[M+Na]^+$

HS-C_{11}-TEG-Zwit

A dichloromethane solution of compound **3** (0.6 g, 0.77 mmol), trifluoroacetic acid (1.78 g, 16 mmol), and triisopropylsilane (0.18 g, 1.1mmol) was stirred at room temperature for 6 h under argon. After removal of the solvent at reduced pressure, the residue was

purified by washing with diethyl ether (20 ml x 5). After drying residue under high vacuum, white solid of product was obtained. (Yield 0.36 g,87 %) ^{1}H NMR (400 MHz, $CDCl_3$) 3.91 (m, 2H, -OC*H*$_2$-CH_2-N$(CH_3)_2$-), 3.79-3.52 (m, 16H, OCH_2-C*H*$_2$-N$(CH_3)_2$-, -C*H*$_2$-*TEG*-, and -CH_2-CH_2-C*H*$_2$-sulfonate), 3.42 (t, J = 6.8 Hz, 2H, -OC*H*$_2$-CH_2-N$(CH_3)_2$-), 3.41 (t, J = 6.8 Hz, 2H, -OC*H*$_2$-CH_2-N$(CH_3)_2$-), 3.04 (s, 6H, -N(C*H*$_3)_2$-), 2.90 (brs, 2H, -C*H*$_2$-CH_2-CH_2-sulfonate), 2.49 (q, J=7.2 Hz, 2H, HS-C*H*$_2$-), 2.26 (brs, 2H, -CH_2-C*H*$_2$-CH_2-sulfonate), 1.40 (m, 18H, -S-CH_2-(C*H*$_2)_9$-); MS (ESI-MS) calcd for $C_{24}H_{52}NO_7S_2$ 530.32, found 552.4 $[M+Na]^+$.

Preparation of AuNPZwit

Gold nanoparticles, C_5 NP were prepared by following the Brust-Schiffrin two-phase method using 1-pentanethiol as capping ligands. To fabricate AuNPZwit via ligand place exchange reaction, 30 mg of C_5 NP were mixed with 100 mg of HS-C_{11}-TEG-Zwit in dichloromethane (10 mL). The solution was stirred at room temperature for 24 hours. Solvent was removed by rotary evaporator and the nanoparticles were washed with diethyl ether (20 mL x 5). The nanoparticles were further purified by dialysis in MiliQ water using SnakeSkin pleated dialysis tubing (10,000 MWCO) for 1days. ^{1}H NMR spectrum is shown in Figure 2.8 (a).

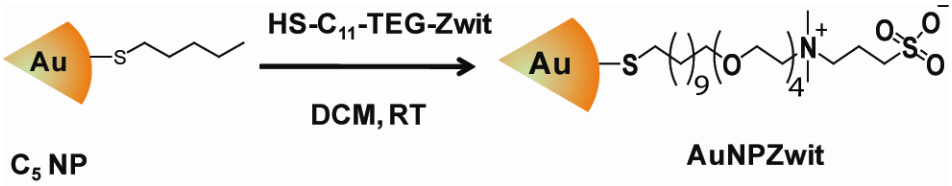

Figure 2.7 Synthetic pathway of AuNPZwit.

2.4.2 Experimental methods

Preparation and characterization of AuNPZwit complexes (AuNPZwit-dye/drug conjugates)

In order to prepare AuNPZwit complexes, solvent displacement method was carried out using water and acetone. An acetone solution of each guest compound (10 mg) and aqueous solution of AuNPZwit (80 μM) were well mixed. Acetone was then removed by rotary evaporator or slow evaporation at room temperature. During the evaporation of acetone, some guest compounds were entrapped in interior of AuNPZwit due to hydrophobic interaction and the rest of guest compounds were precipitated out. The mixture was then filtrated using filter (0.2 μm pore) to remove the precipitate. Any residue of free guest compounds in the aqueous solution may affect to result of cytotoxicity and fluorescence related experiments. For further purification, the AuNPZwit complexes solution was washed with distilled water and centrifuged with Amicon Ultra-4 tube (10,000 MWCO) several times (2 mL x ~5 times) until no absorbance of guest molecules in filtrate was detected by spectrophotometer. AuNPTTMA-Bodipy was also prepared by the same procedure.

AuNPZwit complexes conjugates were characterized by nuclear magnetic resonance (NMR). ^{1}H NMR spectrum of AuNPZwit complexes are shown in Figure 2.8 (b)-(d). A broaden of ^{1}H NMR peak of the guest compounds indicates that guest compounds were entrapped in hydrophobic pocket of the AuNPZwit. It is also noted that the H^{1} NMR peak of guest compounds (TAF and Bodipy) in D_2O was not present until AuNPZwit complex was formed. The stoichiometry of the AuNPZwit complexes was calculated by measuring integral of AuNPZwit and guest compounds. From TGA and TEM analysis, it is

estimated that 100 ligands are placed on each AuNPZwit.[27] Around 10~11 TAFs were entrapped in AuNPZwit. The number of entrapped guest compounds for AuNPZwit-LAP and AuNPZwit-Bodipy were calculated from the NaCN-induced decomposition experiment due to weak ^{1}H NMR signal of guest compound.

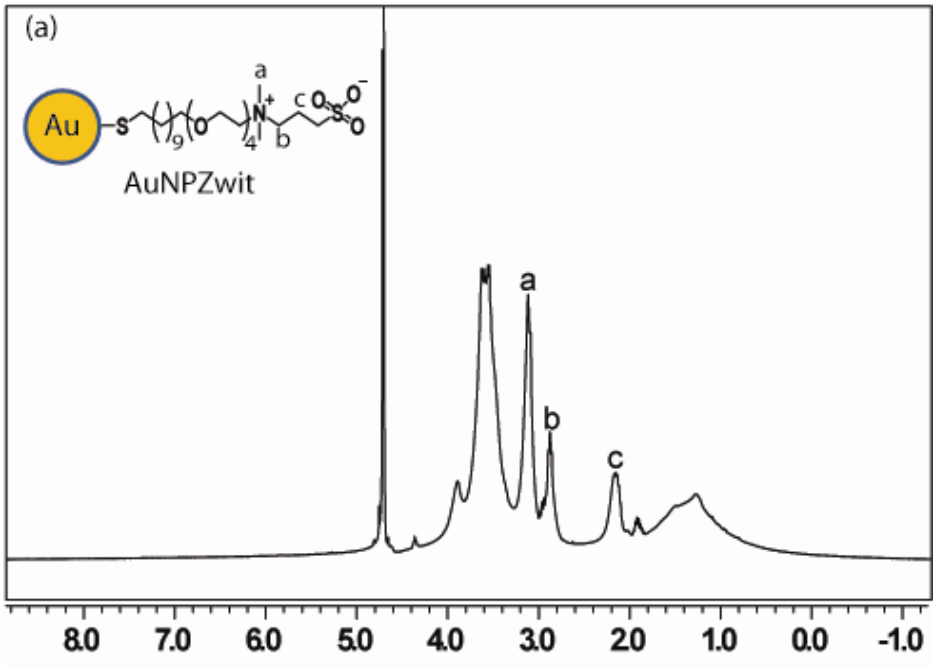

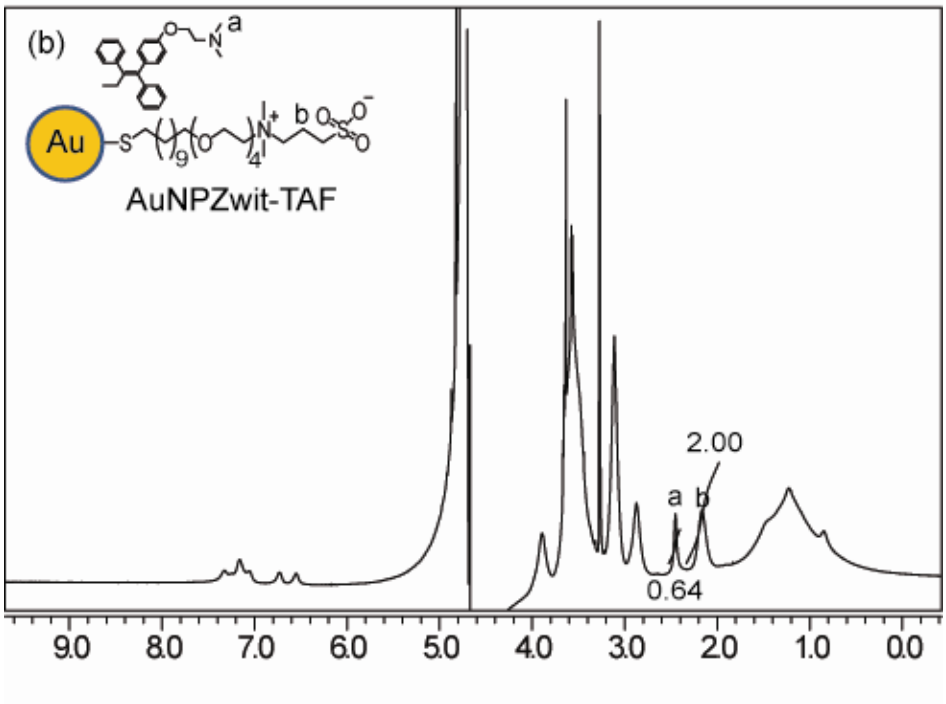
(b)
a
b
Au
AuNPZwit-TAF
2.00
a b
0.64
9.0
8.0
7.0
6.0
5.0
4.0
3.0
2.0
1.0
0.0

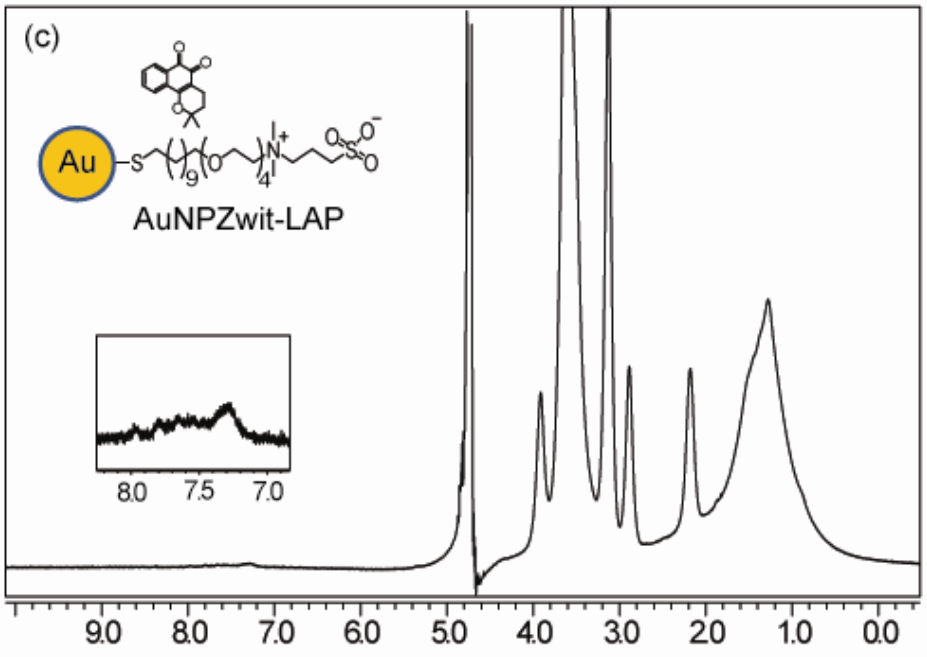
(c)
Au
AuNPZwit-LAP
8.0
7.5
7.0
9.0
8.0
7.0
6.0
5.0
4.0
3.0
2.0
1.0
0.0

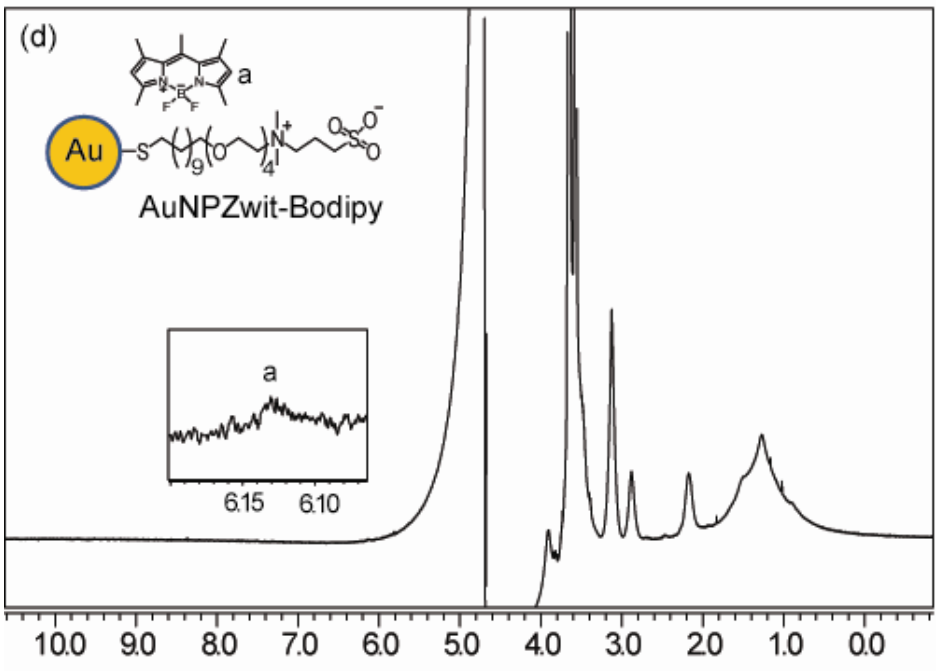

Figure 2.8 ^{1}H NMR spectrum of AuNPZwit and AuNPZwit complexes (a) AuNPZwit (b) AuNPZwit-TAF, (c) AuNPZwti-LAP, (d) AuNPZwit-Bodipy.

NaCN-induced decomposition of AuNPZwit complexes

To 1 ml of a solution of the desired AuNPZwit complexes in THF (final concentration of 0.5 ~ 4 μM) was added 1 mL of an aqueous NaCN solution (final concentration 0.1 M) followed by briefly agitating the mixture. After 2 h, plasmon absorption band of the AuNP at 520 nm completely decayed while absorbance of guest compounds remained. Concentration of guest compounds was then calculated based on the Beer-Lambert law (λ_{max} = 496 nm for Bodipy, λ_{max} = 290 nm for LAP, and λ_{max} = 280 nm for TAF). By comparing with the concentration of AuNPZwit before etching, the number of guest

compounds entrapped in AuNPZwit was estimated. A molar extinction coefficient of free guest compounds in THF/H_2O (1:1) was obtained for this estimation (Bodipy ε = 7.07 x 10^3 at 496 nm, LAP ε = 1.2 x 10^4 at 290 nm, and TAF ε = 1.1 x 10^4 at 280 nm).

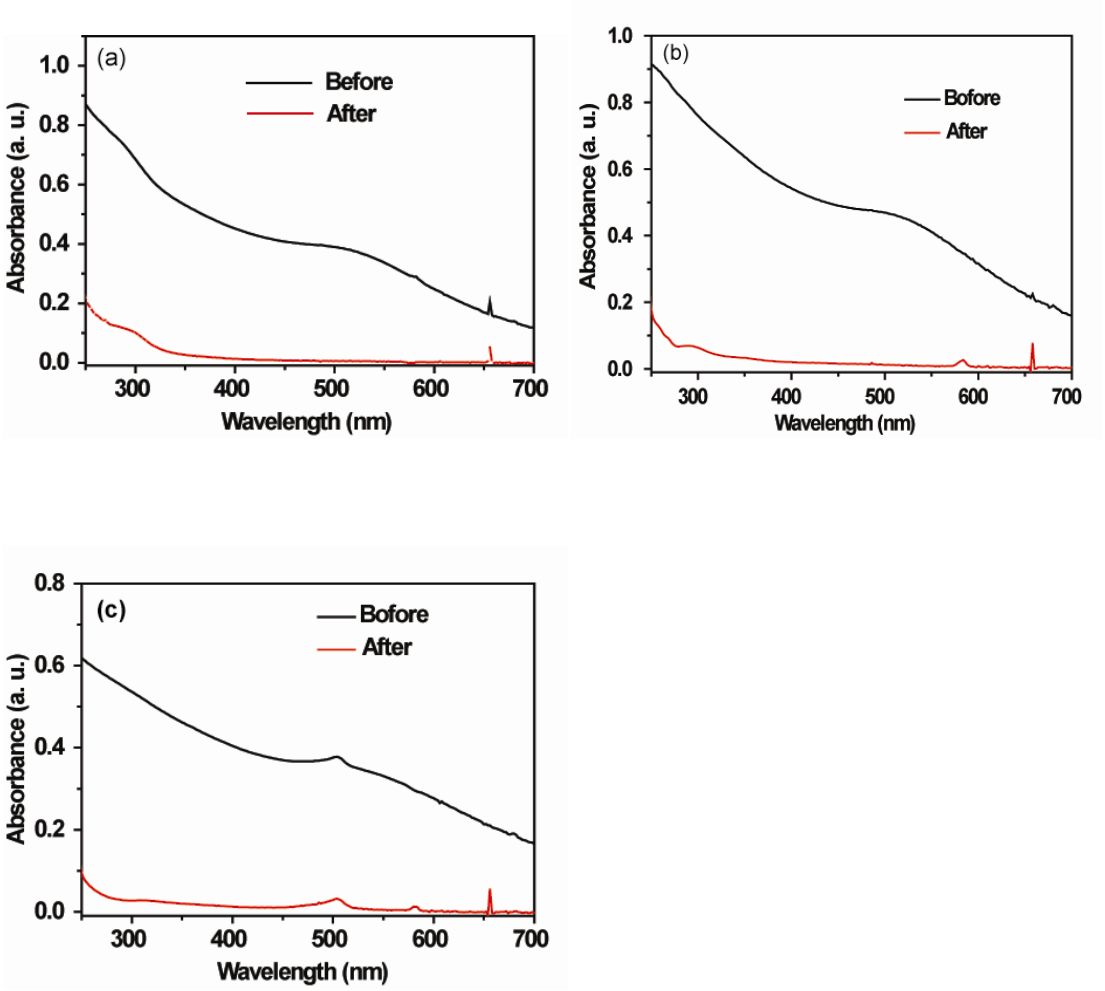

Figure 2.9 UV-vis spectrum of AuNPZwit complexes before and after NaCN-induced decomposition experiment. (a) AuNPZwit-TAF, (b) AuNPZwit-LAP, and (c) AuNPZwit-Bodipy.

Stability test of AuNPZwit complexes in PBS

1 mL of AuNPZwit complexes (5 μM) in PBS was centrifuged with Amicon Ultra-4 tube (10,000 MWCO) at 8,000 rpm for 30 min. Stability of AuNPZwit complexes was examined by measuring the absorbance of the filtrate. Any absorbance of guest compound in filtrate was not observed at least for one month.

Partition Coefficient logP

Partition coefficient, logP was obtained according to our previous study.[28] The logP for the hydrophobic compounds as followings: LAP: 2.68, TAF: 3.64, and Bodipy: 4.0. It indicates that LAP is less hydrophobic than TAF and Bodipy, which might cause the lower number of encapsulated guests in AuNPZwit.

Cell culture

MCF-7 cells were grown in a cell culture flask in low glucose Dulbecco's Modified Eagle Medium supplemented with 10% fetal bovine serum (FBS) and 1 % of antibiotics at 37 °C in a humidified atmosphere of 5 % CO_2.

Cytotoxicity test of AuNPZwit complexes

MCF-7 cells were seeded at 20,000 cells in 0.2 ml per well in 96-well plates 24 h prior to the experiment. The old medium were replaced by different concentrations of TAF, LAP, AuNPZwit-TAF, AuNPZwit-LAP, and AuNPZwit in serum containing medium and incubated for 24 h at 37 °C in a humidified atmosphere of 5 % CO_2. The cells were then completely washed with PBS buffer three times and 10 % Alarmar blue of serum

containing medium was added to each well and further incubated at 37 ºC for 3 h. The cell viability was then determined by measuring the fluorescence intensity at 570 nm using a SpectraMax M5 microplate spectrophotometer. Curves were fitted by DoseRep function in Origin 8.

Confocal laser scanning microscopy

MCF-7 cells were seeded in 35 mm Petri dish (Mat Tek Corporation, MA) at 50,000 cells in 1 mL of serum containing medium 24 h prior to the experiment. The medium was replaced by serum containing medium and AuNPZwit-Bodipy to a final concentration of 1 μM and were incubated for 2 h. Cells were washed with PBS three times before being imaged under a confocal microscope (Zeiss LSM510 meta confocal microscope equipped with an argon-HeNe laser, λ_{ex} = 488 nm).

ICP-MS Instrumentation

All ICP-MS measurements were performed on a Perkin Elmer Elan 6100. Operating conditions of the ICP-MS are listed below: RF power: 1200 W; plasma Ar flow rate: 15 L/min; nebulizer Ar flow rate: 0.96 L/min; isotopes monitored: ^{197}Au; dwell time: 50 ms; nebulizer: cross flow; spray chamber: Scott.

ICP-MS sample preparation and measurements[29]

AuNPZwit-Boidpy and AuNPTTMA-Bodipy (1 μM) was incubated with pre seeded MCF-7 cell line in 24 well plates (200,000 cells/well) for 4h and 24 h (Figure 2.10). After incubation and lysing the cells, the resulting cell lysate was digested overnight using 3

mL of HNO_3 and 1 mL of H_2O_2. On the next day, 3 mL of aqua regia, which is highly corrosive and must be use with extreme caution, was added, and then the sample was allowed to react for another 2-3 h. The sample solution was then diluted to 100 mL with de-ionized water, and aqua regia. The final AuNP sample solution contained 5% aqua regia. The AuNPs sample solution was measured by ICP-MS under the operating conditions described above. Cell uptake experiments with each AuNP were repeated 3 times, and each replicate was measured 5 times by ICP-MS. A series of gold standard solutions (20, 10, 5, 2, 1, 0.5, 0.2, 0 ppb) were prepared before each experiment. Each gold standard solution contained 5% aqua regia. Each standard solution was also measured 5 times by ICP-MS using the operating conditions described above. The resulting calibration line was used to determine the gold amount in taken up by the cells in each sample. A ~100 ppm solution of dithiothreitol was used to wash the instrument between analyses to facilitate gold removal.

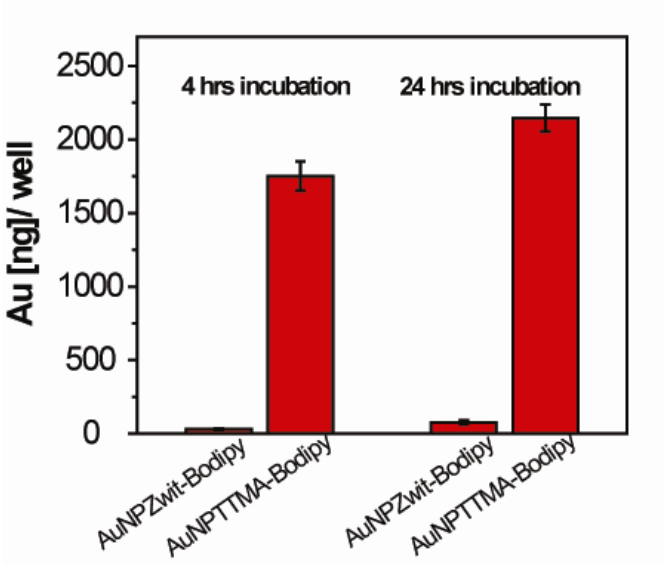

Figure 2.10 ICP-MS measurement of AuNPZwit-Boidpy and AuNPTTMA-Bodipy for 4 and 24 h.

TEM preparation for AuNPZwit complexes and fixed cell treated with AuNPs

MCF-7 cells were seeded and incubated on 15 mm diameter Theramanox® coverslips (Nalge Nunc International, NY) placed in 24 well plates at amount of 100,000 cells in 1 ml of serum containing medium for 24 h prior to the experiment. The medium was replaced by 1 ml of serum containing medium and AuNPZwit-Bodipy or AuNPTTMA to a final concentration of 1 μM and incubated for 4 h.[30] The medium containing the gold nanoparticles not taken up by the cells was discarded, and the cells were completely washed with PBS buffer three times. The cells were then fixed in 2 % glutaraldehyde with 3.75 % sucrose in 0.1 M sodium phosphate buffer (pH 7.0) for 30 min and then washed with 0.1 M PBS containing 3.75% sucrose three times over 30 min. They were postfixed in 1 % osmium tetroxide with 5 % sucrose in 0.05 M sodium phosphate buffer solution (pH 7.0) for 1 hr and the rinsed with distilled water three times. They were

dehydrated in a graded series of acetone (10 % step), and embedded in epoxy resin. The resin was polymerized at 60 °C for 48 h. Ultrathin sections (50−70 nm) obtained with a Reichert Ultracut E Ultramicrotome were stained with 2% aqueous uranyl acetate and 2% aqueous lead citrate and imaged under a JEOL 100S electron microscopy.

TEM samples of AuNPZwit and AuNPZwit complexes were prepared by placing one drop of the desired AuNP solution (3 μM) on to a 300-mesh Cu grid coated with carbon film. These samples were analyzed and photographed using the same instrument. TEM image of AuNPZwit is shown in Figure 2.11 (a). The average diameter of Au core is 2.5 ± 0.4 nm.

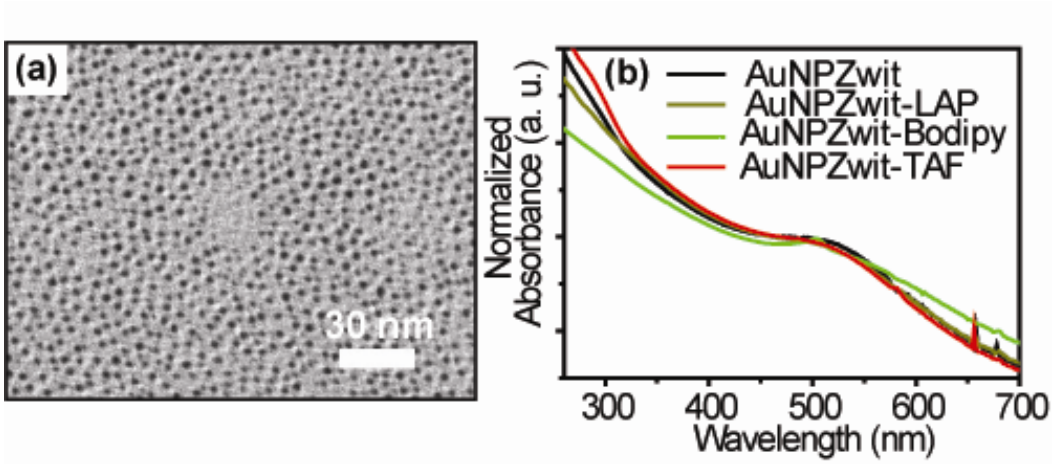

Figure 2.11 (a) TEM images of AuNPZwit. (b) UV-vis spectrum of AuNPZwit and AuNPZwit complexes. No red shift of plasmon absorption band was observed.

Thermogravimetric analysis (TGA)

TGA was performed using a TGA 2950 high-resolution thermo-gravimetric analyzer (TA Instruments, Inc., New Castle, DE), which was equipped with an open platinum pan and an automatically programmed temperature controller. The TGA data were obtained as follows: about 3.0 mg of AuNPZwit was placed in the TGA pan and heated in a nitrogen atmosphere at a rate of 10 °C / min up to 600 °C. TGA curve of AuNPZwit is shown in Figure S5. The TGA data showed that the weight percentage of organic ligands and Au core of AuNPZwit is 35 % and 65 %, respectively. Accordingly, the average number of the lignads is estimated as ~100, which is comparable to the literature.[31]

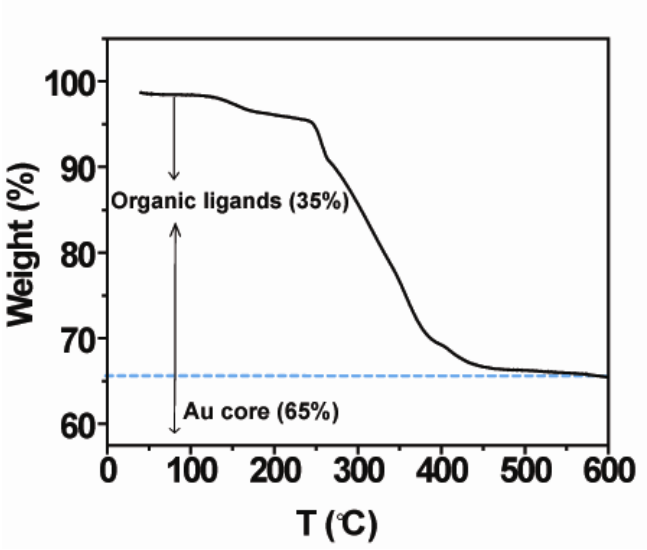

Figure 2.12 Thermal gravimetric analysis (TGA) data of AuNPZwit.

2.5 References

1. Allen, T. M.; Cullis, P. R., Drug delivery systems: Entering the mainstream. *Science* **2004,** *303* (5665), 1818-1822.
2. Peer, D.; Karp, J. M.; Hong, S.; FaroKHzad, O. C.; Margalit, R.; Langer, R., Nanocarriers as an emerging platform for cancer therapy. *Nat. Nanotechnol.* **2007,** *2* (12), 751-760.
3. Torchilin, V. P., Structure and design of polymeric surfactant-based drug delivery systems. *J. Control. Release* **2001,** *73* (2-3), 137-172.
4. Lee, C. C.; MacKay, J. A.; Frechet, J. M. J.; Szoka, F. C., Designing dendrimers for biological applications. *Nat. Biotechnol.* **2005,** *23* (12), 1517-1526..
5. Morgan, M. T.; Nakanishi, Y.; Kroll, D. J.; Griset, A. P.; Carnahan, M. A.; Wathier, M.; Oberlies, N. H.; Manikumar, G.; Wani, M. C.; Grinstaff, M. W., Dendrimer-encapsulated camptothecins: Increased solubility, cellular uptake, and cellular retention affords enhanced anticancer activity in vitro. *Cancer Res.* **2006,** *66* (24), 11913-11921..
6. Templeton, A. C.; Wuelfing, M. P.; Murray, R. W., Monolayer protected cluster molecules. *Acc. Chem. Res.* **2000,** *33* (1), 27-36..
7. De, M.; Ghosh, P. S.; Rotello, V. M., Applications of nanoparticles in biology. *Adv. Mater.* **2008,** *20* (22), 4225-4241..
8. Bhattacharya, R.; Mukherjee, P., Biological properties of "naked" metal nanoparticles. *Adv. Drug Deliv.Rev.* **2008,** *60* (11), 1289-1306.

9. Hong, R.; Han, G.; Fernandez, J. M.; Kim, B. J.; Forbes, N. S.; Rotello, V. M., Glutathione-mediated delivery and release using monolayer protected nanoparticle carriers. *J. Am. Chem. Soc.* **2006,** *128* (4), 1078-1079.

10. Paciotti, G. F.; Kingston, D. G. I.; Tamarkin, L., Colloidal gold nanoparticles: A novel nanoparticle platform for developing multifunctional tumor-targeted drug delivery vectors. *Drug Develop. Res.* **2006,** *67* (1), 47-54.

11. Gibson, J. D.; Khanal, B. P.; Zubarev, E. R., Paclitaxel-functionalized gold nanoparticles. *J. Am. Chem. Soc.* **2007,** *129* (37), 11653-11661..

12. Ghosh, P.; Han, G.; De, M.; Kim, C. K.; Rotello, V. M., Gold nanoparticles in delivery applications. *Adv. Drug Deliv.Rev.* **2008,** *60* (11), 1307-1315..

13. Cheng, Y.; Samia, A. C.; Meyers, J. D.; Panagopoulos, I.; Fei, B. W.; Burda, C., Highly efficient drug delivery with gold nanoparticle vectors for in vivo photodynamic therapy of cancer. *J. Am. Chem. Soc.* **2008,** *130* (32), 10643-10647.

14. Crampton, H. L.; Simanek, E. E., Dendrimers as drug delivery vehicles: non-covalent interactions of bioactive compounds with dendrimers. *Polymer International* **2007,** *56*, 489-496.

15. Hostetler, M. J.; Stokes, J. J.; Murray, R. W., Infrared spectroscopy of three-dimensional self-assembled monolayers: N-alkanethiolate monolayers on gold cluster compounds. *Langmuir* **1996,** *12* (15), 3604-3612.

16. Lucarini, M.; Franchi, P.; Pedulli, G. F.; Gentilini, C.; Polizzi, S.; Pengo, P.; Scrimin, P.; Pasquato, L., Effect of core size on the partition of organic solutes in the monolayer

of water-soluble nanoparticles: An ESR investigation. *J. Am. Chem. Soc.* **2005,** *127* (47), 16384-16385.

17. Kim, C. K.; Ghosh, P.; Pagliuca, C.; Zhu, Z. J.; Menichetti, S.; Rotello, V. M., Entrapment of Hydrophobic Drugs in Nanoparticle Monolayers with Efficient Release into Cancer Cells. *J. Am. Chem. Soc.* **2009,** *131* (4), 1360-1361

18. Rouhana, L. L.; Jaber, J. A.; Schlenoff, J. B., Aggregation-resistant water-soluble gold nanoparticles. *Langmuir* **2007,** *23* (26), 12799-12801.

19. Jin, Q.; Xu, J. P.; Ji, J.; Shen, J. C., Zwitterionic phosphorylcholine as a better ligand for stabilizing large biocompatible gold nanoparticles. *Chem. Commun.* **2008,** (26), 3058-3060.

20. Loudet, A.; Burgess, K., BODIPY dyes and their derivatives: Syntheses and spectroscopic properties. *Chem. Rev.* **2007,** *107* (11), 4891-4932.

21. Jones, M. C.; Leroux, J. C., Polymeric micelles - a new generation of colloidal drug carriers. *Eur. J. Pharm. Biopharm.* **1999,** *48* (2), 101-111.

22. Chen, H. T.; Kim, S. W.; Li, L.; Wang, S. Y.; Park, K.; Cheng, J. X., Release of hydrophobic molecules from polymer micelles into cell membranes revealed by Forster resonance energy transfer imaging. *P. Natl. Acad. Sci. USA* **2008,** *105* (18), 6596-6601..

23. D'Emanuele, A.; Attwood, D., Dendrimer–drug interactions. *Adv. Drug Deliv.Rev.* **2005,** *57* (2147), 2147– 2162.

24. Guo, B. C.; Peng, X. J.; Cui, A. J.; Wu, Y. K.; Tian, M. Z.; Zhang, L. Z.; Chen, X. Q.; Gao, Y. L., Synthesis and spectral properties of new boron dipyrromethene dyes. *Dyes Pigments* **2007,** *73* (2), 206-210.

25. Sun, J. S.; Geiser, A. H.; Frydman, B., A preparative synthesis of lapachol and related naphthoquinones. *Tetrahedron Lett.* **1998,** *39* (45), 8221-8224.

26. You, C. C.; Miranda, O. R.; Gider, B.; Ghosh, P. S.; Kim, I. B.; Erdogan, B.; Krovi, S. A.; Bunz, U. H. F.; Rotello, V. M., Detection and identification of proteins using nanoparticle-fluorescent polymer 'chemical nose' sensors. *Nat. Nanotechnol.* **2007,** *2* (5), 318-323.

27. Gopidas, K. R.; Whitesell, J. K.; Fox, M. A., Nanoparticle-Cored Dendrimers: Synthesis and Characterization. *J. Am. Chem. Soc.* **2003,** *125*, 6491-6502.

28. Phillips, R. L.; Miranda, O. R.; Mortenson, D. E.; Subramani, C.; Rotello, V. M.; Bunz, U. H. F., Gold nanoparticle-PPE constructs as biomolecular material mimics: understanding the electrostatic and hydrophobic interactions. *Soft Matter* **2009,** *5* (3), 607-612

29. Zhu, Z.-J.; Ghosh, P. S.; Miranda, O. R.; Vachet, R. W.; Rotello, V. M., Multiplexed Screening of Cellular Uptake of Gold Nanoparticles Using Laser Desorption/Ionization Mass Spectrometry. *J. Am. Chem. Soc.* **2008,** *130* (43), 14139–14143.

30. Verma, A.; Uzun, O.; Hu, Y.; Hu, Y.; Han, H.-S.; Watson, N.; Chen, S.; Irvine, D. J.; Stellacci, F., Surface-structure-regulated cell-membrane penetration by monolayer-protected nanoparticles. *Nat. Mater.* **2008,** *7*, 588 - 595.

31. Hostetler, M. J.; Wingate, J. E.; Zhong, C. J.; Harris, J. E.; Vachet, R. W.; Clark, M. R.; Londono, J. D.; Green, S. J.; Stokes, J. J.; Wignall, G. D.; Glish, G. L.; Porter, M. D.; Evans, N. D.; Murray, R. W., Alkanethiolate gold cluster molecules with core diameters from 1.5 to 5.2 nm: Core and monolayer properties as a function of core size. *Langmuir* **1998,** *14* (1), 17-30.

CHAPTER 3

TUNING PAYLOAD DELIVERY IN TUMOR CYLINDROIDS USING GOLD NANOPARTICLES

3.1 Introduction

Inefficient delivery limits the efficacy of many chemotherapeutic treatments.[1, 2, 3, 4, 5] Overcoming delivery limitations requires precise control of interstitial diffusion and cellular uptake. Tumors typically have irregularly formed vasculature, with large intervessel distances and heterogeneous populations of cells.[6] These populations are often unresponsive to standard therapy because of their distance from blood vessels and resistance to molecular uptake.[7] This limited efficacy prevents complete cell clearance per drug cycle, which can eventually lead to tumor regrowth, metastatic disease and poor treatment outcomes.[8, 9]

Colloidal gold nanoparticles have great potential to overcome delivery limitations because of their biocompatibility, low toxicity, small size and tunable surface functionalities.[10, 11] Functionality can be tuned by modifying the composition of functional molecules in the mixed monolayer on the surface of gold nanoparticles.[12, 13, 14] In cancer cell cultures, surface properties have been shown to regulate cellular uptake, intracellular release and distribution in subcellular compartments.[15, 16, 17, 18] Modification of the surface properties of gold nanoparticles therefore has the potential to control accumulation in tumors, and the locations at which drug payloads are released.

Three-dimensional *in vitro* tumor models provide an important tool for the optimization of efficient intratumoral drug delivery. Multicellular tumor cylindroids provide a unique platform with which to systematically monitor extracellular diffusion, cellular uptake and molecular release from nanoparticles in real time (Figure 3.1a). Tumor cylindroids are spheroids constrained between two parallel surfaces.[19, 20] The geometry of cylindroids allows only radial diffusion from the peripheral edge to the centre, simplifying analysis. Through the optically accessible cross-section, local concentrations of nanoparticles and dyes can be measured with standard fluorescence microscopy. Importantly, cylindroids consist of heterogeneous cell populations arranged relative to their distance from the peripheral edge: cells in the periphery are predominantly proliferating, and cells in the centre are mostly apoptotic and necrotic.[21, 22, 23] This radial organization mimics the distribution of cells around blood vessels in tumors *in vivo* (Figure 3.1b).[24, 25]

We predict that different surface charges can control the penetration of nanoparticles and the location of cellular uptake and release. Thioalkylated fluorescein-labelled gold nanoparticles (2 nm core diameter, 6 nm overall with ligand) with positive and negative surface charges were synthesized (Figure 3.1c) and administered to cylindroids. Fluorophore concentrations were measured as functions of time and radial position. The diffusion of gold nanoparticles in an extracellular matrix (Matrigel) was measured in a linear cell free chamber. A mathematical model was developed to discriminate between fluorescence from particles and released fluorescein, and to calculate the rates of cellular uptake/release (Figure 3.1d) as a function of position in the cylindroids. The determined parameters were used to predict the dynamics of particle

transport and release from blood vessels in a conceptualized tumor (Figure 3.1b). Positive and negative gold nanoparticles conjugated with doxorubicin (DOX) were similarly synthesized, and our results show that surface charge can be used to control tissue penetration and drug release. This work has been reported as an article in *Nature Nanotechnology*.[26]

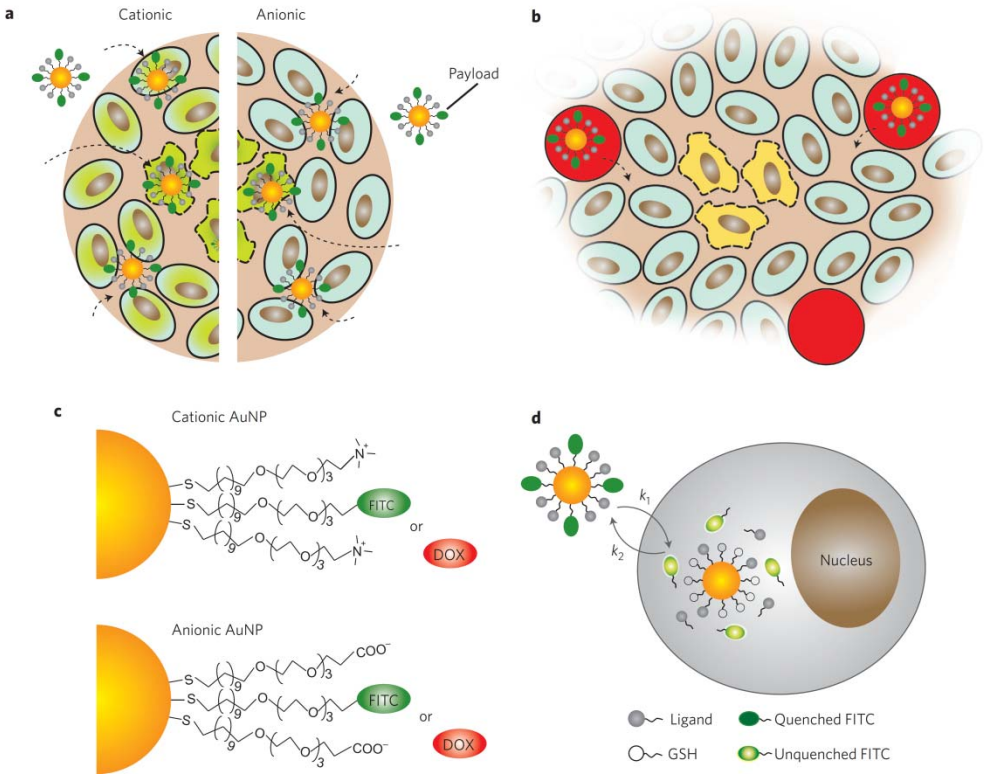

Figure 3.1 Schematic showing the delivery of payload by gold nanoparticles. (a) Delivery of payload (green ovals) into tumor cylindroids by gold nanoparticles. Cells containing released FITC–SH are in green. Viable cells are shown with smooth, solid boundaries, and necrotic cells have irregular, dashed boundaries. Dashed arrows indicate diffusion and cellular uptake. In cylindroids, nanoparticles are present in the medium outside the boundary of the cell mass. (b) Intratumoral delivery by gold nanoparticles following extravasation from the vessel lumen (red circles). (c) Mixed monolayer-protected gold nanoparticles loaded with thioalkylated FITC or doxorubicin (DOX). (d) Cellular uptake and FITC–SH release by thiol-mediated replacement reactions.

3.2 Results and discussion

3.2.1 Uptake of fluorescent gold nanoparticles

Nanoparticles were synthesized with gold cores protected by mixed monolayers[27] to provide tunable probes for delivery. The monolayers on these particles consisted of thioalkylated fluorescein isothiocyanate (FITC–SH) and either thioalkyl tetra(ethylene glycol) lyated trimethyl ammonium or thioalkyl tetra(ethylene glycol)-lyated carboxylic acid to create cationic (p-FITC–AuNP) and anionic (n-FITC–AuNP) gold nanoparticles (Figure 3.1c), respectively.[28] The surface zeta potentials of p-FITC–AuNP and n-FITC–AuNP were measured to be + 30 and - 36 mV, respectively. The fluorescence intensities of p-FITC–AuNP, n-FITC–AuNP and free fluorophore (FITC–SH) were used to calibrate the fluorescence intensity and determine the FITC-SH loading ratio on each gold core. Fluorescence intensities were linearly proportional to concentration (Figure 3.2a). Conjugation to gold cores quenches FITC–SH fluorescence. Treatment with potassium cyanide to recover quenched fluorescence increased the intensities of the p-FITC–AuNP and n-FITC–AuNP solutions by factors of 4 and 2.4, respectively (Figure 3.2a). The ratio of released ligand to free ligand fluorescence indicates that the loading ratios were 7.5 and 8.3 for p-FITC–AuNP and n-FITC–AuNP, respectively. The linear relationship between intensity and concentration indicates that self-quenching did not have a large effect over this concentration range.

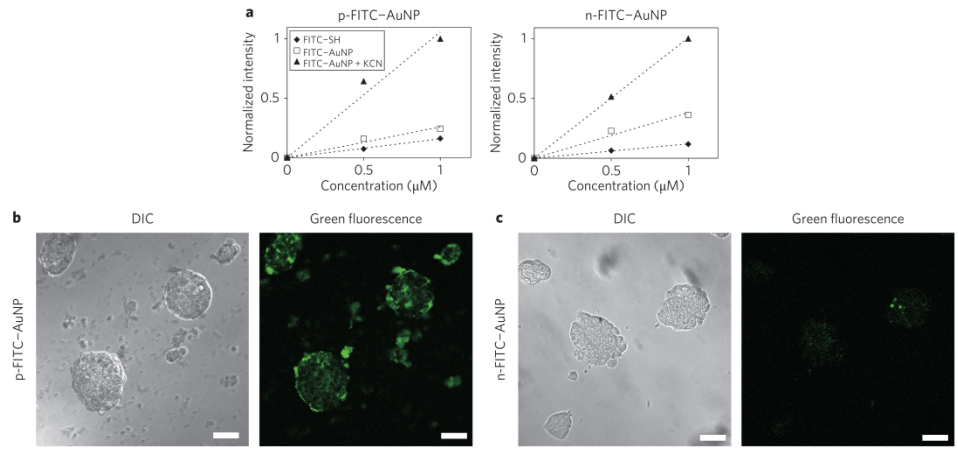

Figure 3.2 Fluorescence calibration and cellular uptake and release of FITC–AuNPs. (a) Normalized fluorescence intensities plotted against nanoparticle concentration. Dotted lines represent linear least-squares fitting results. For all components, fluorescence intensity was linearly proportional to concentration. (b) and (c) Differential interference contrast (DIC) and confocal green fluorescent images of cells in monolayer culture incubated with cationic (b) and anionic (c) gold nanoparticles. Scale bars, 50 mm.

In monolayer cell culture, all FITC–SH release from nanoparticle core was intracellular (Figure 3.2b and c). Intracellular release of FITC–SH is mediated by cytoplasmic thiol compounds, of which reduced glutathione (GSH) is the most abundant.[29] Similar selectivity would be observed *in vivo*, because the intracellular concentration of glutathione (1–10 mM) is considerably higher than that in plasma (2 μM).[30, 31] After removal of media containing FITC–AuNP, stronger green fluorescence was observed across the cells treated with p-FITC–AuNP (Figure 3.2b) compared with n-FITC–AuNP (Figure 3.2c). This observation indicates that cellular uptake and dissociation were greater for cationic gold nanoparticles, potentially mediated by interactions of the particles with serum proteins. Cellular uptake and release in cylindroids was dependent on particle surface charge and radial position (Figure 3.3). Intra- and extracellular

fluorescence was measured in cylindroids in real time using fluorescence microscopy (Figure 3.3a,c, and e). A clear morphological boundary could be observed between the inner and outer regions of the cylindroids (Figure 3.3a, c, and e), which have been shown to contain viable and apoptotic microenvironments, respectively. In the outer region, cationic particles produced more fluorescence than free FITC and anionic particles (Figure 3.3a–f). For positive particles, the fluorescence intensity in the outer region increased with time, and eventually the entire cylindroid became fluorescent (Figure 3.3a and b). For negative particles, the fluorescence intensity in the outer region did not increase (Figure 3.3c) and remained unchanged after 11 h (Figure 3.3d). This preferential uptake of cationic gold nanoparticles by proliferating cells was similar to the difference observed in the monolayer cultures (Figure 3.2b,c). In the inner region, fluorescence appeared at earlier time points than in the outer region and appeared regardless of surface charge (Figure 3.3a–d). Images acquired at 4 and 8 h were spatially similar but fainter than those at 11 h. In cylindroids incubated with free FITC, strong fluorescence appeared only in the inner region (Figure 3.3e), and the intensity profiles remained unchanged for 11 h after treatment (Figure 3.3f). The enhanced cellular uptake of positive particles by proliferating cells may be caused by electrostatic interaction with the net negative surface charge of the plasma membrane,[32, 33] which has also been observed in liposomal and polymeric delivery systems.[34, 35, 36] Particle charge had a pronounced effect on the dynamics of particle uptake and fluorophore release (Figure 3.3g and h). These dynamics were observed by averaging the behavior in the inner and outer regions, which were defined as annuli 175–200 mm from the centre and 25–50 mm from the periphery of three cylindroids (grey bars in Figure 3b and d).

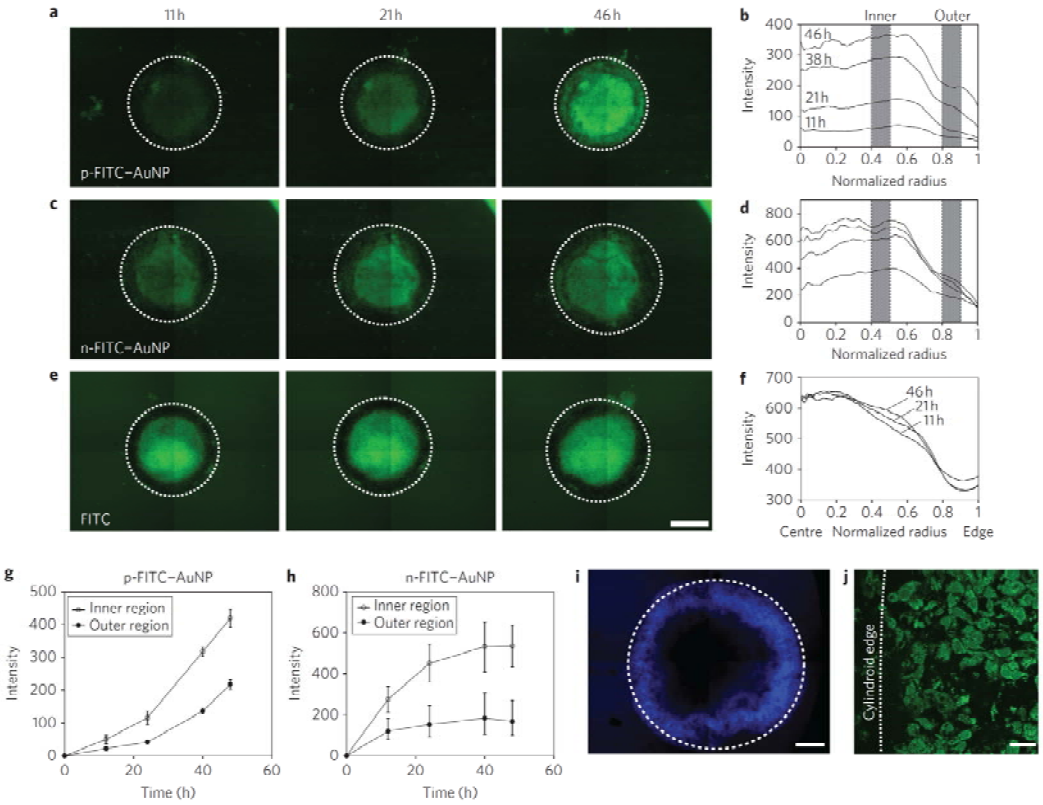

Figure 3.3 Release of FITC–SH from AuNPs in tumour cylindroids. (a)–(f), Green fluorescence images ((a), (c), and (e)) and corresponding intensity profiles ((b), (d), and (f)) of cylindroids treated with nanoparticles. Fluorescence images were acquired after incubation with p-FITC–AuNP (a), n-FITC–AuNP (c) and FITC (e) for 11, 21 and 46 h. Dotted circles indicate cylindroid edges. Scale bar, 300 mm. Fluorescence intensity profiles are shown at 11, 21, 38 and 46 h ((b) and (d)). (g) and (h), Change of average fluorescence intensities over time in the inner and outer regions of the cylindroids (indicated by grey bars in (b) and (d)) after incubation with p-FITC–AuNP (g) and n-FITC–AuNP (h). Errors are standard error of the mean (n=3). (i) Blue fluorescence image of a cylindroid incubated with OPA for 18 h. Scale bar, 200 mm. (j) Green confocal fluorescence microscope image of the outer region of the cylindroid treated with p-FITC–AuNP. Scale bar, 20 μm.

In cylindroids treated with positive particles, fluorescence intensities increased monotonically (Figure 3.3g). The behavior was considerably different for cylindroids

treated with negative particles, in which the fluorescence intensity saturated with time and eventually reached a plateau (Figure 3.3h). Comparing inner and outer regions, the time-dependent behavior of cellular uptake/release was functionally similar for both particle types (Figure 3.3g and h). Two possible causes for the early appearance of fluorescence at the centre of the cylindroids following nanoparticle administration (Figure 3.3a–d) can be suggested: first, an increased rate of uptake by apoptotic/necrotic cells or, second, an increased rate of fluorophore dissociation due to higher thiol concentrations. The dye o-phthaldialdehyde (OPA) reacts non-enzymatically with amino acids and their derivatives in the presence of thiol compounds; this has been widely used to measure intracellular glutathione concentration.[37, 38] Staining with OPA showed that the concentration of thiol compounds was higher in the outer region and decreased toward the centre of the cylindroids (Figure 3.3i). This location of cellular thiol compounds was opposite to the pattern of fluorescence from nanoparticles (Figure 3.3a–d). We have previously shown that centers of cylindroids are composed of apoptotic and necrotic cells and these cells preferentially take up particles when compared to viable cells because they have lost membrane integrity. Together, these observations demonstrate that cellular uptake is the dominant mechanism. If dissociation, and not uptake, were the limiting mechanism, then fluorescence from released fluorophore would have been greater in the periphery than in the centre. Ligand dissociation was expected to be entirely intracellular because of the higher levels of glutathione relative to the extracellular environment. Confocal microscopy was used to verify that extracellular dissociation did not occur (Figure 3.3j). Following incubation with nanoparticles for 36 h, FITC–SH release was observed primarily inside cells (Figure 3.3j). Intracellular

localization of dissociation was consistent across the diameter of the cylindroids; fluorescence was observed only inside cells in both the inner and outer regions. Furthermore, the observed fluorescence patterns were conserved in the z-direction (away from the objective), supporting the use of epifluorescent microscopy for quantitative penetration measurements.

3.2.2 Uptake of doxorubicin nanoparticles

To further probe the potential therapeutic applications of engineered nanoparticles, we fabricated particles featuring a doxorubicin prodrug tethered through an acid-labile hydrazone linkage to a thiol ligand (Figure 3.1c). Similar to FITC–AuNP, a positive surface charge dramatically enhanced uptake of DOX–AuNP into proliferating peripheral cells when compared to negative particles and free drug (Figure 3.4). In cylindroids, positive particles delivered more doxorubicin than negative particles (Figure 3.4a and b). With regard to position, positive particles delivered significantly more doxorubicin to viable cells in the cylindroids periphery when compared to negative particles and free drug, which were preferentially taken up by dead cells at the cylindroids centre ($P < 0.05$; Figure 3.4d). This charge-dependent localization was consistent over the 46 h of the experiment ($P < 0.05$; Figure 3.4e), during which the concentration of particles and free drug increased within the cylindroids (Figure 3.4a–c, radial profiles). The similarity of these results with the FITC results (Figure 3.3) supports the prediction that nanoparticles with positive surface charges will outperform negative particles for most applications, and confirms that charged gold nanoparticles have the

potential to overcome drug penetration barriers and deliver clinically relevant anticancer drugs.

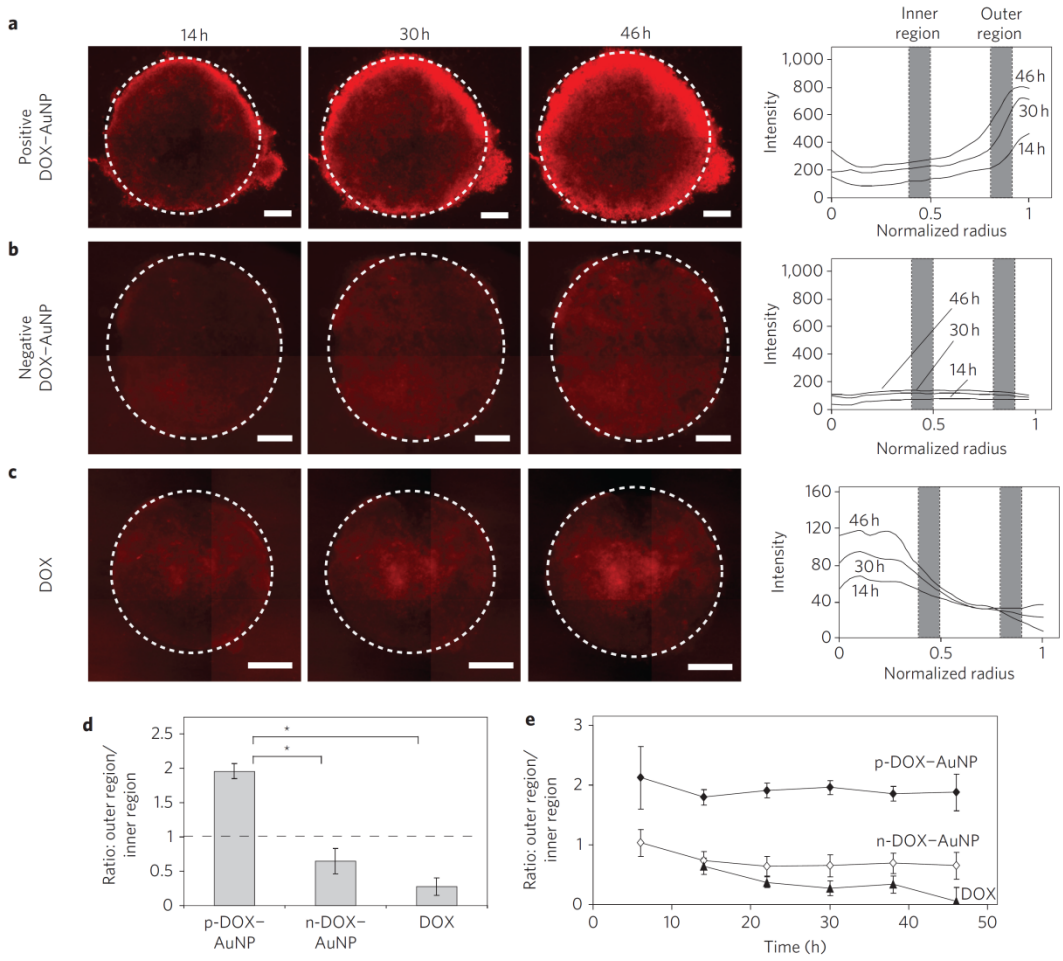

Figure 3.4 Doxorubicin release in cylindroids. (a)–(c), Red fluorescence images and the corresponding radial intensity profiles of cylindroids treated with positive DOX–AuNP (a), negative DOX–AuNP (b), and free DOX (c). Dotted circles indicate cylindroid edges. Scale bars, 200 mm. (d) and (e), Ratio of average fluorescence intensities in the outer region to those in the inner region of the cylindroids, 30 h after treatment (d) and as a function of time (e). Errors are standard error of the mean, and significance was determined using Student's t-test (*$P < 0.05$; $n = 3$).

3.2.3 Diffusion of nanoparticles in matrix material

In addition to regulating cellular uptake, surface charge also significantly affects the diffusivity of gold nanoparticles in the extracellular matrix. Diffusivity in the extracellular matrix was modeled using a cell-free diffusion chamber, which confined Matrigel between a trench cut in a polycarbonate block and the bottom surface of a well plate (Figure 3.5a). In this model, diffusion occurred in only one direction: from the exposed surface to the center of the trench. Concentrations of FITC and FITC–AuNP were measured as a function of time and location by acquiring a series of fluorescence images along the longitudinal direction every 2 h. Intensity gradients decreased from the edge towards the centre of the Matrigel trench, and the slope of the gradients diminished with time (Figure 3.5b and c). Diffusion coefficients were determined by nonlinear least-squares fitting of the intensity gradients to a Fickian diffusion model (Figure 3.5c). The diffusion coefficient for FITC was $(42 \pm 2) \times 10^{-7}$ cm^2 s^{-1}, which was larger than both gold nanoparticles by an order of magnitude (Figure 3.5d). Simulations with this diffusion coefficient matched the concentration profiles seen in the cylindroids (Figure 3.3), suggesting that diffusion alone controlled the delivery of free FITC. Anionic gold nanoparticles had a larger diffusion coefficient, $(9.0 \pm 0.1) \times 10^{-7}$ cm^2 s^{-1}, than cationic nanoparticles, $(7.6 \pm 0.1) \times 10^{-7}$ cm^2 s^{-1} ($P < 0.005$; $n = 3$; Figure 3.5d). The lower diffusion coefficient of positive particles suggests that electrostatic interactions with negatively charged macromolecules in the matrix slowed particle diffusion. The major components of the extracellular matrix in tumors and spheroids are collagen and proteoglycans.[39, 40, 41] Matrigel is derived from tumor matrix materials,[42] which are negatively charged under physiological conditions. Because cationic and anionic particles

have similar molecular weights and hydrodynamic radii, it is likely that electrostatic interactions with the matrix are the primary cause of the difference between the diffusion coefficients. Three mechanisms control the timing and location of drug delivery into tumors using nanoparticles: diffusion, cellular uptake and ligand dissociation. Our results indicate that, of the three, cellular uptake is the dominant mechanism. In all cylindroids, fluorescence appeared early in their centers (Figure 3.3). If diffusion were the limiting mechanism, fluorescence would first appear at the outside edge and progress into the center. The measured diffusion coefficients in the matrix material (Figure 3.5d) confirm that diffusion can account for the rapid appearance of particles in the cylindroid centers.

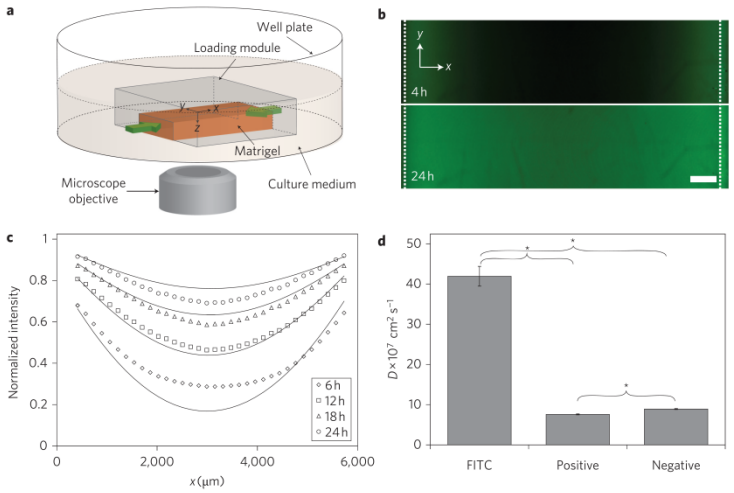

Figure 3.5 Effect of surface charge on diffusivity through extracellular matrix material. (a) Schematic representation of loading module filled with Matrigel. (b) Green fluorescence images acquired from the bottom of the loading module 4 and 24 h after adding particles. Dotted lines at both ends indicate the Matrigel edges. Scale bar, 500 mm. (c) Fluorescence intensity profiles in Matrigel along the x-axis as a function of time (symbols) and intensity profiles generated by fitting to a Fickian diffusion model (solid lines). (d) Comparison of diffusion coefficients of FITC, cationic and anionic gold nanoparticles in Matrigel (*P < 0.005; n = 3).

3.2.4 Modeling diffusion and cellular uptake/release

A descriptive mathematical model was developed to interpret the coupled effects of extracellular diffusion (Figure 3.1b) and cellular uptake/release (Figure 3.1d) on molecular nanoparticle delivery. The model framework was designed to show how dynamic nanoparticle measurements in cylindroids provide preliminary information about nanoparticle behavior under physiological conditions. The model consisted of two transient partial differential equations, one for gold nanoparticles, and the other for free intracellular fluorophore. Concentration profiles for particles and released ligand were predicted using *in vitro* calibrations of ligand release (Figure 3.2a). Based on confocal microscopy results (Figure 3.3j), all ligand dissociation was modeled as an intracellular reaction. Internalization of FITC–AuNPs and release of FITC–SH were modeled as a single reaction with radially dependent forward (k_1) and reverse (k_2) rate constants (Figure 3.1d). Nanoparticle diffusion coefficients were derived from measured diffusivities in Matrigel (Figure 3.5). The modeling results fit the experimental data well, and predict that positively charged particles will outperform negative particles for most, but not all applications (Figure 3.6). The modeling results (solid lines in Figure 3.6a and b) capture a number of key characteristics of the fluorescent patterns shown in Figure 3.3 and the experimental data points (symbols, Figure 3.6a and b). First, a higher fluorescence was observed in the inner regions than in the outer at early time points. Second, positive particles showed a monotonic increase in fluorescence, and this increase was more pronounced in the outer regions. Third, negative particles displayed saturation of fluorescence. By separating the fluorescence contributions from free and bound fluorophore, the modeling results indicate that particle diffusion was rapid, and the

appearance of free fluorophore by uptake and dissociation controlled overall fluorescence (Figure 3.6c). Calculated kinetic rates suggest that viable cells had a higher net uptake of positive particles because of a lower export rate (k_2) in both inner and outer regions ($P < 0.05$; $n = 3$; Figure 3.6d). For negative particles, the forward rate constant was only larger in the inner region ($P < 0.05$; $n = 3$; Figure 3.6d). Modeling predictions were based on a hypothetical tumor for which the geometry was inverted: particles diffused from a blood vessel ($0 < r < 5$ μm) into tumor tissue ($r > 5$ μm). Because of their greater diffusion coefficient, negative particles penetrated deeper into the interstitium at all times (Figure 3.6e). However, the concentration of released intracellular ligand was greater for positive particles, because of their larger net uptake rate (Figure 3.6f). This predicts that deep penetration of negative particles may be mitigated by the elevated interstitial fluid pressures often observed in tumors *in vivo*.[43, 44, 45] For both particles, the concentration of released ligand reached a maximum between 20 and 30 h (Figure 3.6f). Regions of proliferating (10–70 μm) and quiescent (75–120 μm) cells were defined based on single cell analysis performed in cylindroids. The average concentrations of released ligand for positive particles in the proliferating and quiescent regions were more than 11-fold and 8-fold greater at all times, respectively (Figure 3.6g). Deep in the tissue (> 1 mm) the concentration of released ligand was greater for negative particles at later times (> 20 h; Figure 3.6h). These results suggest that positive particles will release more ligand to most cells at all times (Figure 3.6f and g) and therefore would be advantageous for most applications. Complementarily, negative particles would have an advantage in delivering drugs deep into tissue (Figure 5d and figure 6h) and would be useful for treating tumors with large intervessel spacing and high hypoxic tolerance.

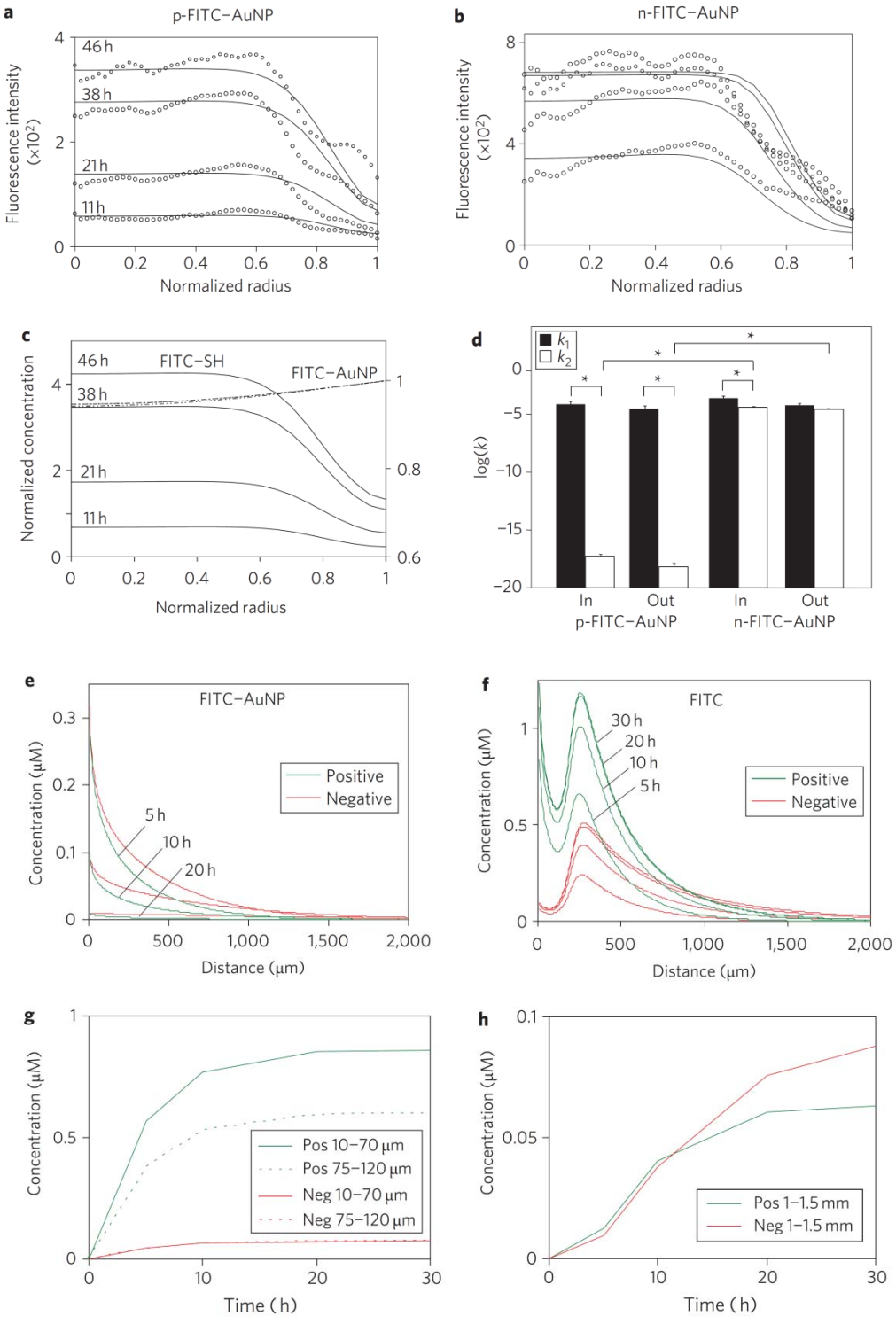
a
p-FITC–AuNP
Fluorescence intensity (×10²)
46 h
38 h
21 h
11 h
Normalized radius
b
n-FITC–AuNP
Fluorescence intensity (×10²)
Normalized radius
c
Normalized concentration
46 h
38 h
21 h
11 h
FITC–SH
FITC–AuNP
Normalized radius
d
k1
k2
log(k)
In
Out
In
Out
p-FITC–AuNP
n-FITC–AuNP
e
FITC–AuNP
Concentration (μM)
Positive
Negative
5 h
10 h
20 h
Distance (μm)
f
FITC
Concentration (μM)
30 h
20 h
10 h
5 h
Positive
Negative
Distance (μm)
g
Concentration (μM)
Pos 10–70 μm
Pos 75–120 μm
Neg 10–70 μm
Neg 75–120 μm
Time (h)
h
Concentration (μM)
Pos 1–1.5 mm
Neg 1–1.5 mm
Time (h)

Figure 3.6 Rate constants of cellular uptake and predictions of particle and ligand distribution in tumors. (a) and (b) Fluorescence intensity profiles measured in fluorescence images of cylindroids (symbols) and those predicted by the mathematical model (solid lines). Concentrations were normalized by the maximum concentration of FITC–AuNP in the cylindroids. (c) Independent concentration profiles of fluorophore bound to nanoparticles (FITC–AuNP) and released fluorophore ligand (FITC–SH) predicted by the computation model. (d) Comparison of forward (k_1) and reverse (k_2) rate constants in different regions. Errors are standard error of the mean, and significance was determined using Student's t-test (*P < 0.05). (e) and (f) Modeled concentrations of FITC–AuNPs and released FITC–SH as a function of distance from blood vessels of a hypothetical tumor. Clearance half-life of FITC–AuNPs was assumed to be 3 h. (g) Average concentrations of FITC–AuNPs in the regions 10–70 μm (proliferating) and 75–120 μm (quiescent) from the blood vessel wall as a function of time. (h) Average concentrations of released FITC in deep tumor regions (1.0–1.5 mm) as a function of time.

3.3 Summary and future outlook

Using a combination of experimental *in vitro* tumor models and mathematical modeling, we have shown that, under most circumstances, positively charged nanoparticles improved delivery of payloads to the majority of cells in tumors, whereas negatively charged particles would perform better when delivering drugs deep into tissues. Positive particles had significantly higher uptake and dissociation by viable cells, whereas negative particles diffused at a faster rate. Both positive and negative particles penetrated tissues rapidly, and for both, the rate of cellular uptake and dissociation was slower than extracellular diffusion. The mathematical models suggested that the rate of cellular uptake of both particles was fast in apoptotic and necrotic tissues. Furthermore, the uptake kinetics of positive particles is irreversible, but is reversible for negative

particles over the timescales investigated. The ability to tune surface charge to control tissue penetration and drug release makes gold nanoparticles a flexible and powerful drug delivery vehicle.

3.4 Synthesis of materials and experimental methods

3.4.1 Synthesis of ligand and fabrication of nanoparticle

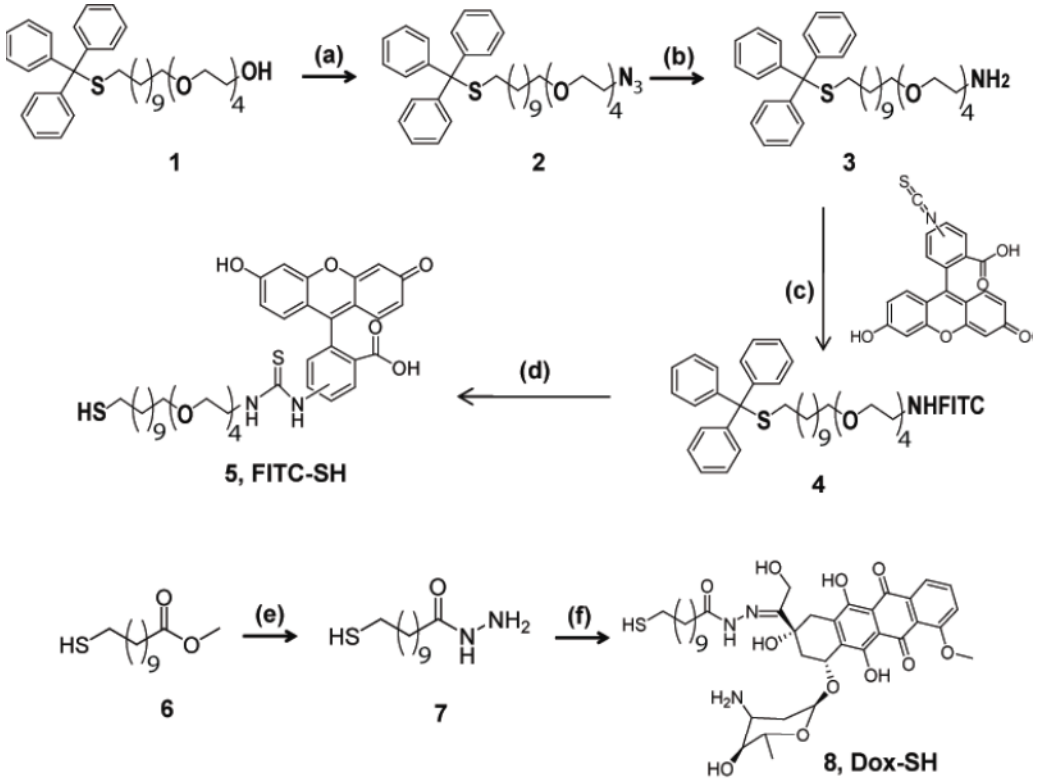

Figure 3.7 Synthetic procedure of the thioalkylate tetra (ethylene glycol) FITC and Dox conjugated ligands (a) 1. methanesulfonyl chloride, TEA, DCM, RT, 4h, 2. sodium azide, DMF, 4h. (b) triphenylphosphine, THF. (c) fluorescein isothiocyanate, acetone. (d) TFA, TIPS, DCM, RT, 4h, (e) hydrazine, MeOH, reflux. (f) Doxorubicin, MeOH

Synthesis of compound 2

Compound 2 Trityl protected thioalkyl tetra (ethylene glycol) alcohol 1 (5 g, 8.02 mmol)[2] was dissolved in dry dichloromethane (80 mL) that was placed in an ice bath. When the temperature reached about 0 °C, triethylamine (1.67 mL, 12.03 mmol) and methanesulfonyl chloride (1.25 mL, 16.04 mmol) were added successively. The mixture was stirred at room temperature for 4 h. The reaction mixture was evaporated to yield the crude product (5.72 g). The crude mesylated compound was then dissolved in dry dimethyl formamide (30 mL). Subsequently, sodium azide powder (1.04 g, 16.04 mmol) was added to the solution. The mixture was stirred at 80 oC for 4 h. After cooling to room temperature, the solution was poured into 100 mL ice-water. The mixture solution was extracted by CH2Cl2 (3 x 25 mL). The organic phases were combined and washed with brine. The crude product was charged on a silica gel chromatographic column with ethyl acetate as eluent for purification. Yields were around 88 %. ^{1}H NMR (400 MHz, $CDCl_3$, TMS): δ 7.41 (m, 6H, HAr), 7.27 (m, 6H, HAr), 7.20 (m, 3H, HAr), 3.68 (m, 12H, $-OCH_2-$), 3.58 (m, 2H,$-CH_2O-$), 3.44 (t, ^{3}J = 6.8 Hz, 2H, $-CH_2O-$), 3.37 (t, ^{3}J = 5.0 Hz, 2H, $-CH_2O-$), 2.13 (t, ^{3}J = 7.4 Hz, 2H, $-SCH_2-$), 1.57 (m, 2H, −CH2−), 1.38 (m, 2H, $-CH_2-$), 1.20 (m, 14H, $-CH_2-$).

Synthesis of compound 3

A mixture of Trityl protected tetra (ethylene glycol) azide 2 (2.0 g, 3.08 mmol) and triphenylphosphine (0.97 g, 3.69 mmol) were dissolved in tetrahydrofuran (20 mL). After that, water (0.5 mL) was added to the solution mixture. The mixture was stirred at room temperature for 12h. The mixture was poured into water. The aqueous suspension was

extracted by dichloromethane (3 x 25 mL) and washed thoroughly with brine and dried over anhydrous magnesium sulfate. After filtration, the combined organic phase was evaporated to provide a white solid. The crude mixture was charged on silica gel column with methanol:dichloromethane:ammonium hydroxide (50:45:5) as eluent for purification to yield compound 3 (1.39 g, 73%) ^{1}H NMR (400 MHz, $CDCl_3$, TMS): δ 7.40 (m, 6H, HAr), 7.27 (m, 6H, HAr), 7.17 (m, 3H, HAr), 3.66 (m, 10H, $-OCH_2-$), 3.58 (m, 2H,$-CH_2O-$), 3.50 (t, ^{3}J = 5.16 Hz, 2H, $-CH_2O-$), 3.44 (t, ^{3}J = 6.68 Hz, 2H, $-CH_2O-$), 2.12 (t, ^{3}J = 7.3 Hz, 2H, $-SCH_2-$), 1.56 (m, 2H, $-CH_2-$), 1.38 (m, 2H, $-CH_2-$), 1.22 (m, 14H, $-CH_2-$). MS (ESI): m/z 622.5 [M^++H] (calcd for 622.4).

Synthesis of compound 4 and 5

To a stirred solution of trityl protected tetra (ethylene glycol) amine 3 (1.0 g, 1.60 mmol) in dry acetone (ca. 10 mL) was subsequently added Fluorescein isothiocyanate (FITC) (0.543 g, 1.33 mmol). After stirred for 6 h at room temperature, the reaction mixture was evaporated to remove acetone. The crude product 4 was then dissolved in dry dichloromethane (ca.10 mL) and stoichiometric trifluoroacetic acid (2.5 mL) was added under stirring. Subsequently, triisopropylsilane (0.65 mL, 3.20 mmol) was added. The reaction was allowed to proceed at room temperature for 12 h. The solvent and excess trifluoroacetic acid and triisopropylsilane were removed under reduced pressure. The product 5 was confirmed by mass spectrometry without purification. MS (ESI): m/z 769.4 [M^++H] (calculated for 769.3).

Synthesis of compound 7

A mixture of hydrazine (1.37 g, 43 mmol) and compound 6 (1.0 g, 4.30 mmol) were dissolved in methanol (5 mL). After stirring for 3h at 70 °C, the solvent was removed under reduced pressure. The crude product was then poured into a mixture of dichloromethane and distilled water. Organic layer was separated and concentrated at reduced pressure to afford compound 7 as a white powder. (0.78 g, 78 %) ^{1}H NMR (400 MHz, $CDCl_3$, TMS): δ 6.98 (s, ^{1}H, -NH-), 3.90 (s, 2H, -NH_2), 2.50 (q, J = 7.2 Hz, 2H, HS-CH_2-), 2.50 (q, J = 7.3 Hz, 2H, -CH_2-CO-), 1.55 (m, 2H, −CH_2−), 1.25 (m, 14H, −CH_2−). ^{13}C NMR (100.64 MHz, $CDCl_3$, TMS) δ 174.05, 34.57, 34.01, 29.42, 29.36, 29.25, 29.02, 28.33, 25.49, 24.65.

Synthesis of compound 7, Dox-SH

A methanol solution of compound 7 (0.03 g, 0.13 mmol) and doxorubicin (0.05 g, 0.08 mmol) was stirred overnight at 60 °C under argon. The reaction mixture was concentrated and precipitated into hexane/ethyl acetate (1:2, v/v). The product was further purified by washing with hexane and ethyl acetate to give compound 8 as a red solid. (0.04 g, 61 %) The product was confirmed by mass spectrometry. MS (ESI): m/z 758.5 [M^{+}+H] (calcd for 757.89).

Synthesis of mixed monolayer-protected gold nanoparticles

Pentanethiol coated gold nanoparticles (2 nm in diameter) were synthesized according to the method reported by You *et. al*.[46] The synthetic procedure of the thioalkylate tetra (ethylene glycol) fluorescein isothiocyanate (FITC) and doxorubicin (Dox) conjugated ligands is represented in Scheme S1 and the details of each reaction step are as follows:

FITC-AuNP fabrication

The cationic and the anionic nanoparticles with FTIC conjugations were afforded by adding 20 mg of 1-pentanethiol coated gold nanoparticles in dichloromethane into the dichloromethane-methanol mixtures of 5mg thioalkylate tetra (ethylene glycol) FITC conjugated ligands (FITC-SH) and 50 mg thiolalkyl tetra (ethylene glycol)lyated trimethyl ammonium ligand (TTMA) or 50 mg thiolalkyl tetra (ethylene glycol)lyated carboxylic acid ligand (TCOOH), respectively. The mixture were then stirred at room temperature for 2~3 days. After all the solvents are evaporated, the ligand-exchanged nanoparticles were washed thoroughly with hexanes, diethyl ether and dichloromethane to remove all the free ligands and were collected by centrifugation. The nanoparticles were dried under high vacuum. The absence of free ligands were confirmed by ^{1}H-NMR.

Fluorescence calibration and loading ratios

Fluorescence intensities of p-FITC-AuNP, n-FITC-AuNP and FITC-SH were measured at 0.5 and 1.0 M in DMEM by fluorimetry (SPECTRAmax GEMINI XS, Molecular

Devices) to calibrate fluorescence intensity and determine the FITC-SH loading ratio. The loading ratio is the number of conjugated FITC ligands per gold core. Conjugation to the gold cores quenches FITC-SH fluorescence, and treatment with potassium cyanide rapidly reacts with the gold cores and triggers FITC-SH release. Potassium cyanide, at a final concentration of 20mM, was added to solutions of p-FITC-AuNP and n-FITC-AuNP in DMEM. The solutions were incubated at 37 ºC for 4 hrs and fluorescence was measured by exciting at 480nm and detecting at 520nm. The ratios of fluorescence intensity to concentration were determined by linear regression and were subsequently used to convert from intensity to concentration. Quenching effects were determined by comparing the fluorescence intensity of the p-FITC-AuNP and n-FITC-AuNP solutions with and without KCN. The loading ratio was determined by dividing the 6fluorescence intensities of FITC ligands released from gold cores by free FITC-SH at the same concentrations.

Dox-AuNP fabrication and characterization

To fabricate Dox-AuNP via ligand place exchange reaction, 10 mg of 1-pentanethiol coated gold nanoparticles was mixed with 3 mg of Dox-SH and 27 mg of TTMA or TCOOH ligands in a mixture of dichloromethane (5 mL) and methanol (5 ml). The solution was stirred at room temperature for 24 hours. Solvent was removed by rotary evaporator and nanoparticles were washed with hexane and diethyl ether (20 mL x 5). Nanoparticles were further purified by dialysis in phosphate buffer (pH: 7.8) using SnakeSkin pleated dialysis tubing (10,000 MWCO) for 2 days to remove all free ligands.

The number of Dox-SH per particles was calculated as followings. Dox-AuNP (0.4 M) was incubated at 37 °C for 24 h in buffer (pH: 2.0) solution. Dox on particle was released as the hydrazone linkage was completely hydrolyzed at low pH. Dox is quenched by gold nanoparticles and photoluminescence was only observed upon Dox release. Release of Dox 7was monitored using fluorimetry (Figure 3.8a). The solution was centrifuged using Amicon Ultra-4 tube (10,000 MWCO) to separate released Dox. Concentration of the filtrate was calculated based on the Beer-Lambert law (λ_{max} = 490 nm) using spectrophotometry (Figure 3.8b). By comparing the absorbance of the filtrate with the absorbance before incubation, the number of Dox-SH attached on a particle was estimated to be 6 Dox-SH ligands per particle. The number of Dox-SH per n-Dox-AuNP was calculated via potassium cyanide decomposition. A 1 ml solution of 4 μM n-Dox-AuNP in THF was added to 1 mL of a 0.1 M aqueous KCN solution, followed by brief agitation. After 2 hr, the plasmon absorption band of n-Dox-AuNP at 520 nm was completely decayed, while absorbance of Dox-SH remained. The concentration of Dox-SH was calculated based on the Beer-Lambert law (λ = 560 nm). A molar extinction coefficient of Dox-SH in THF/H_2O (1:1) was obtained for this estimation (ε = 9.69 x 10^3 at 560 nm). By comparing with the concentration of n-Dox-AuNP before etching, the number of attached Dox-SH was estimated to be 5 ligands per particle.

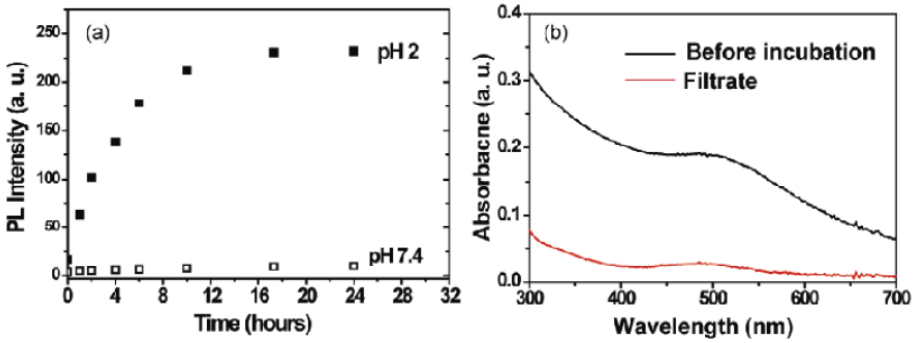

Figure 3.8 (a) The Dox-AuNP released Dox at pH 2 for 24 h incubation but remained stable at pH 7.4. (b) Uv-spectrum of Dox-AuNP before incubation and a filtrate after incubation.

3.4.2 Experimental methods

FITC–AuNP and DOX–AuNP uptake and ligand release in monolayer culture

LS174T human colon carcinoma cells were grown in DMEM (1 g l^{-1} glucose) supplemented with 10% fetal bovine serum at 37 °C with 5% CO_2 in a humidified incubator. Cells in monolayer cultures were incubated with 1 mM FITC–AuNPs for 6 h, and were washed with PBS three times before image acquisition. Confocal fluorescence microscope images were acquired with a Zeiss LSM510 microscope equipped with a ×25 objective lens. A 488-nm argon laser was used for excitation, and emission was acquired at 505 nm (long pass).

FITC–AuNPs and DOX–AuNPs in cylindroids

Cylindroids were prepared from spheroids as described previously and in the Supplementary Information. After equilibration, cylindroids were treated with 125 mM

FITC, 1 mM FITC–AuNP, 1 mM DOX, or 1 mM DOX–AuNP. Transmitted and fluorescence images were acquired with an Olympus IX71 microscope with a ×10 objective at 0, 11, 21, 38, 46 h after treatment. Radial fluorescence intensity profiles in the cylindroids were generated using a customized script in ImageJ (NIH Research Services Branch). Average fluorescence intensities were determined for two annular regions: 175–200 mm from the centre (inner) and 25–50 mm from the periphery (outer). For confocal fluorescence microscopy, cylindroids were prepared in 35-mm glass-bottomed culture dishes. Images were acquired with a Zeiss LSM510 microscope equipped with a × 63 oil-immersion objective. A 488-nm argon laser was used for excitation, and emission was acquired at 505 nm.

Thiol compounds in cylindroids

The distribution of GSH was determined by measuring the fluorescence intensity of OPA derivatives. OPA reacts with amino acids in the presence of thiol compounds to form fluorescent derivatives. Cylindroids were incubated with 250 ml of 100 mM OPA in PBS. Transmitted and fluorescence images were acquired 4, 18 and 36 h after treatment. Samples were excited at 350 nm and measured at 460 nm.

Extracellular diffusion of FITC–AuNP

Diffusion of gold nanoparticles was measured in Matrigel in a loading module (Figure 3.5a) as described in the Supplementary Information. The loading module was prepared by making a channel ($3.1 \times 0.5 \times 6.2$ mm^3; W × H × L) in the top of a polycarbonate block ($9.6 \times 4.8 \times 6.2$ mm^3). Before loading, the well plate was plasma-treated for 5 min

and sterilized with UV for 4 h. The module was loaded with 12 ml Matrigel, which was allowed to gelate at 37 °C for 5 min. Pre-warmed DMEM (2.0 ml) was added to each well and, after 2 h, was replaced with DMEM containing 1 mMFITC–AuNP. Transmitted and green fluorescence images were acquired every 2 h for 36 h. Spatial concentration profiles were obtained by averaging pixel values across the width of the channel. Diffusion coefficients of FITC, p-FITC–AuNP and n-FITC–AuNP were determined by fitting measured fluorescence intensities to a mathematical diffusion model. Numerical solutions were calculated using finite elements, and best-fit diffusion coefficients were determined by nonlinear least-squares optimization in Matlab (MathWorks).

Mathematical modelling of particle diffusion and cellular uptake in cylindroids

Internalization of gold nanoparticles from the extracellular space and glutathionemediated replacement were represented with a one-step reversible reaction:

$$\mathrm{FITC-AuNP} \underset{k_2}{\overset{k_1}{\rightleftharpoons}} \mathrm{FITC-SH} + \mathrm{AuNP}$$

where k_1 and k_2 are forward and reverse reaction constants. Coupled conservation equations for FITC–AuNPs and released FITC–SH incorporated expressions for extracellular nanoparticle diffusion and the kinetics of particle uptake and ligand release:

$$\frac{\partial C_{\mathrm{particle}}}{\partial t} = \frac{D_{\mathrm{eff}}}{r} \cdot \frac{\partial}{\partial r}\left(r \frac{\partial C_{\mathrm{particle}}}{\partial r}\right) - f_{\mathrm{v}}\left(k_1 C_{\mathrm{particle}} - k_2 C_{\mathrm{ligand}}\right) \quad (1)$$

$$\frac{\partial C_{\mathrm{ligand}}}{\partial t} = k_1 C_{\mathrm{particle}} - k_2 C_{\mathrm{ligand}} \quad (2)$$

From confocal measurements, the cell volume fraction fv was found to be 0.48. The effective nanoparticle diffusion coefficients D_{eff} were derived from the Matrigel experiments. Reaction rates were assumed to be functions of position as described in the Supplementary Information. Thismodel was solved using finite elements and fit to measured fluorescence concentrations by nonlinear least-squares optimization in Matlab. Calculated fluorescence values were determined from the sum of the volumefraction-weighted particle (FITC–AuNP) and released ligand (FITC–SH) concentrations. Calculated rate constants were reported as average values inside the inflection point, r,Rt (inner) and between the inflection point and the edge, $R_t < r < 1$ (outer). Significance was determined using unpaired Student's t-tests with unequal variance. Particle diffusion and ligand release was modelled in a hypothetical tumor as described in the Supplementary Information. In thismodel, the blood was assumed to be well mixed, and particles were cleared with a 3-h half-life

Nanoparticle uptake into viable and dead cells in monolayer cultures

To measure the effects of cell viability on uptake, cells were treated with HEPES buffered medium (viable cells) or saline (dead cells), both containing 500 nM positive Dox-AuNP or 500 nM negative Dox-AuNP. Viability was confirmed using 800 nM Ethidium Homodimer (Eth-D1; Invitrogen, Carlsbad, CA). Samples were excited using a 546/10 nm filter and measured through a 590 nm long pass emission filter (Chroma, Rockingham, VT). The increase in fluorescence intensities from 1 hour to 17 hours post treatment was evaluated at nine 8locations for each treatment. Values were normalized by the average increase in intensity of viable cells. Particle uptake was dependent on cell

viability (Figure 3.9). Following growth in medium or saline, cells were either viable or dead as confirmed by staining with ethidium homodimer, Eth-D1 (Figure 3.9). Both positive and negative particles were taken up viable cells, but uptake was significantly greater in necrotic cells. Non-viable cells have greater uptake because they have lost membrane integrity.

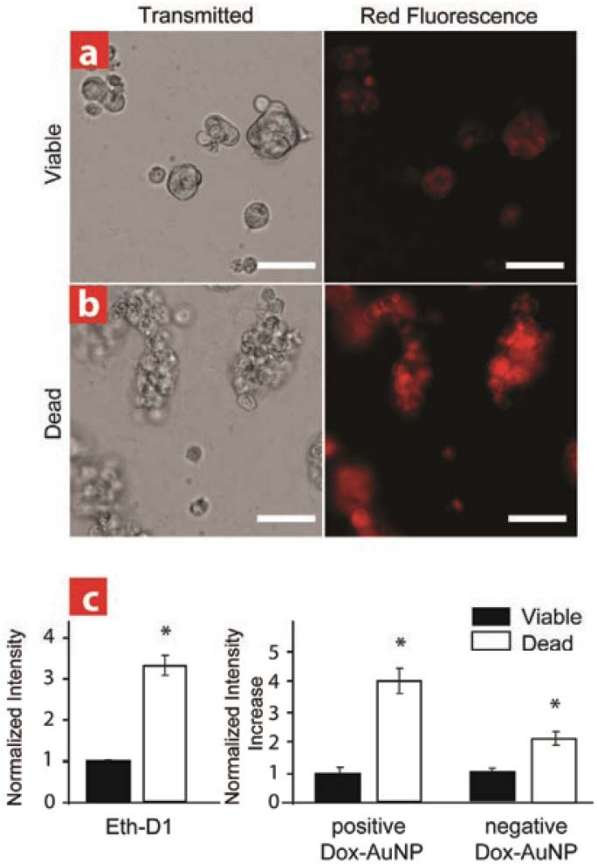

Figure 3.9 Nanoparticle uptake into viable and dead cells a, b, Transmitted and red fluorescent images of viable (a) and dead (b) cells in monolayer culture treated with positive Dox-AuNP. c, Normalized fluorescence intensities of viable and dead cells following uptake of viability stain Eth-D1, positive Dox-AuNP and negative Dox-AuNP. Error bars are standard error of the mean (*$P < 0.05$, n=9). Scale bars are 50µm.

Cylindroid preparation

Cylindroids were formed from spheroids as described previously.[5] To grow spheroids, a single-cell suspension was inoculated into cell culture flasks coated with poly(2-hydroxyethyl methacrylate). After 6-8 days, cylindroids were prepared by placing spheroids in the 150 ± 15μm gap between the bottom of 48 well plates and 3mm diameter cylindrical plugs projecting from the cover. Fresh media (200 μl) was added to each well and cylindroids were allowed to equilibrate overnight.

Image acquisition

Cylindroid images were acquired with an Olympus IX71 microscope with a 10X fluorescence objective. FITC and Dox samples were excited at 470 and 546 nm and measured at 525 and 590 nm, respectively. Careful attention was made during image acquisition to ensure that quantitative comparison was possible, including 1) maintaining a constant exposure time for all image acquisitions and 2) acquiring a background image for all cylindroids before the addition of treatment or fluorophore. Background fluorescence was subtracted before analysis. To cover the large size of cylindroids, 4 (2 × 2) or 9 (3 × 3) individual images were acquired and tiled using a script in IPLab (BD Bioscience).

Radial fluorescence intensity profiles

Radial fluorescence intensity profiles in cylindroids were generated using a customized script in ImageJ (NIH Research Services Branch). Cylindroid radii were determined from transmitted light images. Average radial intensities were obtained by summing the

intensities of all pixels at a given radius and dividing by the number of pixels. Distances were normalized by the cylindroid radius and fluorescence intensities were normalized by the maximum fluorescence intensity. Background autofluorescence was corrected by subtracting the intensity profile of the fluorescence image at 0 hrs. Average temporal behavior was determined for the four time points by averaging all pixels in two annular regions: an inner region (175 - 200 μm from the center) and an outer region (25 - 50 μm from the periphery).

Extracellular diffusion of FITC-AuNP

Diffusion of gold nanoparticles was measured in Matrigel in a loading module attached to the center of a well plate (Figure 3.5a). The loading module was prepared by making a channel (3.1 x 0.5 x 6.2 mm; W x H x L) in the top of a polycarbonate block (9.6 x 4.8 x 6.2 mm). Before loading, the well plate was cleaned by plasma treatment for 5 min and sterilized with UV for 4hrs. Matrigel was kept at 4 ºC to prevent gelation. After loading, 12 μl added Matrigel was allowed to gelate at 37 °C for 5min. Pre-warmed DMEM (2.0ml) was added to each well. After 2hrs, the medium was replaced with fresh DMEM containing 1μM FITC-AuNPs. Transmitted and green fluorescence images (excitation: 470/40nm, emission 525/50nm) were acquired every 2 hrs for 36 hrs using a 4X UPlanApo objective. To cover the large area of the module, four images were acquired and tiled using IPLab. Background autofluorescence was corrected by subtracting the fluorescence image taken at 0hrs from all fluorescence images.

Mathematical modeling of diffusion in Matrigel

Diffusion coefficients of FITC, p-FITC-AuNP and n-FITC-AuNP in Matrigel were determined by fitting measured fluorescence intensities as a function of time and location in the loading module (Figure 3.5a) to a mathematical model of diffusion

$$\frac{\partial C}{\partial t} = D\frac{\partial^2 C}{\partial x^2}$$

with the following initial and boundary conditions

$$\begin{aligned} t = 0, \quad 0 < x < L: \qquad & C = 0 \\ t > 0, \qquad x = 0: \qquad & C = f_1(t) \\ t > 0, \qquad x = L: \qquad & C = f_2(t) \end{aligned}$$

where C is nanoparticle concentration, L is length in the x-axis direction, and $f_1(t)$ and $f_2(t)$ are the measured concentrations at the boundaries as functions of time. Gradients of diffusing components in y- and z-axis were assumed to be negligible compared to the gradient along the x-axis (Figure 3.5a). The model assumes that the initial concentrations in the matrix were zero. Particle concentrations were determined from fluorescence intensities using the calibration described above. Particle concentration profiles as a function of distance from the edge (x-axis) were obtained by averaging pixel values across the width (y-axis). Numerical solutions were calculated using finite elements and diffusion coefficients were determined by nonlinear least square optimization using Matlab (The MathWorks).

Mathematical modeling of diffusion and reaction in cylindroids

A mathematical model was constructed to couple particle diffusion and cellular uptake. Effective diffusivities were derived from measured diffusivities in Matrigel, and were proportional to the volume of extracellular space, 1 - f_v, and inversely proportional to the tortuosity, which was assumed to have a value of 2.7. Internalization of gold nanoparticles from extracellular space and glutathione-mediated replacement were represented with a one-step reversible reaction. A reversible reaction was used to model cellular uptake and release, because it was the most likely cause of the saturation kinetics observed with negative particles. Reaction rates were assumed to be first order with respect to FITC-AuNPs and released FITC-SH. Released FITC-SH was assumed to not diffuse in the extracellular space. Initially neither species was assumed to be present throughout the cylindroid, and the symmetric boundary condition was assumed at the center. At the interface between the cylindroids and the culture media the measured particle concentrations were used as boundary conditions.

Reaction rates as functions of position

Reaction rates were assumed to be functions of position and were modeled with a sigmoidal function that asymptotically approaches maximum and minimum values with a smooth transition.

$$k_j = \frac{1}{2}\left(k_j^{min} + k_j^{max}\right) + \frac{1}{2}\left(k_j^{min} - k_j^{max}\right)\tanh\left(\frac{r - R_t}{\sigma}\right)$$

The subscript j indicates the direction of the reaction (forward, 1 or backward, 2); k_j^{min} and k_j^{max} are the minimum and maximum reaction rates; R_t is the location of the inflection;

and σ is the width of the transition (Figure 3.11). This equation asymptotically approaches k_j^{min} and k_j^{max} as the normalized radius, r, approaches 0 and 1, respectively (Figure 3.11). In figure 3.11 $R_t = 0.6$ and $\sigma = 0.1$. With these parameters, k is within 10^{-6} of k_{max} at r = 0 and 10^{-4} of k_{min} at r = 1. Additionally, k is at 10% of the maximum and minimum values at r = 0.45 and r = 0.75. Nonlinear least square optimization determined k_j^{min}, k_j^{max} and R_t by minimizing the error between measured and calculated radial concentration profiles. The width of transition (σ) was fixed at 60 m based on the fluorescence images (Figure 3.3), which was less than 10% of the radius of most cylindroids. The location of the inflection, R_t, was found to be between 0.6 and 0.8 for all cylindroids. All parameters were determined for the forward and reverse reactions of both particle types.

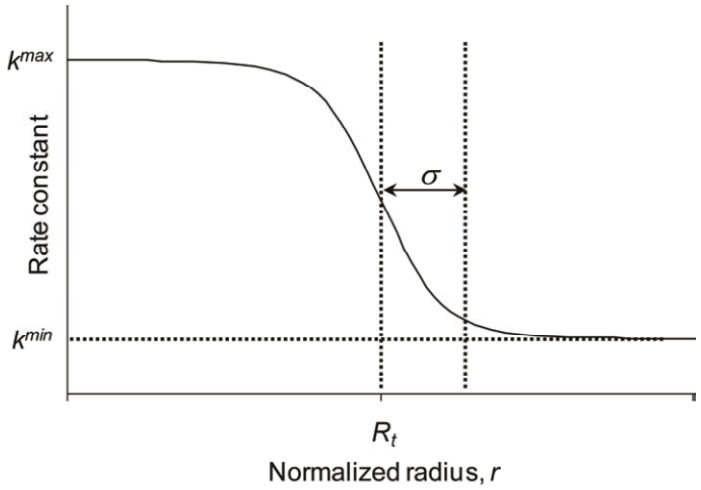

Figure 3.10 Profile of the reaction constant as a function of the radial distance from the center of the cylindroid. The values k_{min} and k_{max} are the maximum and minimum value of the sigmoidal function; R_t is the location of the inflection; and σ is the width of the transition.

Modeling particle diffusion and ligand released in a hypothetical tumor

Particle and released ligand concentrations were predicted using the calculated diffusion and reaction kinetic parameters. To more closely describe tumor biology, the cylindrical geometry was inverted; diffusion was assumed to originate from the lumen of a 10 μm blood vessel. The concentration of particles in the blood was assumed to be well mixed and be cleared by simple two-compartment, monotonically decreasing pharmacokinetics. Previous measurements in mice estimated that the clearance half-life of PEG-coated gold nanoparticles is approximately three hours. The average released ligand concentration was determined in three regions as a function of time, 10-70, 75-120, and 1000-1500μm.

3.5 References

1. Hicks, K. O.; Pruijn, F. B.; Sturman, J. R.; Denny, W. A.; Wilson, W. R., Multicellular resistance to tirapazamine is due to restricted extravascular transport: A pharmacokinetic/pharmacodynamic study in HT29 multicellular layer cultures. *Cancer Res.***2003,** *63* (18), 5970-5977
2. Lankelma, J.; Dekker, H.; Luque, R. F.; Luykx, S.; Hoekman, K.; van der Valk, P.; van Diest, P. J.; Pinedo, H. M., Doxorubicin gradients in human breast cancer. *Clin. Cancer Res.* **1999,** *5* (7), 1703-1707
3. Minchinton, A. I.; Tannock, I. F., Drug penetration in solid tumours. *Nat. Rev. Cancer* **2006,** *6* (8), 583-592.

4. Jain, R. K., Transport of molecules, particles, and cells in solid tumors. *Annu. Rev. Biomed. Eng.* **1999,** *1*, 241-263.

5. Primeau, A. J.; Rendon, A.; Hedley, D.; Lilge, L.; Tannock, I. F., The distribution of the anticancer drug doxorubicin in relation to blood vessels in solid tumors. *Clin. Cancer Res.* **2005,** *11* (24), 8782-8788.

6. Vaupel, P.; Kallinowski, F.; Okunieff, P., Blood-Flow, Oxygen and Nutrient Supply, and Metabolic Microenvironment of Human-Tumors - a Review. *Cancer Res.* **1989,** *49* (23), 6449-6465

7. Tredan, O.; Galmarini, C. M.; Patel, K.; Tannock, I. F., Drug resistance and the solid tumor microenvironment. *J. Natl. Cancer I* **2007,** *99* (19), 1441-1454

8. Grantab, R.; Sivananthan, S.; Tannock, I. F., The penetration of anticancer drugs through tumor tissue as a function of cellular adhesion and packing density of tumor cells. *Cancer Res.* **2006,** *66* (2), 1033-1039.

9. Goldacre, R. J.; Sylven, B., On the Access of Blood-Borne Dyes to Various Tumour Regions. *Brit. J. Cancer* **1962,** *16* (2), 306-322.

10. You, C. C.; Verma, A.; Rotello, V. M., Engineering the nanoparticle-biomacromolecule interface. *Soft Matter* **2006,** *2* (3), 190-204.

11. You, C. C.; De, M.; Han, G.; Rotello, V. M., Tunable inhibition and denaturation of alpha-chymotrypsin with amino acid-functionalized gold nanoparticles. *J. Am. Chem. Soc.* **2005,** *127* (37), 12873-12881.

12. Goodman, C. M.; Chari, N. S.; Han, G.; Hong, R.; Ghosh, P.; Rotello, V. M., DNA-binding by functionalized gold nanoparticles: Mechanism and structural requirements. *Chem. Biol. Drug Des.* **2006,** *67* (4), 297-304.

13. McIntosh, C. M.; Esposito, E. A.; Boal, A. K.; Simard, J. M.; Martin, C. T.; Rotello, V. M., Inhibition of DNA transcription using cationic mixed monolayer protected gold clusters. *J. Am. Chem. Soc.* **2001,** *123* (31), 7626-7629.

14. You, C. C.; De, M.; Han, G.; Rotello, V. M., Tunable inhibition and denaturation of alpha-chymotrypsin with amino acid-functionalized gold nanoparticles. *J. Am. Chem. Soc.* **2005,** *127* (37), 12873-12881

15 . Thomas, M.; Klibanov, A. M., Conjugation to gold nanoparticles enhances polyethylenimine's transfer of plasmid DNA into mammalian cells. *P. Natl. Acad. Sci. USA* **2003,** *100* (16), 9138-9143.

16. Rosi, N. L.; Giljohann, D. A.; Thaxton, C. S.; Lytton-Jean, A. K. R.; Han, M. S.; Mirkin, C. A., Oligonucleotide-modified gold nanoparticles for intracellular gene regulation. *Science* **2006,** *312* (5776), 1027-1030.

17. Jain, P. K.; El-Sayed, I. H.; El-Sayed, M. A., Au nanoparticles target cancer. *Nano Today* **2007,** *2* (1), 18-29.

18. Chithrani, B. D.; Chan, W. C. W., Elucidating the mechanism of cellular uptake and removal of protein-coated gold nanoparticles of different sizes and shapes. *Nano Lett.* **2007,** *7* (6), 1542-1550.

19. Kasinskas, R. W.; Forbes, N. S., Salmonella typhimurium specifically chemotax and proliferate in heterogeneous tumor tissue in vitro. *Biotechnol. Bioeng.* **2006,** *94* (4), 710-721.

20. Kim, B. J.; Forbes, N. S., Flux analysis shows that hypoxia-inducible-factor-1-alpha minimally affects intracellular metabolism in tumor spheroids. *Biotechnol. Bioeng.* **2007,** *96* (6), 1167-1182.

21. Freyer, J. P.; Sutherland, R. M., Selective Dissociation and Characterization of Cells from Different Regions of Multicell Tumor Spheroids. *Cancer Res.* **1980,** *40* (11), 3956-3965.

22 . Kasinskas, R. W.; Forbes, N. S., Salmonella typhimurium lacking ribose chemoreceptors localize in tumor quiescence and induce apoptosis. *Cancer Res.* **2007,** *67* (7), 3201-3209.

23. Sutherland, R. M., Cell and Environment Interactions in Tumor Microregions - the Multicell Spheroid Model. *Science* **1988,** *240* (4849), 177-184.

24 . Kim, B. J.; Forbes, N. S., Single-Cell Analysis Demonstrates How Nutrient Deprivation Creates Apoptotic and Quiescent Cell Populations in Tumor Cylindroids. *Biotechnol. Bioeng.* **2008,** *101* (4), 797-810.

25. Helmlinger, G.; Yuan, F.; Dellian, M.; Jain, R. K., Interstitial pH and pO(2) gradients in solid tumors in vivo: High-resolution measurements reveal a lack of correlation. *Nat. Med.* **1997,** *3* (2), 177-182.

26. Kim, B.; Han, G.; Toley, B. J.; Kim, C. K.; Rotello, V. M.; Forbes, N. S., Tuning payload delivery in tumour cylindroids using gold nanoparticles. *Nat. Nanotechnol.* **2010,** *5* (6), 465-472.

27. De, M.; You, C. C.; Srivastava, S.; Rotello, V. M., Biomimetic interactions of proteins with functionalized nanoparticles: A thermodynamic study. *J. Am. Chem. Soc.* **2007,** *129* (35), 10747-10753.

28. Chompoosor, A.; Han, G.; Rotello, V. M., Charge dependence of ligand release and monolayer stability of gold nanoparticles by biogenic thiols. *Bioconjugate Chem.* **2008,** *19* (7), 1342-1345.

29. Hong, R.; Han, G.; Fernandez, J. M.; Kim, B. J.; Forbes, N. S.; Rotello, V. M., Glutathione-mediated delivery and release using monolayer protected nanoparticle carriers. *J. Am. Chem. Soc.* **2006,** *128* (4), 1078-1079.

30. Jones, D. P.; Carlson, J. L.; Samiec, P. S.; Sternberg, P.; Mody, V. C.; Reed, R. L.; Brown, L. A. S., Glutathione measurement in human plasma Evaluation of sample collection, storage and derivatization conditions for analysis of dansyl derivatives by HPLC. *Clin. Chim. Acta* **1998,** *275* (2), 175-184.

31. Hassan, S. S. M.; Rechnitz, G. A., Determination of Glutathione and Glutathione-Reductase with a Silver Sulfide Membrane-Electrode. *Anal. Chem.* **1982,** *54* (12), 1972-1976.

32. Baldwin, A. L.; Wu, N. Z.; Stein, D. L., Endothelial Surface-Charge of Intestinal Mucosal Capillaries and Its Modulation by Dextran. *Microvasc. Res.* **1991,** *42* (2), 160-178.

33. Ghitescu, L.; Fixman, A., Surface-Charge Distribution on the Endothelial-Cell of Liver Sinusoids. *J. Cell. Biol.* **1984,** *99* (2), 639-647.

34. Chen, A. M.; Santhakumaran, L. M.; Nair, S. K.; Amenta, P. S.; Thomas, T.; He, H. X.; Thomas, T. J., Oligodeoxynucleotide nanostructure formation in the presence of

polypropyleneimine dendrimers and their uptake in breast cancer cells. *Nanotechnology* **2006,** *17* (21), 5449-5460.

35. Holzapfel, V.; Musyanovych, A.; Landfester, K.; Lorenz, M. R.; Mailander, V., Preparation of fluorescent carboxyl and amino functionalized polystyrene particles by miniemulsion polymerization as markers for cells. *Macromol. Chem. Physic.* **2005,** *206* (24), 2440-2449.

36. Mislick, K. A.; Baldeschwieler, J. D., Evidence for the role of proteoglycans in cation-mediated gene transfer. *P. Natl. Acad. Sci. USA* **1996,** *93* (22), 12349-12354.

37. Helmlinger, G.; Yuan, F.; Dellian, M.; Jain, R. K., Interstitial pH and pO(2) gradients in solid tumors in vivo: High-resolution measurements reveal a lack of correlation. *Nat. Med.* **1997,** *3* (2), 177-182.

38. Orwar, O.; Fishman, H. A.; Ziv, N. E.; Scheller, R. H.; Zare, R. N., Use of 2,3-Naphthalenedicarboxaldehyde Derivatization for Single-Cell Analysis of Glutathione by Capillary Electrophoresis and Histochemical-Localization Ion by Fluorescence Microscopy. *Anal. Chem.* **1995,** *67* (23), 4261-4268.

39. Davies, C. D.; Berk, D. A.; Pluen, A.; Jain, R. K., Comparison of IgG diffusion and extracellular matrix composition in rhabdomyosarcomas grown in mice versus in vitro as spheroids reveals the role of host stromal cells. *Brit. J. Cancer* **2002,** *86* (10), 1639-1644.

40. Pluen, A.; Boucher, Y.; Ramanujan, S.; McKee, T. D.; Gohongi, T.; di Tomaso, E.; Brown, E. B.; Izumi, Y.; Campbell, R. B.; Berk, D. A.; Jain, R. K., Role of tumor-host

interactions in interstitial diffusion of macromolecules: Cranial vs. subcutaneous tumors. *P. Natl. Acad. Sci. USA* **2001,** *98* (8), 4628-4633.

41. Ramanujan, S.; Pluen, A.; McKee, T. D.; Brown, E. B.; Boucher, Y.; Jain, R. K., Diffusion and convection in collagen gels: Implications for transport in the tumor interstitium. *Biophys J.* **2002,** *83* (3), 1650-1660.

42. Kleinman, H. K.; Mcgarvey, M. L.; Liotta, L. A.; Robey, P. G.; Tryggvason, K.; Martin, G. R., Isolation and Characterization of Type-Iv Procollagen, Laminin, and Heparan-Sulfate Proteoglycan from the Ehs Sarcoma. *Biochemistry-Us* **1982,** *21* (24), 6188-6193.

43. Boucher, Y.; Baxter, L. T.; Jain, R. K., Interstitial Pressure-Gradients in Tissue-Isolated and Subcutaneous Tumors - Implications for Therapy. *Cancer Res.* **1990,** *50* (15), 4478-4484.

44. Jain, R. K., Transport of Molecules in the Tumor Interstitium - a Review. *Cancer Res.* **1987,** *47* (12), 3039-3051.

45. Young, J. S.; Lumsden, C. E.; Stalker, A. L., The Significance of the Tissue Pressure of Normal Testicular and of Neoplastic (Brown-Pearce Carcinoma) Tissue in the Rabbit. *J. Pathol. Bacteriol.* **1950,** *62* (3), 313-333.

46. You, C. C.; De, M.; Rotello, V. M., Contrasting effects of exterior and interior hydrophobic moieties in the complexation of amino acid functionalized gold clusters with alpha-chymotrypsin. *Org. Lett.* **2005,** *7* (25), 5685-5688.

CHAPTER 4

RECOGNITION-MEDIATED ACTIVATION OF THERAPEUTIC GOLD NANOPARTICLES INSIDE LIVING CELLS

4.1 Introduction

Supramolecular chemistry provides a versatile tool for the organization of molecular systems into functional structures and the actuation of these assemblies for a myriad of applications through the reversible association between complementary components. Supramolecular chemistry uses non-covalent interactions to provide controlled assembly of molecular building blocks.[1, 2, 3, 4, 5, 6] By virtue of reversible non-covalent interactions (e.g. hydrogen bonding, ion-ion, pi-pi stacking and van der Waals interactions), supramolecular complexes are inherently dynamic in nature and highly selective toward other complementary guest molecules through these various weak and reversible interactions.[7] As a result of the modularity and the reversibility, supramolecular systems can be engineered to assemble and disassemble spontaneously in response to a range of triggers.[8]

The versatility of supramolecular chemistry makes this strategy a promising tool for biomedical science. A number of host-guest supramolecular systems (e.g. nanovalves and artificial molecular machines) have been reported for the delivery of drugs and other therapeutic materials.[9, 10, 11] The engineering of such systems has been achieved principally through the design of molecular recognition partners, thereby fine tuning the

molecular recognition event to meet the demands of specific applications. A number of synthetic receptors including cucurbit[n]uril (CB[n]),[12] cyclodextrins,[13, 14] cyclophanes,[15] calixarenes,[16] and crown ethers[17, 18] have been used for this purpose. Of these host systems, the cucurbit[n]uril (CB[n]) family of macrocyclic receptors is particularly useful due to their well defined structure and recognition properties coupled with their ability to form stable host-guest inclusion complexes with a wide variety of guest molecules in aqueous media.[19, 20, 21] This capability has been exploited for the creation of delivery vectors, including the encapsulation of platinum drugs inside the cavity of CB[7] to increase the stability of the drugs in biological environments.[22, 23, 24, 25] In another example, the strong affinity of spermine towards CB[n] has been utilized to tailor a DNA delivery vector for enhanced transfection efficiency and target specificity.[26, 27] In these systems, the properties of the guest molecule have been modified as a result of the supramolecular complexation with the host molecules, enhancing delivery properties.

In addition to modification of molecular properties, supramolecular chemistry provides the capability of actuation.[28, 29] Engineering of host-guest systems to function inside the cell provides a potentially powerful strategy for the regulation of therapeutics. We present here a supramolecular system featuring complementary diaminohexane-terminated gold nanoparticles (AuNP-NH_2) and cucurbit[7]uril (CB[7]) that form a non-toxic assembly that is readily taken up by the cells (Figure 4.1). This host-guest complex can be disassembled intracellularly by the orthogonal guest molecule 1-adamantylamine (ADA) that features a very high affinity to CB[7]. Intracellular removal of CB[7] from the nanoparticle surface results in a endosomal escape by the AuNP-NH_2, thereby activating the cytotoxicity of AuNP-NH_2 and hence inducing cell death (Figure 4.1). This

result presents a new strategy for triggering therapeutic systems through the use of competitive interactions of orthogonally presented guest molecules, with immediate advantages in dosage control and potential utility for dual-targeting therapies. This work has been published as an article in the *Nature Chemistry* journal. [30]

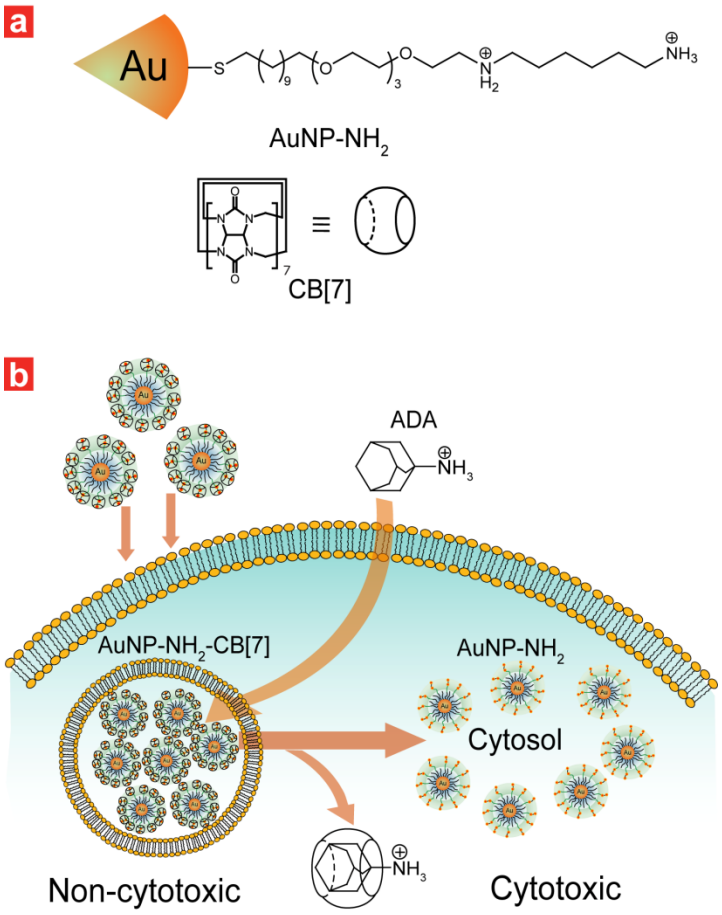

Figure 4.1 Structure of gold nanoparticle and use of intracellular host-guest complexation to trigger nanoparticle cytotoxicity. (a) Structure of diaminohexane-terminated gold nanoparticle (AuNP-NH_2) and cucurbit[7]uril (CB[7]). (b) Activation of AuNP-NH_2-CB[7] cytotoxicity by dethreading of CB[7] from the nanoparticle surface by ADA.

4.2 Results and discussion

4.2.1 Complexation/decomplexation between AuNP-NH_2 and CB[7]

The therapeutic component of the system is provided by AuNP-NH_2 (2.5 ± 0.4 nm core size) featuring a self-assembled monolayer of diaminohexane terminated thiol ligands (Figure 4.1a).[31] The terminal diaminohexane moiety both renders the particle cytotoxic (vide infra) and serves as a recognition unit for the formation of host-guest inclusion complex with CB[7]. The association constant of this diamine-CB[7] complexation process is ~ 10^8 M^{-1} and the complex has been shown to be stable under biological conditions. [32] The complexation between AuNP-NH_2 and CB[7] was investigated using NMR titration experiments as shown in Figure 4.2. As the ratio of CB[7]/ AuNP-NH_2 increases, the peaks for the methylene groups of AuNP-NH_2-CB[7] are shifted upfield relative to those of AuNP-NH_2. This behavior indicates that terminal diaminohexane units were encapsulated inside the shielding zone of CB[7] cavity as AuNP-NH_2-CB[7] complex forms.[33] At the ratio of 1:40 (AuNP-NH_2:CB[7]), the signal shift of the methylene groups was completely saturated, revealing the number of CB[7] around a single nanoparticle is ~40. According to the thermogravimetric analysis (TGA), the number of diaminohexane-terminated ligands on a single nanoparticle estimated is ~43 (Figure 4.2b), indicating almost complete encapsulation of diaminohexane units by CB[7].

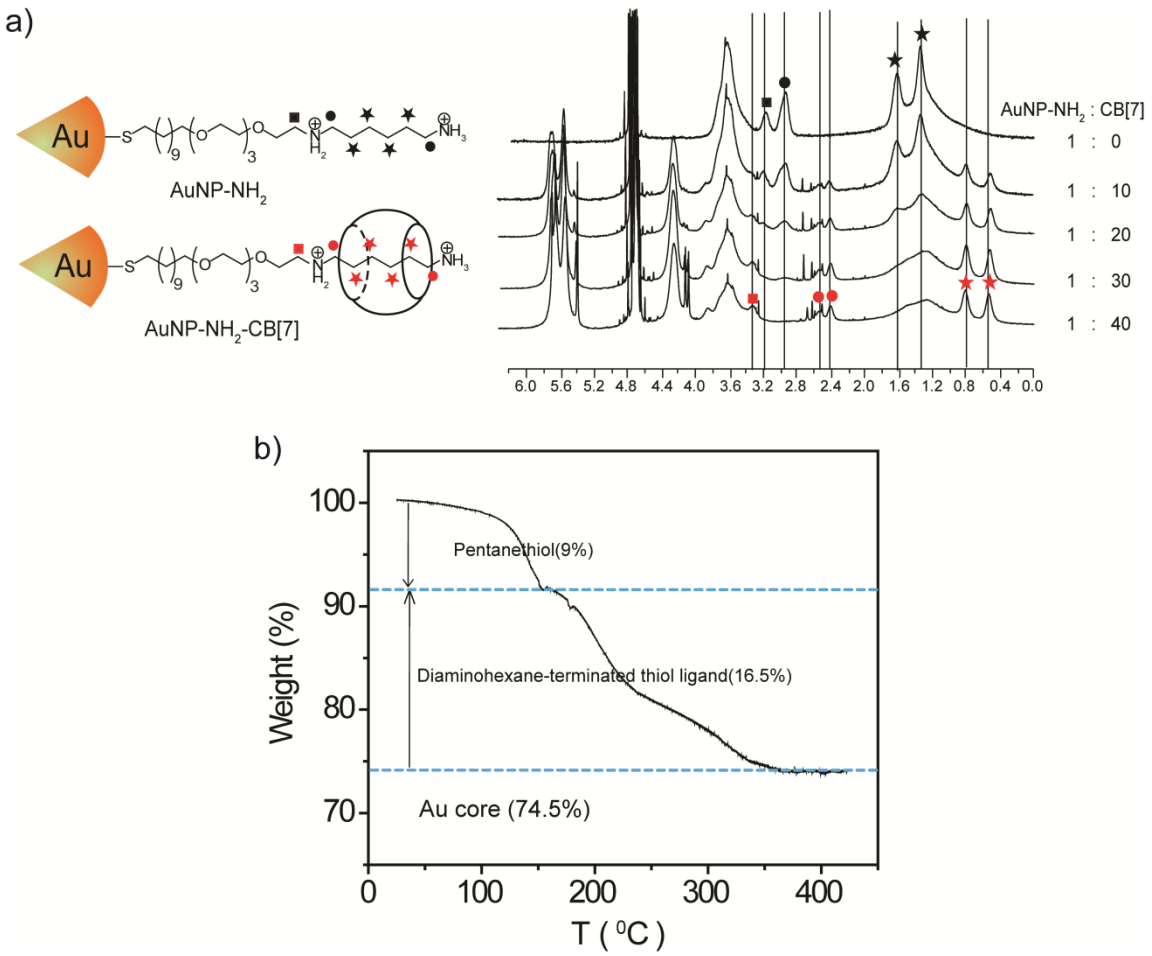

Figure 4.2 (a) NMR titration between AuNP-NH_2 and CB[7]. The resonance signals for the methylene groups (• and ★) of AuNP-NH_2-CB[7] were shifted upfield, relatively to those in AuNP-NH_2. (b) Thermogravimetric analysis (TGA) data of AuNP-NH_2. The average number of diaminohexane-terminated thiol ligand in a single nanoparticle estimated is ~43.

The AuNP-NH_2-CB[7] complex was further characterized through transmission electron microscopy (TEM) as shown in Figure 4.3. TEM images taken after uranyl acetate staining showed that each gold nanoparticle was encapsulated by CB[7]. The average overall diameter of the nanoparticles calculated from the TEM image of AuNP-NH_2-CB[7] is 11.4 ± 0.8 nm, which is in good agreement with the hydrodynamic diameter observed by DLS experiment (12.1 ± 0.8 nm). In addition, no size change or aggregation of nanoparticles was observed from UV-Vis spectra of the nanoparticles, indicating no morphological change after complexation (Figure 4.4).

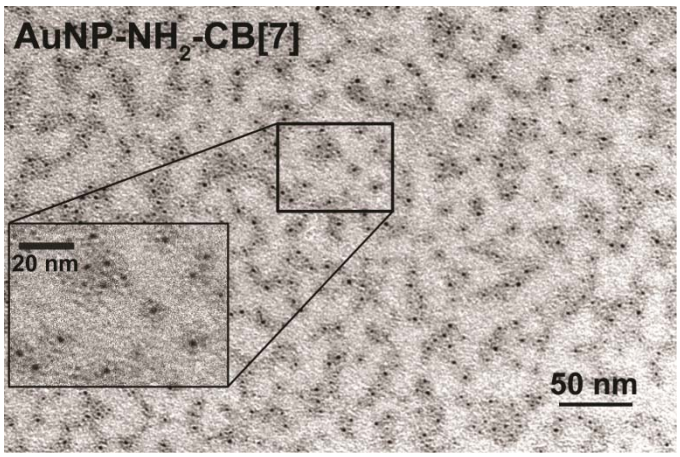

Figure 4.3 TEM image of AuNP-NH_2-CB[7] complex after uranyl acetate staining.

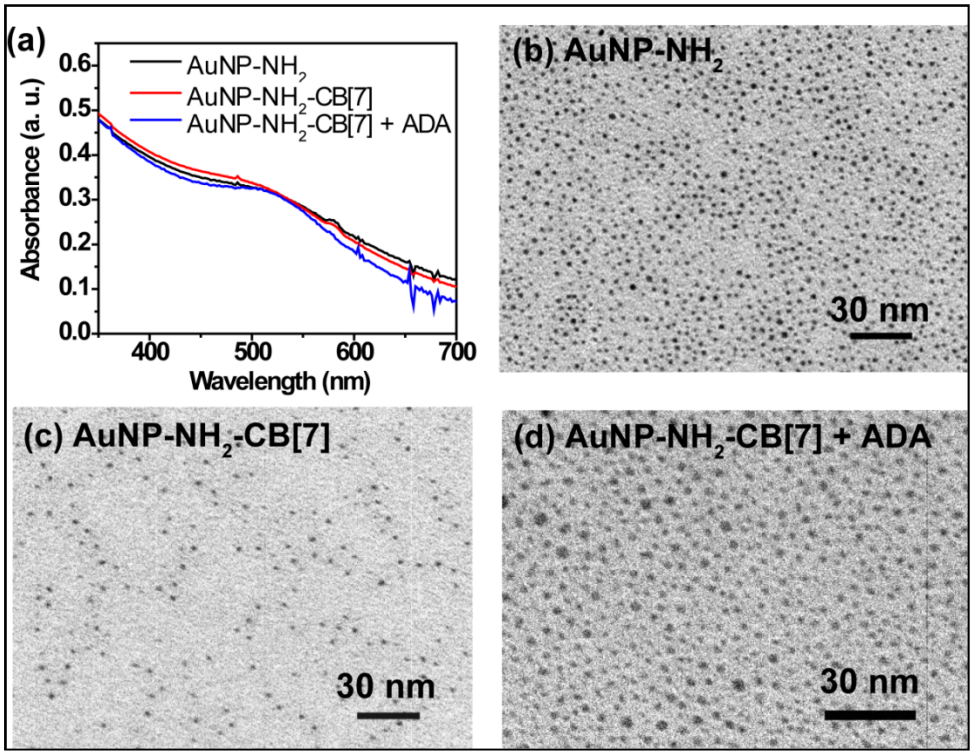

Figure 4.4 (a) UV-Vis spectra of nanoparticles. 0.6 μM nanoparticles were used to measure the absorption spectra. No change in UV-Vis absorption band was observed during complexation/decomplexaion process. TEM images of (b) AuNP-NH_2, (c) AuNP-NH_2-CB[7], and (d) AuNP-NH_2-CB[7] + ADA. No size change or aggregation of nanoparticles was observed from TEM images, indicating no morphological change during complexation/decomplexation process. TEM samples of AuNP-NH_2, AuNP-NH_2-CB[7], and AuNP-NH_2-CB[7] unsheathed by ADA were prepared by placing one drop of the desired solution (3 μM) on to a 300-mesh Cu grid coated with carbon film. These samples were analyzed and photographed using the same instrument without staining. The average diameter of Au core is 2.5 ± 0.4 nm.

The competitive unsheathing of the AuNP-NH_2-CB[7] complex by ADA (commonly used as an antiviral or anti-Parkinsonian drug [34, 35, 36]) was confirmed using NMR and matrix-assisted laser desorption/ionization mass spectroscopy (MALDI-MS).

Addition of ADA triggered the release of CB[7] from nanoparticles through creation of the more favorable 1:1 ADA-CB[7] complexes ($K_a = 1.7 \times 10^{12}$). As expected, the shifted resonance signals of the methylene groups of the ligands induced by complexation with CB[7] were fully recovered as soon as ADA was added (Figure 4.5a). In MALDI-MS, the AuNP-NH_2 and AuNP-NH_2-CB[7] exhibit characteristic ion peaks at m/z 479.44 and 1641.8 respectively, corresponding to the molecular ion (M^+) of [HS-NH_2] and [HS-NH_2-CB[7]]. After addition of ADA, the ion peak of [HS-NH_2-CB[7]] disappeared and a new peak of [ADA-CB[7]] appeared, indicating efficient complexation/decomplxation process (Figure 4.5b).

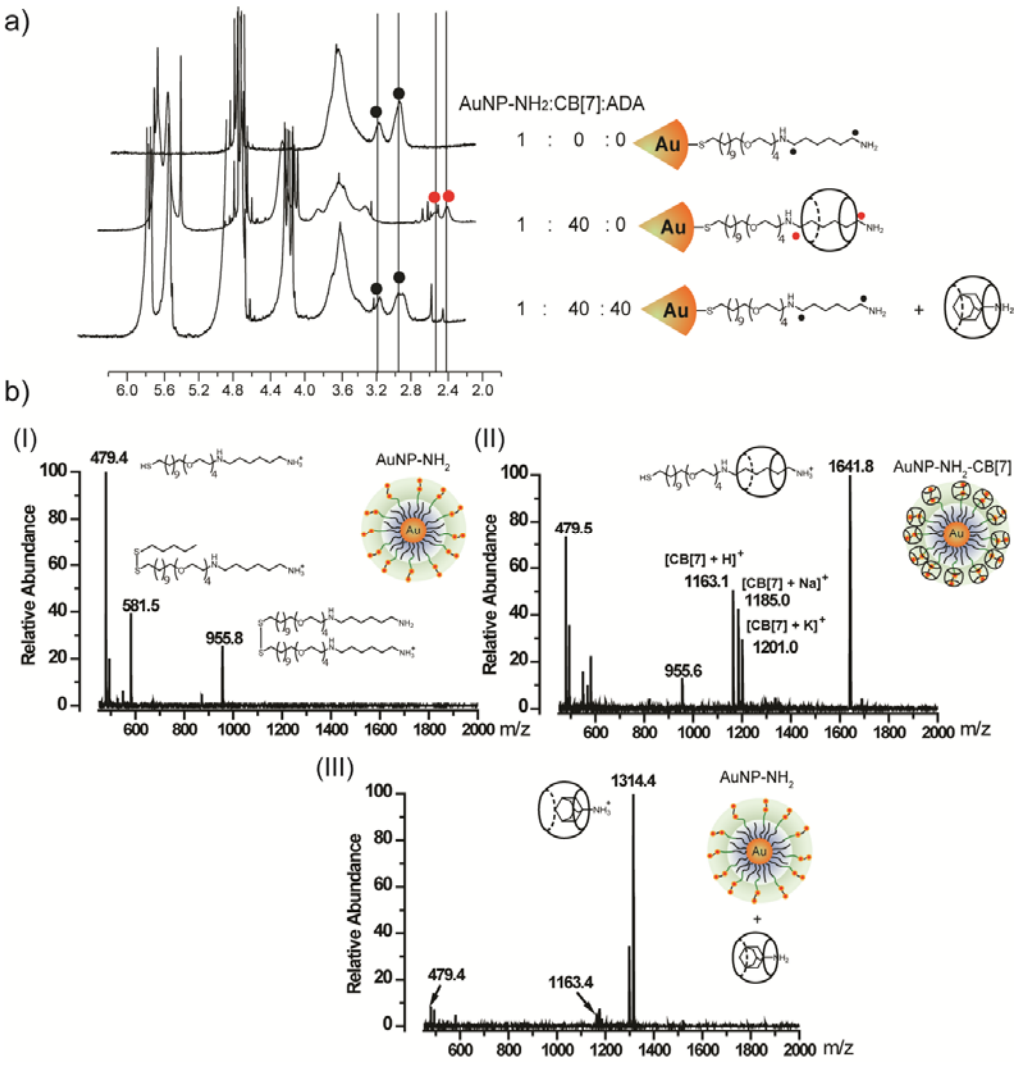

Figure 4.5 (a) Competitive behavior of host-guest binding equilibrium on nanoparticle was demonstrated by NMR data. The shifted resonance signals of the methylene groups of the surface ligands induced by complexation with CB[7] were fully recovered as soon as ADA was added to the complex (AuNP-NH_2-CB[7]) solution. (b) Matrix-assisted laser desorption/ionization mass spectroscopy (MALDI-MS) spectrum. (I) AuNP-NH_2, (II) AuNP-NH_2-CB[7], and (III) AuNP-NH_2-CB[7] + ADA

4.2.2 Cellular uptake, cytotoxicity and intracellular localization of the nanoparticles

The cellular uptake of the nanoparticles was quantified using inductively coupled plasma mass spectrometry (ICP-MS). ICP-MS analysis revealed that the total amount of the nanoparticles taken up by the cells was nearly identical for AuNP-NH_2 and AuNP-NH_2-CB[7] (Figure 4.6). TEM analysis of the cells was employed to evaluate the impact of CB[7] complexation on the intracellular fate/localization of the nanoparticles. As shown in Figure 4.7, after 3 h incubation, both AuNP-NH_2 and AuNP-NH_2-CB[7] are trapped within vesicular structures morphologically consistent with endosomes. This observation is consistent with the behavior observed with other cationic nanoparticles, as reported in our previous work.[37, 38] After 24 h of incubation, however, AuNP-NH_2 particles had escaped from the endosome and were dispersed in the cytosol (Figure 4.8). In contrast, AuNP-NH_2-CB[7] particles remained sequestered in the endosome with no free particles observed in the cytosol (Figure 4.8) after the same period. Significantly, incubation of AuNP-NH_2-CB[7]-treated cells with ADA for 24 h resulted in the escape of a substantial number of particles into the cytosol (Figure 4.8c), consistent with intracellular transformation of AuNP-NH_2-CB[7] to AuNP-NH_2 via dethreading.

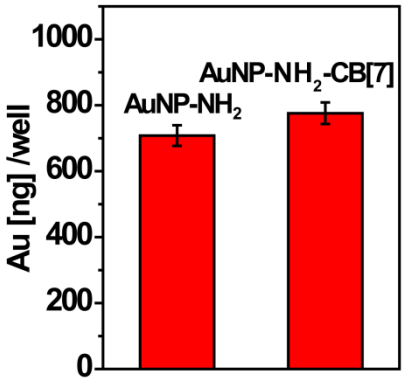

Figure 4.6 Cellular uptake of the gold nanoparticles. Quantification of the amount of gold present in cells. Samples were analyzed by ICP-MS to determine the amount of gold in MCF-7 cell after 3 h incubation with 0.5 M of AuNP-NH_2 and AuNP-NH_2-CB[7]. Both particles showed almost same cellular uptake. Cellular uptake experiments with each gold nanoparticle were repeated 3 times, and each replicate was measured 5 times by ICP-MS. Error bars represent the standard deviations of these measurements.

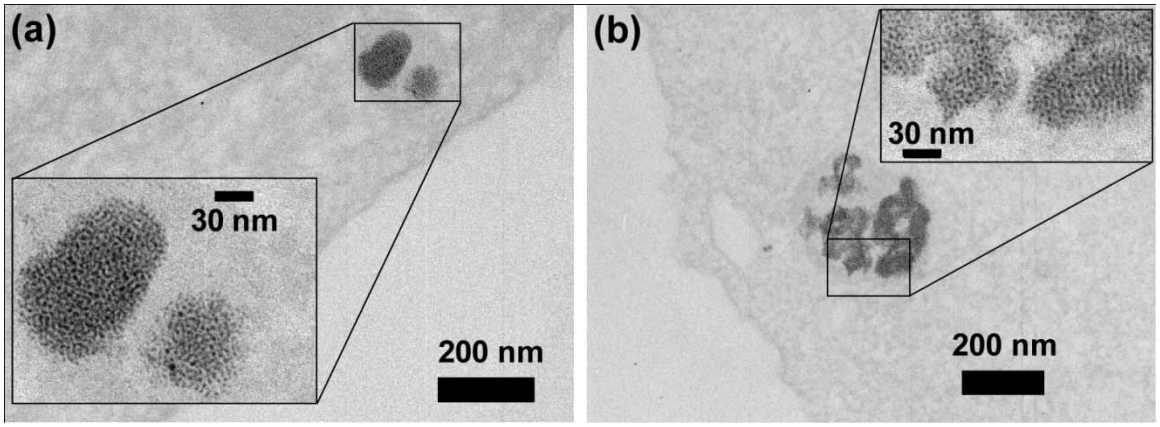

Figure 4.7 TEM images of cross sectional MCF-7 cells incubated for 3h with 0.5 μM (a) AuNP-NH_2 and (b) AuNP-NH_2-CB[7]. Both particles were similarly trapped in organelles such as endosomes.

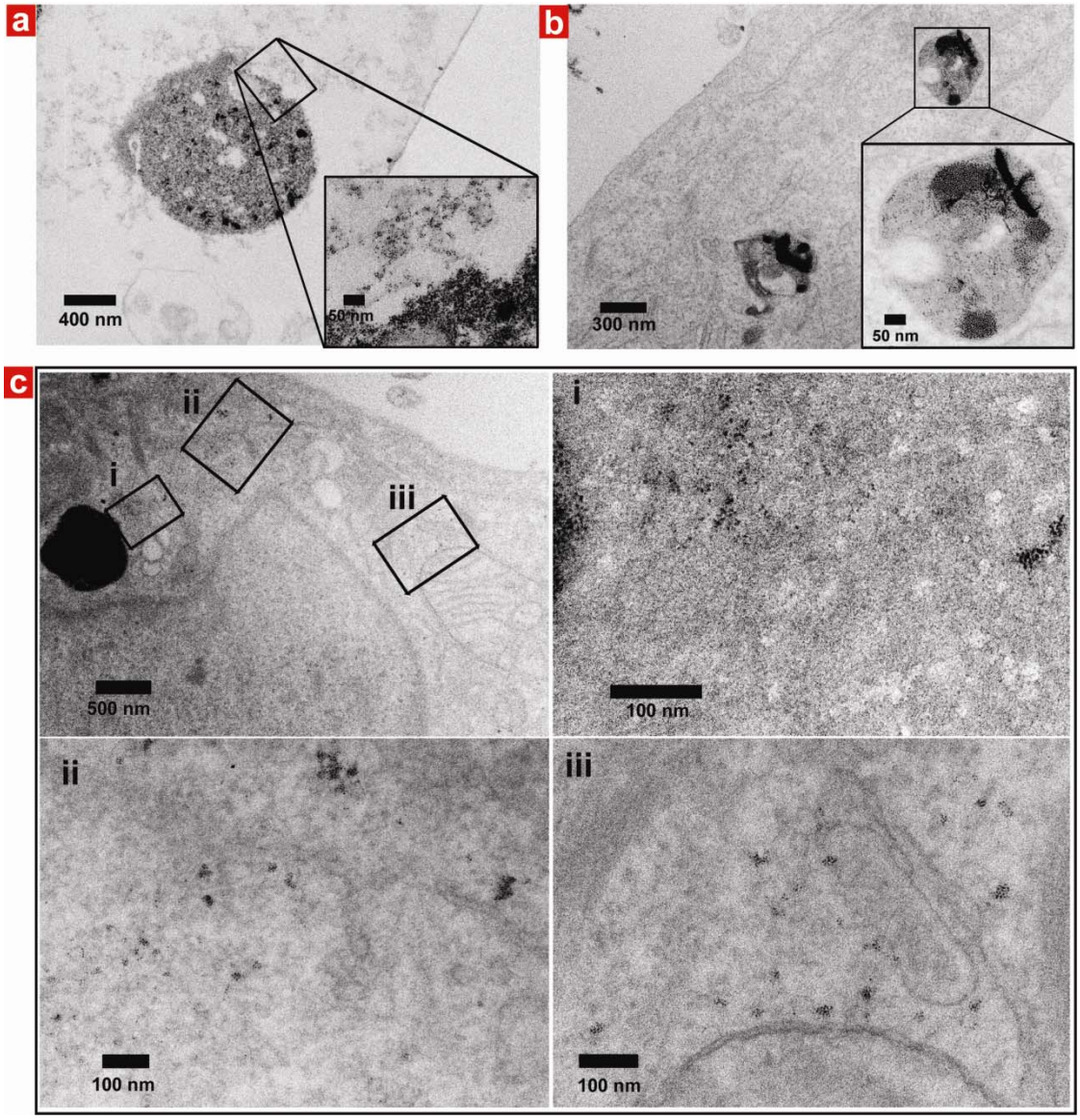

Figure 4.8 Intracellular localization of the gold nanoparticles. TEM images of cross sectional MCF-7 cells incubated for 24 h with 2 μM (a) AuNP-NH_2 and (b) AuNP-NH_2-CB[7]. Significant amount of AuNP-NH_2 is present in the cytosol, however most of the AuNP-NH_2-CB[7] seems to be trapped in organelles such as endosome. (c) TEM images of cross sectional MCF-7 cells incubated for 3 h with 2 μM of AuNP-NH_2-CB[7] and then further incubation with ADA for 24 h. In the intracellular environment ADA

transforms AuNP-NH_2-CB[7] to AuNP-NH_2, which then escaped from the endosome and observed to be dispersed in the cytosol. i, ii and iii are the magnified sections of part (c).

4.2.3 Activating therapeutic efficacy by ADA

Polyamine functionalized macromolecules[39, 40, 41] and nanoparticles[42, 43, 44, 45] interact strongly with cell membranes and subcellular compartments, resulting in membrane disruption and cytotoxicity. Complexation of AuNP-NH_2 with CB[7] should attenuate the positive charge of the particle surfaces, reducing the ability of the particles to disrupt membranes (including the endosomal) and hence lower toxicity. The cytotoxicity of AuNP-NH_2 and AuNP-NH_2-CB[7] was investigated in the human breast cancer MCF-7 cell line using an Alamar blue assay. The AuNP-NH_2-CB[7] complex was substantially less toxic as compared to AuNP-NH_2. After 24 h incubation, AuNP-NH_2 exhibited cytotoxicity with an IC_{50} value of 1.3 μM (Figure 4.9). On the other hand, AuNP-NH_2-CB[7] complex did not inhibit cell proliferation at concentrations ≤ 50 μM under the same experimental conditions, presumably arising from sequestration of the particle in the endosome. Significantly, when the free thiol ligand was added to the cells at concentrations consistent with those used in the study (80 μM, corresponding to the same per-ligand concentration as 2 μM nanoparticle) toxicity was observed with both threaded and unthreaded ligand, demonstrating the modulation of ligand toxicity on the particle.

Given the observed intracellular dethreading of AuNP-NH_2-CB[7] with ADA and concomitant release from the endosome, the endosomal escape of the nanoparticles after ADA treatment raises the possibility that toxicity of the AuNP-NH_2-CB[7] complex can be triggered by ADA. To test this hypothesis MCF-7 cells were incubated with 2 μM of

AuNP-NH_2-CB[7] in culture medium for 3h, to allow endocytosis of nanoparticles.[46] Cells were then washed three times with PBS buffer, and then ADA was added to the culture medium. Cells were then incubated for an additional 24 h. Cells treated with AuNP-NH_2 and AuNP-NH_2-CB[7] alone exhibited 34 % and 100 % cell viability after 24 h incubation, respectively (Figure 4.9b). Treatment with 0.4 mM ADA led to 40 % cell viability, approaching the level of lethality observed for the AuNP-NH_2 control. The result indicates that ADA acts as an effective trigger for the competitive release of CB[7] from particles within the cell, with attendant activation of cytotoxicity.

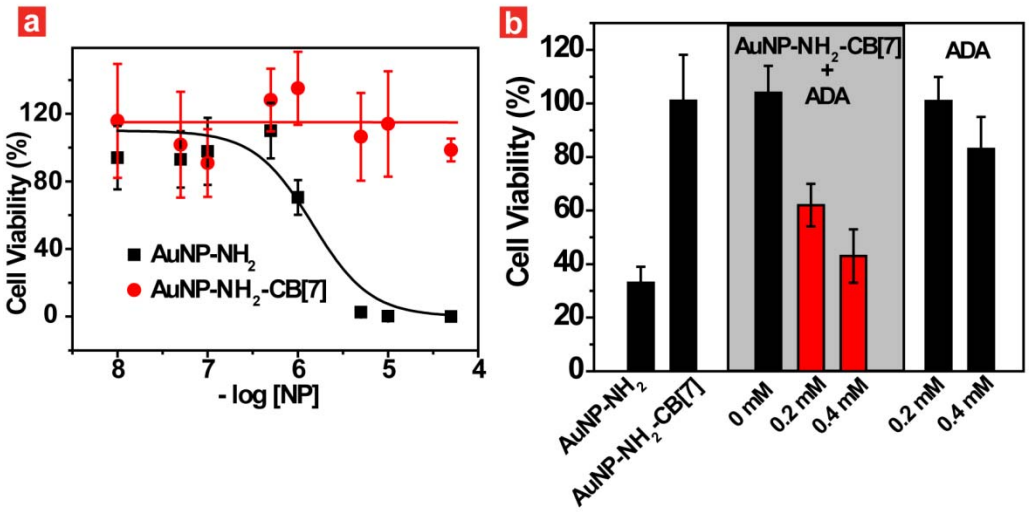

Figure 4.9 Cytotoxicity of AuNP-NH_2 and AuNP-NH_2-CB[7] and modulating cytotoxicity of the gold nanoparticles. (a) Cytotoxicity of AuNP-NH2 and AuNP-NH_2-CB[7] measured by Alamar blue assay after 24 h incubation in MCF-7. IC_{50} of AuNP-NH_2 was 1.3 μM and no cytotoxicity of AuNP-NH2-CB[7] was observed up to 50 μM. (b) Triggering cytotoxicity using ADA. After 3h incubation of AuNP-NH_2-CB[7] (2 μM) in MCF-7 cell, different concentrations (0, 0.2 and 0.4 mM) of ADA in medium added and further incubated at 37 ºC for 24 h. The cell viability was then determined by using an Alamar blue assay. As controls, cell viability of AuNP-NH_2 and AuNP-NH_2-CB[7] was measured after 24 h incubation (34 % and 100 %, respectively). Cell viability

experiments were performed as triplicate and the error bars represent the standard deviations of these measurements.

4.3 Summary and future outlook

In summary, we have demonstrated the use of synthetic host-guest chemistry to provide triggered activation of a therapeutic system via competitive complexation. This approach provides a potential strategy for the construction of synthetic host-guest supramolecular systems capable of complex and sophisticated behavior within living cells. Triggering therapeutic systems through the use of competitive interactions of orthogonally presented guest molecules can be potentially useful for dual-targeting therapies, i.e. targeting of both host and guest component. This provides the potential for orthogonal ("effector/trigger") drug delivery and therapeutic activation[47, 48] that would be capable of achieving higher levels of site specific activity, and reduced amounts of collateral damage. Currently, we are exploring this strategy *in vivo* and thoroughly considering issues (e.g. the practical use of ADA) related to the real-world application of this system.

4.4 Synthesis of materials and experimental methods

General

All the chemicals were purchased from Sigma-Aldrich or Fischer Scientific, unless otherwise specified. The chemicals were used as received. Dichloromethane (DCM) used as a solvent for chemical synthesis was dried according to standard procedure. The yields of the compounds reported here refer to the yields of spectroscopically pure compounds after purification. ^{1}H NMR spectra of the nanoparticles and the complexes were recorded on a Bruker AVANCE 400 at 400 MHz. MALDI-MS analyses were performed using a Bruker Omniflex time-of-flight mass spectrometer. UV-Vis spectra were recorded on Hewlett-Packard 8452A spectrophotometer. Dynamic light scattering (DLS) was measured by Zetasizer Nano ZS.

4.4.1 Synthesis of ligand and fabrication of nanoparticle

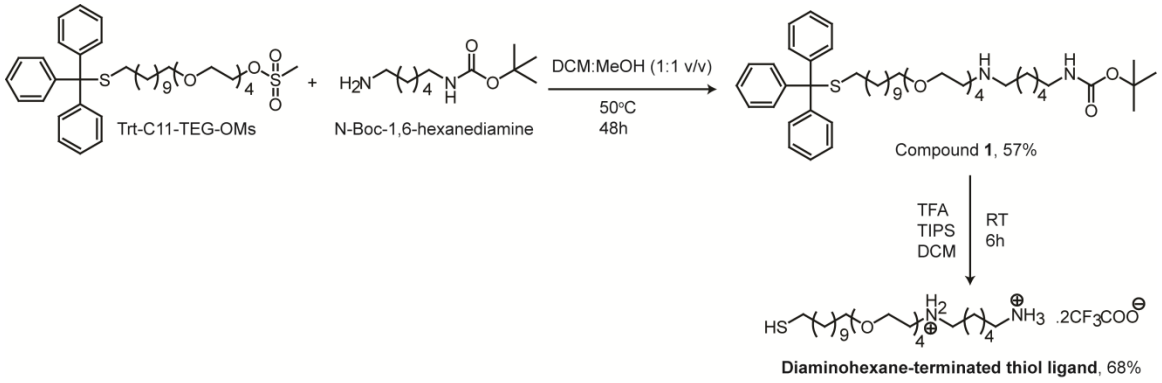

Figure 4.10 Synthetic scheme for the preparation of diaminohexane-terminated ligand.

Synthesis of compound 1

The trityl-protected thiol ligand (Trt-C11-TEG-OMs) was prepared according to our previously reported procedure.[49] Trt-C11-TEG-OMs (0.150 g, 0.214 mmol) was first dissolved in 2 mL of DCM: MeOH (1:1 v/v) mixture. The solution was then placed in a 20 mL glass vial and N-Boc-1,6-hexanediamine (0.479 mL, 2.143 mmol) was added to it. The reaction mixture was heated to 50°C and stirred for ~48 h. The reaction mixture was concentrated under reduced pressure and the residue was directly charged on a SiO_2 column for purification (eluent: a gradient eluent of 0-10% methanol in DCM v/v). Yield 0.100 g (0.122 mmol, 57%, viscous pale yellow color liquid). ^{1}H NMR (400MHz, $CDCl_3$): 7.40 (m, 6H, $TrtH_{Ar}$), 7.27 (m, 6H, $TrtH_{Ar}$), 7.20 (m, 3H, $TrtH_{Ar}$), 4.59 (br, 1H, –NHCO–), 3.88 (t, ^{3}J = 4.64 Hz, 2H, $–OCH_2–$), 3.68-3.57 (m, 12H, $–CH_2O–$ + $–OCH_2–$), 3.44 (t, ^{3}J = 7.02 Hz, 2H, $–CH_2O–$), 3.11-3.06 (m, 4H, $–CH_2NCO–$ + $C–CH_2N–$), 2.90 (t, ^{3}J = 8 Hz, 2H, $–NCH_2–C$), 2.12 (t, ^{3}J = 7.32 Hz, 2H, $–SCH_2–$), 1.83 (m, 2H, $–CH_2–$), 1.59-1.14 (m, 33H, $–CH_2–$ + $–C(CH_3)_3$). MS (ESI-MS) calculated for $C_{49}H_{76}N_2O_6S$ 820.5, found 821.8 $[M+H]^+$.

Synthesis of diainohexane-terminated thiol ligand

The protected thiol ligand (compound 1, 0.300 g, 0.365 mmol) was dissolved in dry DCM. The solution was purged with argon and an excess of trifluoro acetic acid (TFA, 0.600 mL) was added. During the addition period of TFA the color of the solution was turned to yellow. Subsequently, triisopropylsilane (TIPS, 0.250 mL) was added to the reaction mixture and the color of mixture slowly recovered to colorless. The reaction

mixture was allowed to stir at room temperature for 6 h under argon atmosphere. The volatile components (solvent, TFA and TIPS) were then distilled off under reduced pressure. The pale yellow residue was purified by washing with hexane (15 mL × 3) and diethyl ether (15 mL × 3). After drying under high vacuum a viscous colorless liquid was obtained. Yield 0.175 g (0.248 mmol, 68%). ^{1}H NMR (400MHz, CDCl3): 3.77 (brt, ^{3}J = 4.14 Hz, 2H, –OCH_2–), 3.64-3.57 (m, 12H, –CH_2O– + –OCH_2–), 3.44 (t, ^{3}J = 6.94 Hz, 2H, –CH_2O–), 3.18 (br, 2H, C–CH_2N–), 2.99 (m, 4H, –CH_2N + –NCH_2–C), 2.51 (q, ^{4}J = 7.38 Hz, 2H, –SCH_2–), 1.78-1.26 (m, 26H, –CH_2–).

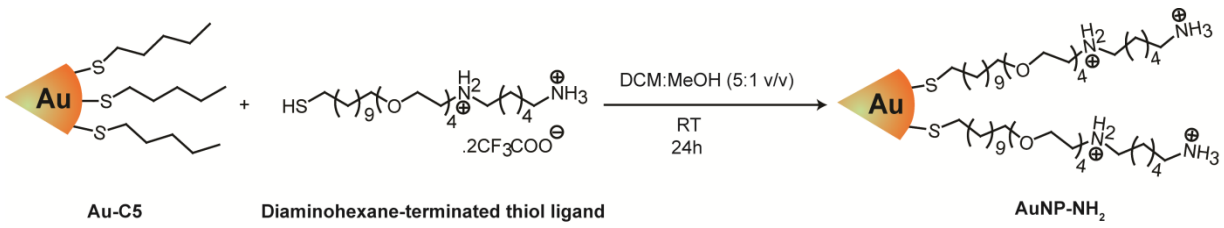

Figure 4.11 Construction of diaminohexane-terminated gold nanoparticle (AuNP-NH2) through place exchange reaction.

Procedure for construction of diaminohexane-terminated gold nanoparticle (AuNP-NH_2)

Gold nanoparticle (AuNP-NH2) was prepared through place-exchange reaction of 1-pentanethiol protected gold nanoparticle (Au-C5). Au-C5 was prepared by following the procedure reported by Brust et al.[50]As shown in Figure 5.11, nanoparticle was decorated with diaminohexane-terminated thiol ligand by following the general procedure reported by Murray et al. In a typical reaction, 0.015 g of Au-C5 was first dissolved in 1 mL of dry

DCM. Then, 0.038 g of diaminohexane-terminated thiol ligand dissolved in 5 ml DCM:MeOH (4:1 v/v) was added carefully to the solution of Au-C5. The reaction mixture was allowed to stir at room temperature for ~ 24 h. After ~ 24 h, argon was bubbled through the nanoparticle solution to evaporate the solvents. The dark black color nanoparticle residue was then washed with DCM (10 mL × 3) and 5% MeOH in DCM v/v (10 mL × 2). After washing the nanoparticle was immediately dissolved in MiliQ water and was allowed to stay at room temperature for ~12 h to remove the volatile components. The aqueous solution of the nanoparticle was further purified and concentrated by using molecular cut off filter (Amicon Ultra-4 tube, 10000 MWCO). The filtrate was discarded and the trapped nanoparticle residue (on the cut off filter) was then dissolved in D_2O. ^1H NMR spectra in D_2O was then recorded in a 400 MHz Bruker machine. The nanoparticle was stable in solution for months and was stored in MiliQ water at 4 °C.

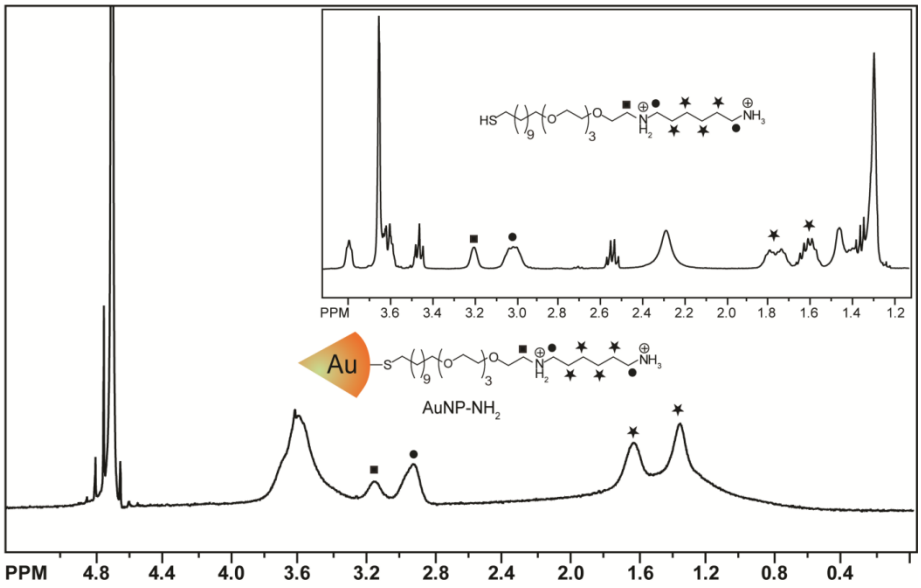

Figure 4.12 400 MHz ^{1}H NMR spectrum of AuNP-NH2 in D_2O. Inset shows the ^{1}H NMR spectrum of the diaminohexane-terminated thiol ligand in $CDCl_3$.

4.4.2 Experimental methods

Cell Culture Experiment

MCF-7 cells were grown in a cell culture flask using low glucose Dulbecco's Modified Eagle Medium supplemented with 10% fetal bovine serum (FBS) at 37°C in a humidified atmosphere of 5% CO_2. For cytotoxicity tests involving AuNP-NH_2 and AuNP-NH_2-CB[7], MCF-7 cells were seeded at 20,000 cells in 0.2 ml per well in 96-well plates 24 h prior to the experiment. During experiment old media was replaced by different concentrations of AuNP-NH_2 and AuNP-NH_2-CB[7] in serum containing media and the cells were incubated for 24 h at 37°C in a humidified atmosphere of 5 % CO_2. The cells were then completely washed with PBS buffer for three times and 10% Alarmar blue in serum containing media was added to each well and further incubated at 37 °C for 4 h.

The cell viability was then determined by measuring the fluorescence intensity at 570 nm using a SpectraMax M5 microplate spectrophotometer. Curves were fitted by DoseRep function in Origin 8. For measuring cytotoxicity of AuNP-NH_2-CB[7] upon adding ADA, MCF-7 cells were seeded at 20,000 cells per well in 96-well plate 24 h prior to the experiment. The old medium was replaced by 2 μM of AuNP-NH_2-CB[7] in medium containing serum and incubated for 3h. The cells were then completely washed with PBS buffer for three times and different concentration (0, 0.2 and 0.4 mM) of ADA in serum containing media was added to the cells and further incubated at 37 ºC for 24 h. The cell viability was then determined by using Alamar blue assay.

TEM sample preparation

TEM samples of nanoparticles were prepared by placing one drop of the desired nanoparticles solution (1~3 μM) on to a 300-mesh Cu grid coated with carbon film, followed by 2 % of uranyl acetate staining for 15 min. These samples were analyzed and photographed using JEOL 100S electron microscopy.

For the preparation of cellular TEM samples, MCF-7 cells were seeded and incubated on 15 mm diameter Theramanox® coverslips (Nalge Nunc International, NY) placed in 24 well plates at amount of 100,000 cells in 1 ml of serum containing media for 24 h prior to the experiment. The media was replaced by 0.5 ml of 2 μM AuNP-NH_2 or AuNP-NH_2-CB[7] in serum containing media and incubated for 24 h. The medium containing the gold nanoparticles was then discarded and the cells were completely washed with PBS buffer for three times. The cells were then fixed in 2 % glutaraldehyde with 3.75 % sucrose in 0.1 M sodium phosphate buffer (pH 7.0) for 30 min and then

washed with 0.1 M PBS containing 3.75% sucrose three times over 30 min. They were postfixed in 1 % osmium tetroxide with 5 % sucrose in 0.05 M sodium phosphate buffer solution (pH 7.0) for 1 hr and the rinsed with distilled water three times. They were dehydrated in a graded series of acetone (10 % step), and embedded in epoxy resin. The resin was polymerized at 70 °C for 12 h. Ultrathin sections (50 nm) obtained with a Reichert Ultracut E Ultramicrotome and imaged under a JEOL 100S electron microscopy.

For the preparation of TEM samples for the cells treated with AuNP-NH_2-CB[7] and subsequent incubation with ADA, pre-seeded MCF-7 cell on 15 mm diameter Theramanox® coverslips was treated by AuNP-NH_2-CB[7] (2 μM) for 3h. After washing three times with PBS buffer, the cells were further incubated with ADA (0.4 mM) in serum containing media for 24 h. Cellular TEM sample was prepared according to the above described procedure.

ICP-MS sample preparation and experimental setup

ICP-MS measurements were performed on a Perkin Elmer Elan 6100. Operating conditions of the ICP-MS are listed below: RF power: 1200 W; plasma Ar flow rate: 15 L/min; nebulizer Ar flow rate: 0.96 L/min; isotopes monitored: ^{197}Au; dwell time: 50 ms; nebulizer: cross flow; spray chamber: Scott. AuNP-NH_2 and AuNP-NH_2-CB[7] (0.5 μM) was incubated with pre seeded MCF-7 cell line in 24 well plates (20,000 cells/well) for 3h. After incubation, cells were washed three times with PBS buffer and then lysis buffer (250 μl) was added to the cells. The resulting cell lysate was digested overnight using 3 mL of HNO_3 and 1 mL of H_2O_2. On the next day, 3 mL of aqua regia was added, and

then the sample was allowed to react for another 2-3 h. The sample solution was then diluted to 100 mL with de-ionized water, and aqua regia. The final gold nanoparticle sample solution contained 5% aqua regia. The gold nanoparticle sample solution was measured by ICP-MS under the operating conditions described above. Cellular uptake experiments with each gold nanoparticle were repeated 3 times, and each replicate was measured 5 times by ICP-MS. A series of gold standard solutions (20, 10, 5, 2, 1, 0.5, 0.2, 0 ppb) were prepared before each experiment. Each gold standard solution contained 5% aqua regia. The resulting calibration line was used to determine the gold amount in taken up by the cells in each sample.

Matrix Assisted Laser Desorption/Ionization Mass Spectrometry (MALDI-MS)

The MALDI analyses were done on a Bruker Omniflex time-of-flight mass spectrometer. The spectrometers are equipped with a 337 nm nitrogen laser, a 1.0 m flight tube, and a stainless steel sample target. All mass spectra were acquired in a reflectron mode, using a reflectron voltage of 20 kV. All reported spectra represent an average of 100 shots. A saturated matrix (α-cyano-4-hydroxycinnamic acid (α-CHCA)) solution was prepared in 70% acetonitrile, 30% H_2O, and 0.1% trifluoroacetic acid. 1 μL of matrix solution was mixed with 1 μL of nanoparticle solution. 1 μL of this mixture was applied to target, and after allowing it to dry, the MALDI-MS analysis was performed.

Thermogravimetric analysis (TGA)

TGA was performed using a TGA 2950 high-resolution thermo-gravimetric analyzer (TA Instruments, Inc., New Castle, DE), which was equipped with an open platinum pan

and an automatically programmed temperature controller. The TGA data were obtained as follows: about 3.0 mg of AuNP-NH_2 was placed in the TGA pan and heated in a nitrogen atmosphere at a rate of 5 °C / min up to 500 °C. The mass change was plotted against temperature to generate the thermogravimetric combustion profile of AuNP-NH_2.

4.5 References

1. Lehn, J. M., Toward self-organization and complex matter. *Science* **2002,** *295* (5564), 2400-2403.
2. Lehn, J. M., From supramolecular chemistry towards constitutional dynamic chemistry and adaptive chemistry. *Chem. Soc. Rev.* **2007,** *36* (2), 151-160.
3. Reinhoudt, D. N.; Crego-Calama, M., Synthesis beyond the molecule. *Science* **2002,** *295* (5564), 2403-2407.
4. Yaghi, O. M.; O'Keeffe, M.; Ockwig, N. W.; Chae, H. K.; Eddaoudi, M.; Kim, J., Reticular synthesis and the design of new materials. *Nature* **2003,** *423* (6941), 705-714.
5. Lehn, J. M. *Supramolecular Chemistry: Concepts and Perspectives.* (VCH, New York, 1995).
6. Dankers, P. Y. W.; Harmsen, M. C.; Brouwer, L. A.; Van Luyn, M. J. A.; Meijer, E. W., A modular and supramolecular approach to bioactive scaffolds for tissue engineering. *Nat. Mater.* **2005,** *4* (7), 568-574.
7. Hennig, A.; Bakirci, H.; Nau, W. M., Label-free continuous enzyme assays with macrocycle-fluorescent dye complexes. *Nat. Methods* **2007,** *4* (8), 629-632.

8. Klajn, R.; Olson, M. A.; Wesson, P. J.; Fang, L.; Coskun, A.; Trabolsi, A.; Soh, S.; Stoddart, J. F.; Grzybowski, B. A., Dynamic hook-and-eye nanoparticle sponges. *Nat. Chem.* **2009,** *1* (9), 733-738.

9. Angelos, S.; Yang, Y. W.; Patel, K.; Stoddart, J. F.; Zink, J. I., pH-responsive supramolecular nanovalves based on cucurbit[6]uril pseudorotaxanes. *Angew. Chem. Int. Edit.* **2008,** *47* (12), 2222-2226.

10. Angelos, S.; Khashab, N. M.; Yang, Y. W.; Trabolsi, A.; Khatib, H. A.; Stoddart, J. F.; Zink, J. I., pH Clock-Operated Mechanized Nanoparticles. *J. Am. Chem. Soc.* **2009,** *131* (36), 12912-12914.

11. Coti, K. K.; Belowich, M. E.; Liong, M.; Ambrogio, M. W.; Lau, Y. A.; Khatib, H. A.; Zink, J. I.; Khashab, N. M.; Stoddart, J. F., Mechanised nanoparticles for drug delivery. *Nanoscale* **2009,** *1* (1), 16-39.

12. Lee, H. K.; Park, K. M.; Jeon, Y. J.; Kim, D.; Oh, D. H.; Kim, H. S.; Park, C. K.; Kim, K., Vesicle formed by amphiphilc cucurbit[6]uril: Versatile, noncovalent modification of the vesicle surface, and multivalent binding of sugar-decorated vesicles to lectin. *J. Am. Chem. Soc.* **2005,** *127* (14), 5006-5007.

13. Park, C.; Oh, K.; Lee, S. C.; Kim, C., Controlled release of guest molecules from mesoporous silica particles based on a pH-responsive polypseudorotaxane motif. *Angew. Chem. Int. Edit.* **2007,** *46* (9), 1455-1457.

14. Du, L.; Liao, S. J.; Khatib, H. A.; Stoddart, J. F.; Zink, J. I., Controlled-Access Hollow Mechanized Silica Nanocontainers. *J. Am. Chem. Soc.* **2009,** *131* (42), 15136-15142.

15. Hayashida, O.; Uchiyama, M., Multivalent macrocyclic hosts: Histone surface recognition, guest binding, and delivery by cyclophane-based resorcinarene oligomers. *J. Org. Chem.* **2007,** *72* (2), 610-616.

16. Sansone, F.; Dudic, M.; Donofrio, G.; Rivetti, C.; Baldini, L.; Casnati, A.; Cellai, S.; Ungaro, R., DNA condensation and cell transfection properties of guanidinium calixarenes: Dependence on macrocycle lipophilicity, size, and conformation. *J. Am. Chem. Soc.* **2006,** *128* (45), 14528-14536.

17. Weimann, D. P.; Winkler, H. D. F.; Falenski, J. A.; Koksch, B.; Schalley, C. A., Highly dynamic motion of crown ethers along oligolysine peptide chains. *Nat. Chem.* **2009,** *1* (7), 573-577.

18. Darwish, I. A.; Uchegbu, I. F., The evaluation of crown ether based niosomes as cation containing and cation sensitive drug delivery systems. *Int. J. Pharm.* **1997,** *159* (2), 207-213.

19. Lee, J. W.; Samal, S.; Selvapalam, N.; Kim, H. J.; Kim, K., Cucurbituril homologues and derivatives: New opportunities in supramolecular chemistry. *Acc. Chem. Res.* **2003,** *36* (8), 621-630.

20. Kim, K.; Selvapalam, N.; Ko, Y. H.; Park, K. M.; Kim, D.; Kim, J., Functionalized cucurbiturils and their applications. *Chem. Soc. Rev.* **2007,** *36* (2), 267-279.

21. Lagona, J.; Mukhopadhyay, P.; Chakrabarti, S.; Isaacs, L., The cucurbit[n]uril family. *Angew. Chem. Int. Edit.* **2005,** *44* (31), 4844-4870.

22. Wheate, N. J.; Day, A. I.; Blanch, R. J.; Arnold, A. P.; Cullinane, C.; Collins, J. G., Multi-nuclear platinum complexes encapsulated in cucurbit[n]uril as an approach to reduce toxicity in cancer treatment. *Chem. Commun.* **2004,** (12), 1424-1425.

23. Jeon, Y. J.; Kim, S. Y.; Ko, Y. H.; Sakamoto, S.; Yamaguchi, K.; Kim, K., Novel molecular drug carrier: encapsulation of oxaliplatin in cucurbit[7]uril and its effects on stability and reactivity of the drug. *Org. Biomol. Chem.* **2005,** *3* (11), 2122-2125.

24 . Wheate, N. J., Improving platinum(II)-based anticancer drug delivery using cucurbit[n]urils. *J. Inorg. Biochem.* **2008,** *102* (12), 2060-2066.

25. Wheate, N. J.; Buck, D. P.; Day, A. I.; Collins, J. G., Cucurbit[n]uril binding of platinum anticancer complexes. *Dalton T.* **2006,** (3), 451-458.

26. Lim, Y. B.; Kim, T.; Lee, J. W.; Kim, S. M.; Kim, H. J.; Kim, K.; Park, J. S., Self-assembled ternary complex of cationic dendrimer, cucurbituril, and DNA: Noncovalent strategy in developing a gene delivery carrier. *Bioconjugate Chem.* **2002,** *13* (6), 1181-1185.

27. Kim, S. K.; Park, K. M.; Singha, K.; Kim, J.; Ahn, Y.; Kim, K.; Kim, W. J., Galactosylated cucurbituril-inclusion polyplex for hepatocyte-targeted gene delivery. *Chem. Commun.* **2010,** *46* (5), 692-694.

28. Angelos, S.; Yang, Y. W.; Khashab, N. M.; Stoddart, J. F.; Zink, J. I., Dual-Controlled Nanoparticles Exhibiting AND Logic. *J. Am. Chem. Soc.* **2009,** *131* (32), 11344 -11346.

29. Ghosh, S.; Isaacs, L., Biological Catalysis Regulated by Cucurbit[7]uril Molecular Containers. *J. Am. Chem. Soc.* **2010,** *132* (12), 4445-4454.

30. Kim, C.; Agasti, S. S.; Zhu, Z. J.; Isaacs, L.; Rotello, V. M., Recognition-mediated activation of therapeutic gold nanoparticles inside living cells. *Nat. Chem.* **2010,** *2* (11), 962-966.

31. Templeton, A. C.; Wuelfing, M. P.; Murray, R. W., Monolayer protected cluster molecules. *Acc. Chem. Res.* **2000,** *33* (1), 27-36.

32. Liu, S. M.; Ruspic, C.; Mukhopadhyay, P.; Chakrabarti, S.; Zavalij, P. Y.; Isaacs, L., The cucurbit[n]uril family: Prime components for self-sorting systems. *J. Am. Chem. Soc.* **2005,** *127* (45), 15959-15967.

33. Lee, J. W.; Ko, Y. H.; Park, S. H.; Yamaguchi, K.; Kim, K., Novel pseudorotaxane-terminated dendrimers: Supramolecular modification of dendrimer periphery. *Angew. Chem. Int. Edit.* **2001,** *40* (4), 746-749.

34. Davies, W. L.; Hoffmann, C. E.; Paulshock, M.; Wood, T. R.; Haff, R. F.; Grunert, R. R.; Watts, J. C.; Hermann, E. C.; Neumayer, E. M.; Mcgahen, J. W., Antiviral Activity of 1-Adamantanamine (Amantadine). *Science* **1964,** *144* (362), 862 -863.

35. Maassab, H. F.; Cochran, K. W., Rubella Virus - Inhibition in Vitro by Amantadine Hydrochloride. *Science* **1964,** *145* (363), 1443 -1444.

36. Hagan, J. J.; Middlemiss, D. N.; Sharpe, P. C.; Poste, G. H., Parkinson's disease: Prospects for improved drug therapy. *Trends Pharmacol. Sci.* **1997,** *18* (5), 156-163.

37. Zhu, Z.-J.; Ghosh, P. S.; Miranda, O. R.; Vachet, R. W.; Rotello, V. M., Multiplexed Screening of Cellular Uptake of Gold Nanoparticles Using Laser Desorption/Ionization Mass Spectrometry. *J. Am. Chem. Soc.* **2008,** *130* (43), 14139–14143.

38. Kim, C. K.; Ghosh, P.; Pagliuca, C.; Zhu, Z. J.; Menichetti, S.; Rotello, V. M., Entrapment of Hydrophobic Drugs in Nanoparticle Monolayers with Efficient Release into Cancer Cells. *J. Am. Chem. Soc.* **2009,** *131* (4), 1360 -1361.

39. Godbey, W. T.; Wu, K. K.; Mikos, A. G., Poly(ethylenimine) and its role in gene delivery. *J. Control. Release* **1999,** *60* (2-3), 149-160.

40. Leroueil, P. R.; Berry, S. A.; Duthie, K.; Han, G.; Rotello, V. M.; McNerny, D. Q.; Baker, J. R.; Orr, B. G.; Holl, M. M. B., Wide varieties of cationic nanoparticles induce defects in supported lipid bilayers. *Nano Lett.* **2008,** *8* (2), 420-424.

41. Fischer, D.; Bieber, T.; Li, Y. X.; Elsasser, H. P.; Kissel, T., A novel non-viral vector for DNA delivery based on low molecular weight, branched polyethylenimine: Effect of molecular weight on transfection efficiency and cytotoxicity. *Pharmaceut. Res.* **1999,** *16* (8), 1273-1279.

42. Ghosh, P. S.; Kim, C. K.; Han, G.; Forbes, N. S.; Rotello, V. M., Efficient Gene Delivery Vectors by Tuning the Surface Charge Density of Amino Acid-Functionalized Gold Nanoparticles. *Acs Nano.* **2008,** *2* (11), 2213-2218.

43. Lovric, J.; Bazzi, H. S.; Cuie, Y.; Fortin, G. R. A.; Winnik, F. M.; Maysinger, D., Differences in subcellular distribution and toxicity of green and red emitting CdTe quantum dots. *J. Mol. Med.-Jmm.* **2005,** *83* (5), 377-385.

44. Goodman, C. M.; McCusker, C. D.; Yilmaz, T.; Rotello, V. M., Toxicity of gold nanoparticles functionalized with cationic and anionic side chains. *Bioconjugate Chem.* **2004,** *15* (4), 897-900.

45. Fuller, J. E.; Zugates, G. T.; Ferreira, L. S.; Ow, H. S.; Nguyen, N. N.; Wiesner, U. B.; Langer, R. S., Intracellular delivery of core-shell fluorescent silica nanoparticles. *Biomaterials* **2008,** *29* (10), 1526-1532.

46. Verma, A.; Uzun, O.; Hu, Y.; Hu, Y.; Han, H.-S.; Watson, N.; Chen, S.; Irvine, D. J.; Stellacci, F., Surface-structure-regulated cell-membrane penetration by monolayer-protected nanoparticles. *Nat. Mater.* **2008,** *7*, 588 - 595.

47. Taylor, S. K.; Pei, R. J.; Moon, B. C.; Damera, S.; Shen, A. H.; Stojanovic, M. N., Triggered Release of an Active Peptide Conjugate from a DNA Device by an Orally Administrable Small Molecule. *Angew. Chem. Int. Edit.* **2009,** *48* (24), 4394-4397.

48. Sarkar, D.; Su, Z. Z.; Vozhiila, N.; Park, E. S.; Gupta, P.; Fisher, P. B., Dual cancer-specific targeting strategy cures primary and distant breast carcinomas in nude mice. *P. Natl. Acad. Sci. USA* **2005,** *102* (39), 14034-14039.

49. Chompoosor, A.; Han, G.; Rotello, V. M., Charge dependence of ligand release and monolayer stability of gold nanoparticles by biogenic thiols. *Bioconjugate Chem.* **2008,** *19* (7), 1342-1345.

50. Brust, M.; Walker, M.; Bethell, D.; Schiffrin, D. J.; Whyman, R., Synthesis of Thiol-Derivatized Gold Nanoparticles in a 2-Phase Liquid-Liquid System. *J. Chem. Soc. Chem. Comm.* **1994,** (7), 801-802.

CHAPTER 5

REGULATING EXOCYTOSIS OF GOLD NANOPARTICLES VIA HOST-GUEST CHEMISTRY

5.1 Introduction

Drug delivery systems (DDSs) improve the efficacy of conventional pharmaceutics through enhanced pharmacokinetics and biodistribution.[1] Drugs can be both covalently and non-covalently incorporated into DDSs.[2] Successful therapy with DDSs achieves accurate delivery of their associated drugs to target cells through controlled drug release.[3] Release of drugs from carriers can be regulated by employing tunable activation strategies (e.g. hydrolysis or degradation) via relevant stimuli (e.g. the low endosomal pH, light, and cytosolic reductive conditions).[4, 5, 6] Because greater antiproliferative activity of the drugs relies on the sustained therapeutic effect inside cells, cellular uptake and subsequent long-term retention of the drug carriers within the cells are required for efficient DDSs.[7, 8, 9]

One of the main obstacles of DDSs, however, is the rapid removal of the internalized drug carriers by exocytosis from the cells before the loaded therapeutics are effective.[10, 11] Exocytosis is the process of expelling wastes and other large molecules out of the cells,[12] which is also commonly observed with a wide variety of drug carriers.[13, 14]

As an example, internalized poly (D,L-lactide-*co*-glycolide) nanoparticles undergo exocytosis to the extent of 65 % at 30 min and 85 % at 6 h.[15] Reducing exocytosis of the nanoparticulate drug carriers thus can lead their prolonged retention and sustained release of the loaded drugs inside of the cells, enhancing therapeutic efficiency of the DDSs.[16, 17] To date, there have been no reported strategies preventing exocytosis of the nanoparticles. Furthermore, developing strategies for an orthogonal control of the exocytosis in the cellular environment is a major challenge because of the intracellular chemical complexity and a potential toxicity of relevant reagents. To solve the issues, an orthogonally non-toxic modular system under biological condition should be addressed.

Supramolecular chemistry can develop controlled assemblies from molecular building blocks by virtue of reversible non-covalent interactions including hydrogen bonding and van der Waals interactions.[18] Due to their modular properties toward other complementary molecules, host-guest supramolecular complexes can be tuned to assemble and dissemble in response to various triggers,[19] providing a powerful tool for creating a number of host-guest systems for therapeutic applications.[20, 21, 22] Of the host-guest systems, the use of cucurbit[n]ril (CB[n]) family is useful due to its ability to form stable host-guest complexes with a wide variety of guest molecules in aqueous media,[23, 24] and its non-toxic behavior *in vitro* and *in vivo*.[25, 26] Various CB[n]-guest systems have been developed to create delivery vectors for the drugs and other therapeutic materials, and an actuator system to control catalytic activity of an enzyme.[27, 28, 29] Moreover, owing to the high binding affinity of CB[n] to guest molecules (up to 10^{13} M^{-1}), engineering of the host-guest systems provides the capability of actuation for the regulation of therapeutics in living cells.[30, 31]

In this work, we describe a strategy to regulate exocytosis of AuNPs by utilizing the host-guest system on gold nanoparticles (AuNPs).[32, 33] Quaternary amine head group terminated cationic gold nanoparticles (AuNP-TBen) were readily taken up by the cells via endocytosis (Figure 5.1). Afterward, *in situ* treatment of a complementary cucurbit[7]uril (CB[7]) resulted in threading of the CB[7] on AuNP-TBen inside the cells. The AuNP-TBen-CB[7] complexation rendered the surface of the particles less hydrophilic, inducing the assemblies of AuNP-TBen-CB[7] sequestered in the endosome. Exocytosis of the AuNP-TBen-CB[7] was then blocked by the increased size of the induced assemblies. This approach provide a new strategy for improving efficacy of drug delivery systems through prolonged retention of drug carriers within the cells.

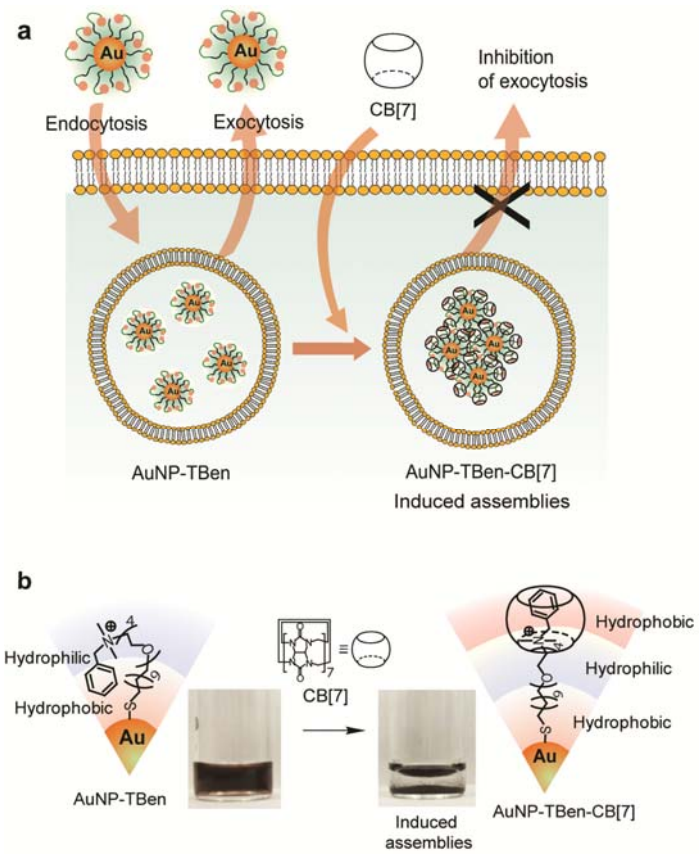

Figure 5.1 Controlling exocytosis of the nanoparticle by using intracellular host-guest complexation. (a) Inhibition of AuNP-TBen exocytosis by threading of CB[7] on the nanoparticle surface. (b) Inducement of the AuNP-TBen-CB[7] assemblies.

5.2 Results and discussion

5.2.1 Complexation between AuNP-TBen and CB[7]

Exocytosis of nanoparticles is dependent on their size.[7] Larger nanoparticles (more than 100 nm in diameter) undergo exocytosis at slower rate and lower amount than smaller nanoparticles. Therefore, the underlying principle of controlling exocytosis of nanoparticles is to induce *in situ* growth of assemblies from the internalized individual nanoparticles entrapped in endocytic vesicles by using a host-guest supramolecular system. The exocytosis of the particles then would be blocked by the increased size of the

induced assemblies [34] and the host-guest system provides an orthogonal stimulus, allowing temporal control of the exocytosis (Figure 5.1 (b)).

To provide an effective host-guest supramolecular system, we synthesized a water-soluble gold nanoparticle, AuNP-TBen, featuring a tetra(ethylene glycol) and quaternary benzyl amine head group at terminal ligand via a Murray's place-exchange reaction.[35] The detailed syntheses and characterization of the AuNPs are available in the Supporting Information. The gold core had an average size of 2.1 ± 0.5 nm with hydrodynamic diameter of the AuNP-TBen being 9.7 ± 0.1 nm determined by TEM and dynamic light scattering, respectively. The AuNP-TBen had a positive potential of + 14.2 mV. The terminal quaternary benzyl amine moiety serves as a recognition unit for the formation of a host-guest inclusion complex with CB[7] with the association constant of ~ 10^{-8} M^{-1}.[36] This higher binding constant is strong enough for the complexes to remain stable under biological conditions.[37]

5.2.2 Inducing assemblies of AuNP-TBen-CB[7]

The complexation between AuNP-TBen and CB[7] was investigated by using DLS experiments as shown in Figure 5.2(a). At the molar ratio of 1:1 and 1:2 (AuNP-TBen:CB[7]), the hydrodynamic diameter of the AuNP-TBen slightly increased from 9.7 ± 0.1 to 11.6 ± 0.5 nm. At a ratio of 1:4 (AuNP-TBen:CB[7]), the particles began to assemble to each other and were completely assembled (aggregated) precipitating at the ratio of 1:10 (AuNP-TBen:CB[7]) as shown in Figure 5.1 (b). The controls, AuNP-TTMA and AuNP-TCOOH showed no observable change of diameter upon adding CB[7] as both particles have no interaction with CB[7].

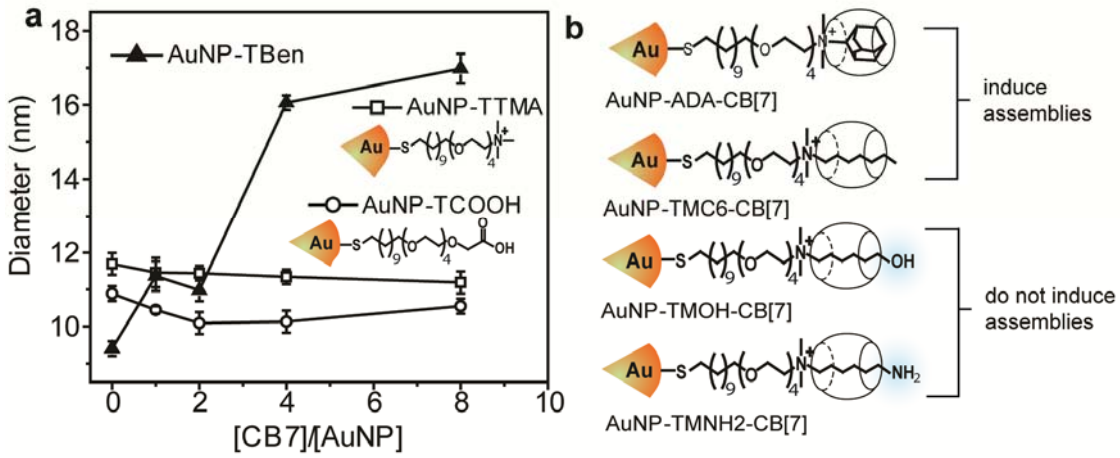

Figure 5.2 Inducing assemblies of the nanoparticle upon binding with CB[7] and effect of surface functional group of the particle. (a) DLS experiments of the nanoparticles depending on addition of CB[7]. It is noted that AuNP-TBens were completely assembled (aggregated) and precipitated at the ratio of 1:10 (AuNP-TBen:CB[7]). (b) AuNP-ADA and AuNP-TMC6 induce the assemblies upon binding with CB[7] (at the ratio of 1:10 (AuNPs:CB[7]), but not for AuNP-TMOH and AuNP-TMNH2 with polar end groups. Inducement of the assemblies of the particles is dependent on surface functional group of the particles

To explain the rationale of the induced assemblies of the AuNP-TBen-CB[7], inducement of the assemblies upon binding with CB[7] was carried out with nanoparticles having different surface functional groups (Figure 5.2 (b)). AuNP-ADA and AuNP-TMC6 induced the assemblies (aggregates) upon binding with CB[7] (at the ratio of 1:10 (AuNPs:CB[7]) as AuNP-TBen-CB[7] complex. In contrast, AuNP-TMOH and AuNP-TMNH2 could not induce assemblies although the particles-CB[7] complexes

were formed. This indicates that the surface end group of the particles plays important role in inducing the assemblies of the particles.

The amphiphilic nanoparticle, AuNP-TBen (also AuNP-ADA and AuNP-TMC6) are soluble in both aqueous and organic solvent (e.g. dichloromethane), respectively. In the aqueous solution, the hydrophobic benzyl units on the particles are probably hidden from the external environment, making the surface of the particles hydrophilic and soluble in aqueous media. Upon binding with CB[7], the benzyl units on the particle presumably became stretched out along the particle, rendering the surface of the particle forcefully less hydrophilic, decreasing their solubility, and inducing the assemblies (Figure 5.1 (b)). AuNP-TMOH and AuNP-TMNH2 can bind with CB[7] but hydroxyl and amine end group potentially kept the surface of particles hydrophilic, and therefore not allowing assemble of the particles. It indicates that inducing assemblies is dependent on surface functional group of the particles.

When the particle assemblies of AuNP-TBen-CB[7] were treated with excess of 1-adamantyl amine (ADA), CB[7] is dethreaded from the particle through creation of the more favorable 1:1 ADA-CB[7] complexes (K_a = 1.7 x 10^{12}).[24] Addition of ADA triggered the particle assemblies to disassemble, making the particles soluble back into the PBS (Figure 5.3). This indicates that exploiting host-guest systems on AuNPs can control solubility (hydrophobicity) of the AuNPs by using precise 'lock and key' modulation over their molecular-level interactions.

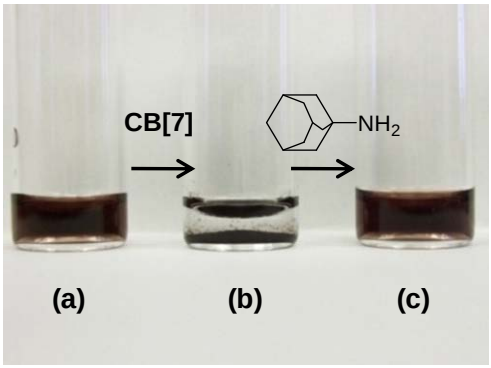

Figure 5.3 (a) AuNP-TBen in PBS. (b) AuNP-TBen-CB[7] assemblies (c) When the particle assemblies of AuNP-TBen-CB[7] were treated with excess of 1-adamantyl amine (ADA), ADA triggered the particle assemblies to disassemble, making the particles soluble back in PBS.

5.2.3 Controlling exoctosis of AuNP-TBen-CB[7]

Cellular uptake behaviors of the nanoparticles were investigated by TEM analysis of the cell. After 3h incubation of the cationic AuNP-TBen (200 nM), the particles were shown to be trapped in the endosomal vesicles in cytoplasm as shown in Figure 5.4 (a). This observation is consistent with a endocytotic behavior of other cationic nanoparticles previously reported in literatures.[38, 39] To study the exocytotic behaviors of the nanoparticle, after 3h incubation of the AuNP-TBen (200 nM), the cells were washed off and incubated with fresh media or CB[7] (0.2 mM) media for an additional 24h. When the cells were treated by fresh media, the number of the particle-entrapped vesicles was significantly decreased (Figure 5.4 (b)). Only a few particles remained within the vesicles or dispersed in various organelles, indicating a major portion of the removed AuNP-TBen

from the cells were involved in exocytosis. In contrast, when the cells were treated by the CB[7] media (0.2 mM) to induce assemblies of AuNP-TBen-CB[7], the particles remained trapped in the endosome (Figure 5.4 (c)). These results indicate that treatment of CB[7] caused intracellular assemblies of the AuNP-TBen-CB[7] as the CB[7] can cross the cell membrane[40] and the induced bulky assemblies remained sequestered in endocytic vesicles without exocytosis.

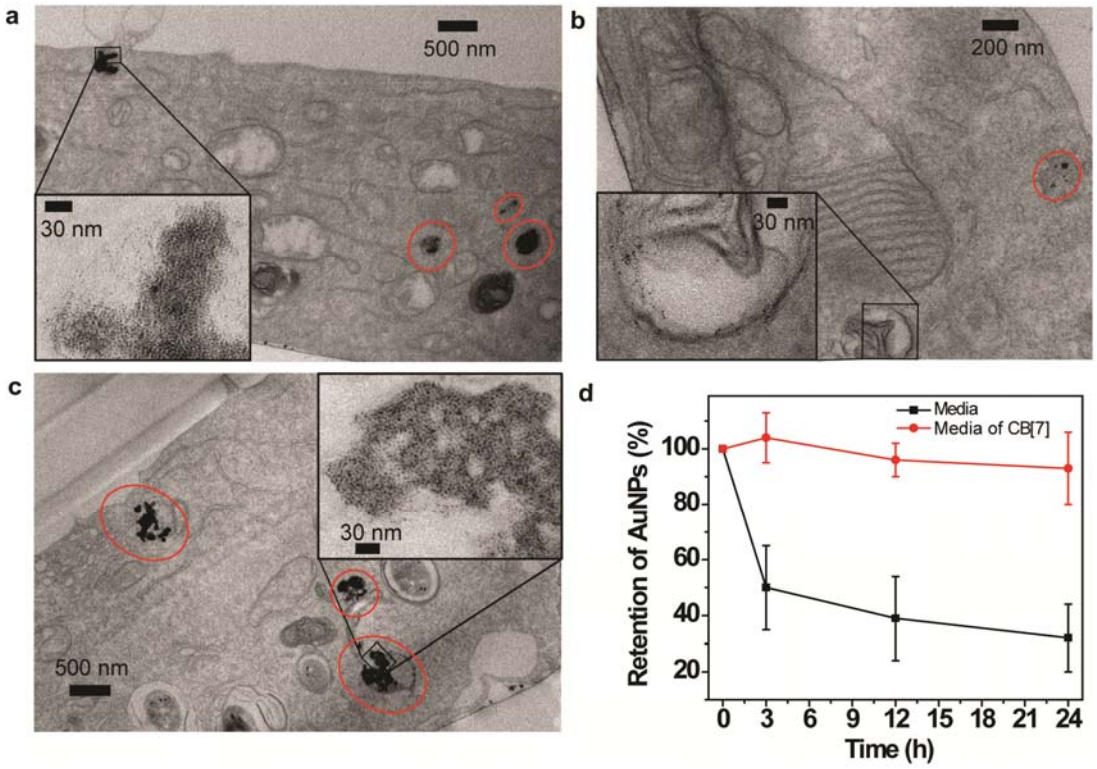

Figure 5.4 Cellular uptake and intracellular behavior of the gold nanoparticles. (a) TEM images of cross sectional MCF-7 cells incubated for 3 h with 200 nM of AuNP-TBen. The cationic AuNP-TBen seems to be trapped in organelles such as an endosome (in the red circle). (b) TEM images of cross sectional MCF-7 cells incubated for 3 h with 200

nM of AuNP-TBen and then washed off and further incubation with only cell culture media for 24 h. The number of the particle-entrapped endosomal vesicles was significantly decreased. (c) TEM images of cross sectional MCF-7 cells incubated for 3 h with 200 nM of AuNP-TBen and then washed off and further incubation with cell culture media of CB[7] (0.2 mM) for 24 h. (d) Quantification of the amount of gold retained in cells at different time (0 h, 3 h, 12 h, and 24 h). Samples at each time point were analyzed by ICP-MS to determine the amount of gold in MCF-7 cell after 3 h incubation with 200 nM of AuNP-TBen and washed off and further incubation with media or media of CB[7] (0.2 mM). Cellular uptake experiments with each gold nanoparticle were repeated 3 times, and each replicate was measured 5 times by ICP-MS. Error bars represent the standard deviations of these measurements.

The excocytosis of the nanoparticles was further quantified by using inductively coupled plasma mass spectrometry (ICP-MS). After 3h incubation of AuNP-TBen (200 nM), the cells were completely washed off and replaced by fresh cell culture media or CB[7] (0.2 mM) media. The cells were then incubated for different additional times (0 h, 3 h, 12 h, and 24 h) and the amount of the gold nanoparticle retained by the cells was determined by measuring ICP-MS. Retention of the AuNP-TBen treated by only cell culture media decreased 34 % at 24 hours while no significant change was observed for the media of CB[7] treatment (Figure 5.4 (d)). This result revealed that treatment of the CB[7] on the cells inhibited exocytosis of the AuNP-TBen along with the observed TEM results.

5.2.4 Effect of an end group on the exocytosis

To further investigate the effect of an end group of AuNPs on the exocytosis, retention of the particles with different functional head groups in the cells was measured by using ICP-MS. AuNP-TTMA and AuNP-TMOH (Figure 5.4 (a) and (b)) exhibited no significant difference of exocytotic behavior for both media and media of CB[7] treatments, showing no effect of CB[7] on exocytosis of the AuNPs. Retention of the AuNP-TTMA and AuNP-TMOH decreased to ~ 62 % and ~ 70 % at 24h, respectively, regardless of CB[7] treatment. In the other hand, exocytosis of the AuNP-ADA and AuNP-TMC6 was blocked when the cells were treated by media of CB[7] as the AuNP-TBen (Figure 5.5 (c) and (d)). Amount of the retained AuNP-ADA and AuNP-TMC6 in the cells reduced to ~ 75 % and ~ 70 % at 24h for the media treatment. Both AuNP-ADA and AuNP-TMC6 induced assemblies of the particle upon binding with CB[7] as AuNP-TBen. It indicates that CB[7] itself does not affect cellular uptake of the particles and exocytosis of the particles was caused increased size of the assemblies.

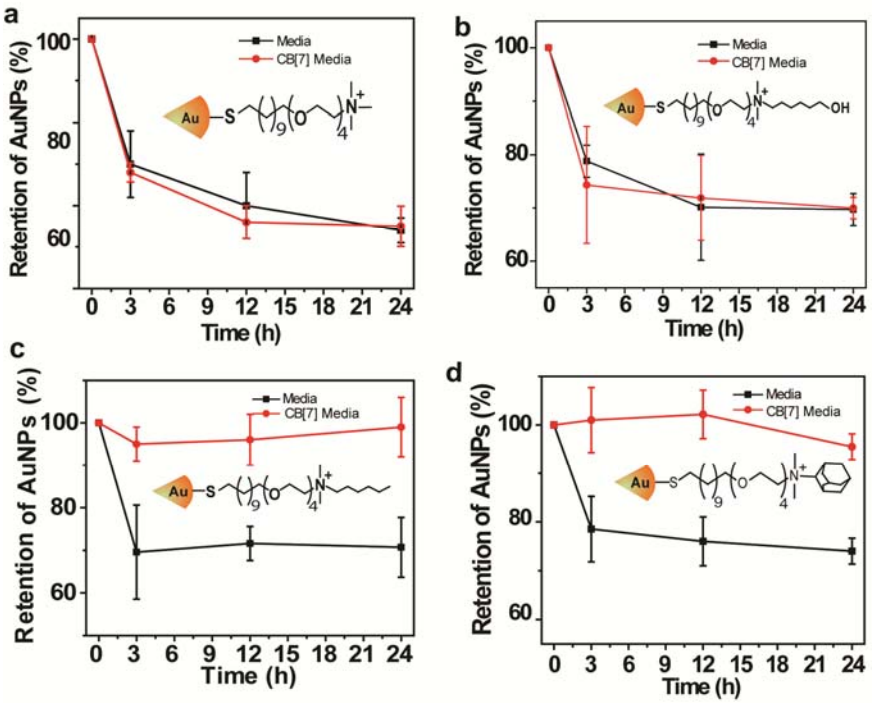

Figure 5.5 Effect of a surface functional group on exocytotic behavior of AuNPs. ICM-MS measurements of (a) AuNP-TTMA, (b) AuNP-TMOH, (c) AuNP-TMC6, and (d) AuNP-ADA. Quantification of exocytosis of the particles were determined by analyzing ICP-MS on MCF-7 cell with same experimental condition carried out on the AuNP-TBen. AuNP-TTMA does not bind with CB[7]. AuNP-TMOH binds with CB[7] but does not induce assemblies. Both AuNP-ADA and AuNP-TMC6 induced assemblies of the particle upon binding with CB[7]. Cellular uptake experiments with each gold nanoparticle were repeated 3 times, and each replicate was measured 5 times by ICP-MS. Error bars represent the standard deviations of these measurements.

5.2.5 Cellular viability

Cellular proliferative activity was measured by alamar blue assay to evaluate possible toxicity that might arise from nanoparticles while retained in the cells. As shown

in Figure 5.6, all the nanoparticles exhibited no decrease in cell viability for the treatment of both media and media of CB[7] (0.2 mM). It shows that the induced assemblies of the particles sequestered in endocytic vesicles do not affect cell viability.

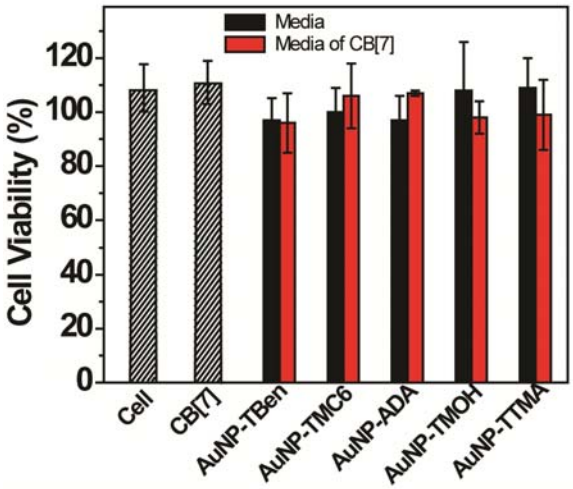

Figure 5.6 Cytotxicity of gold nanoparticles. After 3h incubation of AuNPs (200 nM) in MCF-7 cell, the cells were washed off and further incubated with media and media of CB[7] (0.2 mM) at 37 ºC for 24 h. The cell viability was then determined by using Alamar blue assay. As a control, CB[7], cell viability of CB[7] (0.2 mM) was measured after 24 h incubation.

5.3 Summary and future outlook

In conclusion, we have demonstrated a methodology for regulating exocytosis of the internalized nanoparticles. Utilizing supramolecular host-guest system on the AuNPs induced the assemblies of the particles in the living cells, preventing their exocytosis without any observed cytotoxicity. This approach would provide a potential strategy for prolonged retention of drug carriers within endosome, enabling sustained therapeutic

effect of the carriers. We are currently exploring this strategy with AuNPs featuring prodrugs tethered with labile linkage which can be degraded by external stimuli. Additionally, this approach also will be applied to other nanomaterials with potential utility of their prolonged transplantation in a wide variety of cells for *in vivo* cellular tracking[41] and tumor-targeted delivery of therapeutic systems.[42]

5.4 Synthesis of materials and experimental methods

General

All the chemicals were purchased from Sigma-Aldrich or Fischer Scientific, unless otherwise specified. The chemicals were used as received. Gold nanoaprticles used in this work have been reported previously. [43] ^{1}H NMR spectra were recorded at 400 MHz on a Bruker AVANCE 400 machine. Hewlett-Packard 8452A UV-Vis spectrophotometer was used to record UV-Vis spectra. Dynamic light scattering (DLS) was measured by Zetasizer Nano ZS. The fluorescence from the Alamar blue assay was measured in a SpectraMax M5 microplate spectrophotometer.

ICP-MS sample preparation and measurements

ICP-MS measurements were performed on a Perkin Elmer Elan 6100. Operating conditions of the ICP-MS are listed below: RF power: 1200 W; plasma Ar flow rate: 15 L/min; nebulizer Ar flow rate: 0.96 L/min; isotopes monitored: ^{197}Au; dwell time: 50 ms; nebulizer: cross flow; spray chamber: Scott. Gold nanoparticles (200 nM, 0.5 ml) was incubated with pre-seeded MCF-7 cell line in 24 well plates (20,000 cells/well) for 3h.

After incubation, cells were washed three times with PBS buffer and then 0.5 mL of media or media of CB[7] (0.2 mM) was added to the cells. The wells of the plates then connected to a peristaltic pump which provides a continuous flow of the media and media of CB[7] to remove exocytosed nanoparticles. The cells were then incubated for different additional times (0 h, 3 h, 12 h, and 24 h). Cells were washed three times with PBS buffer and then lysis buffer (300 μl) was added to the cells. The resulting cell lysate was digested overnight using 3 mL of HNO_3 and 1 mL of H_2O_2. On the next day, 3 mL of aqua regia was added, and then the sample was allowed to react for another 2-3 h. The sample solution was then diluted to 100 mL with de-ionized water, and aqua regia. The final gold nanoparticle sample solution contained 5% aqua regia. The gold nanoparticle sample solution was measured by ICP-MS under the operating conditions described above. Cellular uptake experiments with each gold nanoparticle were repeated 3 times, and each replicate was measured 5 times by ICP-MS. A series of gold standard solutions (20, 10, 5, 2, 1, 0.5, 0.2, 0 ppb) were prepared before each experiment. Each gold standard solution contained 5% aqua regia. The resulting calibration line was used to determine the gold amount in taken up by the cells in each sample.

Cellular TEM measurements

For a preparation of cellular TEM samples, MCF-7 cells were seeded and incubated on 15 mm diameter Theramanox® coverslips (Nalge Nunc International, NY) placed in 24 well plates at amount of 100,000 cells in 1 ml of serum containing media for 24 h prior to the experiment. The media was replaced by 0.5 ml of 200 nM AuNP-TBen in serum containing media and incubated for 3 h. The cells were completely washed with PBS

buffer for three times and then 0.5 mL of media or media of CB[7] (0.2 mM) was added to the cells. After another 24 h incubation, the cells were then fixed in 2 % glutaraldehyde with 3.75 % sucrose in 0.1 M sodium phosphate buffer (pH 7.0) for 30 min and then washed with 0.1 M PBS containing 3.75% sucrose three times over 30 min. They were postfixed in 1 % osmium tetroxide with 5 % sucrose in 0.05 M sodium phosphate buffer solution (pH 7.0) for 1 hr and the rinsed with distilled water three times. They were dehydrated in a graded series of acetone (10 % step), and embedded in epoxy resin. The resin was polymerized at 70 °C for 12 h. Ultrathin sections (50 nm) obtained with a Reichert Ultracut E Ultramicrotome and imaged under a JEOL 100S electron microscopy.

Cell culture and cytoxicity TEM measurements

MCF-7 cells were grown in a cell culture flask using low glucose Dulbecco's Modified Eagle Medium supplemented with 10% fetal bovine serum (FBS) at 37°C in a humidified atmosphere of 5% CO_2. For a cytotoxicity test, MCF-7 cells were seeded at 20,000 cells in 0.2 ml per well in 96-well plates 24 h prior to the experiment. During experiment old media was replaced by 0.2 ml of nanoparticles (200 nM) in serum containing media and the cells were incubated for 3 h at 37°C in a humidified atmosphere of 5 % CO_2. The cells were then completely washed with PBS buffer for three times and media or media of CB[7] (0.2 mM) was added to the cell. After another 24h incubation, the cells were then completely washed off and 10% Alarmar blue in serum containing media was added to each well and further incubated at 37 °C for 4 h. The cell viability was then determined

by measuring the fluorescence intensity at 570 nm using a SpectraMax M5 microplate spectrophotometer.

5.5 References

1. Allen, T. M.; Cullis, P. R., Drug delivery systems: Entering the mainstream. *Science* **2004,** *303* (5665), 1818-1822.
2. Torchilin, V. P., Structure and design of polymeric surfactant-based drug delivery systems. *J. Control. Release.* **2001,** *73* (2-3), 137-172.
3. Peer, D.; Karp, J. M.; Hong, S.; FaroKHzad, O. C.; Margalit, R.; Langer, R., Nanocarriers as an emerging platform for cancer therapy. *Nat. Nanotechnol.* **2007,** *2* (12), 751-760.
4. Duncan, R., The dawning era of polymer therapeutics. *Nat. Rev. Drug. Discov.* **2003,** *2* (5), 347-360.
5. Agasti, S. S.; Chompoosor, A.; You, C. C.; Ghosh, P.; Kim, C. K.; Rotello, V. M., Photoregulated Release of Caged Anticancer Drugs from Gold Nanoparticles. *J. Am. Chem. Soc.* **2009,** *131* (16), 5728-5729.
6. Hong, R.; Han, G.; Fernandez, J. M.; Kim, B. J.; Forbes, N. S.; Rotello, V. M., Glutathione-mediated delivery and release using monolayer protected nanoparticle carriers. *J. Am. Chem. Soc.* **2006,** *128* (4), 1078-1079
7. Chithrani, B. D.; Chan, W. C. W., Elucidating the mechanism of cellular uptake and removal of protein-coated gold nanoparticles of different sizes and shapes. *Nano. Lett.* **2007,** *7* (6), 1542-1550.

8. Klostranec, J. M.; Chan, W. C. W., Quantum dots in biological and biomedical research: Recent progress and present challenges. *Adv. Mater.* **2006,** *18* (15), 1953-1964.

9. Hong, R.; Han, G.; Fernandez, J. M.; Kim, B. J.; Forbes, N. S.; Rotello, V. M., Glutathione-mediated delivery and release using monolayer protected nanoparticle carriers. *J. Am. Chem. Soc.* **2006,** *128* (4), 1078-1079

10. Panyam, J.; Zhou, W. Z.; Prabha, S.; Sahoo, S. K.; Labhasetwar, V., Rapid endo-lysosomal escape of poly(DL-lactide-co-glycolide) nanoparticles: implications for drug and gene delivery. *Faseb. J.* **2002,** *16* (10).

11. Panyam, J.; Labhasetwar, V., Sustained cytoplasmic delivery of drugs with intracellular receptors using biodegradable nanoparticles. *Mol. Pharmaceut.* **2004,** *1* (1), 77-84.

12. Pickett, J. A.; Edwardson, J. M., Compound exocytosis: Mechanisms and functional significance. *Traffic* **2006,** *7* (2), 109-116.

13. Slowing, I. I.; Vivero-Escoto, J. L.; Zhao, Y.; Kandel, K.; Peeraphatdit, C.; Trewyn, B. G.; Lin, V. S. Y., Exocytosis of Mesoporous Silica Nanoparticles from Mammalian Cells: From Asymmetric Cell-to-Cell Transfer to Protein Harvesting. *Small* **2011,** *7* (11), 1526-1532.

14. Chavanpatil, M. D.; Handa, H.; Mao, G.; Panyam, J., Incorporation of phospholipids enhances cellular uptake and retention of surfactant-polymer nanoparticles. *J. Biomed. Nanotechnol.* **2007,** *3* (3), 291-296.

15. Panyam, J.; Labhasetwar, V., Dynamics of endocytosis and exocytosis of poly(D,L-lactide-co-glycolide) nanoparticles in vascular smooth muscle cells. *Pharmaceut. Res.* **2003,** *20* (2), 212-220.

16. Sahoo, S. K.; Labhasetwar, V., Enhanced anti proliferative activity of transferrin-conjugated paclitaxel-loaded nanoparticles is mediated via sustained intracellular drug retention. *Mol. Pharmaceut* **2005,** *2* (5), 373-383.

17. Vasir, J. K.; Labhasetwar, V., Quantification of the force of nanoparticle-cell membrane interactions and its influence on intracellular trafficking of nanoparticles. *Biomaterials* **2008,** *29* (31), 4244-4252.

18. Lehn, J. M. *Supramolecular Chemistry: Concepts and Perspectives.* (VCH, New York, 1995).

19. Klajn, R.; Olson, M. A.; Wesson, P. J.; Fang, L.; Coskun, A.; Trabolsi, A.; Soh, S.; Stoddart, J. F.; Grzybowski, B. A., Dynamic hook-and-eye nanoparticle sponges. *Nat. Chem.* **2009,** *1* (9), 733-738.

20. Angelos, S.; Yang, Y. W.; Patel, K.; Stoddart, J. F.; Zink, J. I., pH-responsive supramolecular nanovalves based on cucurbit[6]uril pseudorotaxanes. *Angew. Chem. Int. Edit.* **2008,** *47* (12), 2222-2226.

21. Angelos, S.; Khashab, N. M.; Yang, Y. W.; Trabolsi, A.; Khatib, H. A.; Stoddart, J. F.; Zink, J. I., pH Clock-Operated Mechanized Nanoparticles. *J. Am. Chem. Soc.* **2009,** *131* (36), 12912.

22. Coti, K. K.; Belowich, M. E.; Liong, M.; Ambrogio, M. W.; Lau, Y. A.; Khatib, H. A.; Zink, J. I.; Khashab, N. M.; Stoddart, J. F., Mechanised nanoparticles for drug delivery. *Nanoscale* **2009,** *1* (1), 16-39.

23. Kim, K.; Selvapalam, N.; Ko, Y. H.; Park, K. M.; Kim, D.; Kim, J., Functionalized cucurbiturils and their applications. *Chem. Soc. Rev.* **2007,** *36* (2), 267-279.

24. Lagona, J.; Mukhopadhyay, P.; Chakrabarti, S.; Isaacs, L., The cucurbit[n]uril family. *Angew. Chem. Int. Edit.* **2005,** *44* (31), 4844-4870.

25. Hettiarachchi, G.; Nguyen, D.; Wu, J.; Lucas, D.; Ma, D.; Isaacs, L.; Briken, V., Toxicology and Drug Delivery by Cucurbit[n]uril Type Molecular Containers. *Plos One* **2010,** *5* (5).

26. Uzunova, V. D.; Cullinane, C.; Brix, K.; Nau, W. M.; Day, A. I., Toxicity of cucurbit[7]uril and cucurbit[8]uril: an exploratory in vitro and in vivo study. *Org. Biomol. Chem.* **2010,** *8* (9), 2037-2042.

27. Lim, Y. B.; Kim, T.; Lee, J. W.; Kim, S. M.; Kim, H. J.; Kim, K.; Park, J. S., Self-assembled ternary complex of cationic dendrimer, cucurbituril, and DNA: Noncovalent strategy in developing a gene delivery carrier. *Bioconjugate Chem.* **2002,** *13* (6), 1181-1185.

28. Kim, S. K.; Park, K. M.; Singha, K.; Kim, J.; Ahn, Y.; Kim, K.; Kim, W. J., Galactosylated cucurbituril-inclusion polyplex for hepatocyte-targeted gene delivery. *Chem. Commun.* **2010,** *46* (5), 692-694.

29. Ghosh, S.; Isaacs, L., Biological Catalysis Regulated by Cucurbit[7]uril Molecular Containers. *J. Am. Chem. Soc.* **2010,** *132* (12), 4445-4454.

30. Kim, C.; Agasti, S. S.; Zhu, Z. J.; Isaacs, L.; Rotello, V. M., Recognition-mediated activation of therapeutic gold nanoparticles inside living cells. *Nat. Chem.* **2010,** *2* (11), 962-966.

31. Kim, J.; Ahn, Y.; Park, K. M.; Kim, Y.; Ko, Y. H.; Oh, D. H.; Kim, K., Carbohydrate wheels: Cucurbituril-based carbohydrate clusters. *Angew. Chem. Int. Edit.* **2007,** *46* (39), 7393-7395.

32. Kim, C. K.; Ghosh, P.; Rotello, V. M., Multimodal drug delivery using gold nanoparticles. *Nanoscale* **2009,** *1* (1), 61-67.

33. Ghosh, P.; Han, G.; De, M.; Kim, C. K.; Rotello, V. M., Gold nanoparticles in delivery applications. *Adv. Drug Deliver. Rev.* **2008,** *60* (11), 1307-1315.

34. Nam, J.; Won, N.; Jin, H.; Chung, H.; Kim, S., pH-Induced Aggregation of Gold Nanoparticles for Photothermal Cancer Therapy. *J. Am. Chem. Soc.* **2009,** *131* (38), 13639-13645.

35. Templeton, A. C.; Wuelfing, M. P.; Murray, R. W., Monolayer protected cluster molecules. *Acc. Chem. Res.* **2000,** *33* (1), 27-36.

36. Yuan, L. N.; Wang, R. B.; Macartney, D. H., Chiroptic behaviour of a chiral guest in an achiral cucurbit[7]uril host. *Tetrahedron: Asymmetry* **2007,** *18* (4), 483-487.

37. Wheate, N. J., Improving platinum(II)-based anticancer drug delivery using cucurbit[n]urils. *J. Inorg. Biochem.* **2008,** *102* (12), 2060-2066.

38. Zhu, Z. J.; Ghosh, P. S.; Miranda, O. R.; Vachet, R. W.; Rotello, V. M., Multiplexed Screening of Cellular Uptake of Gold Nanoparticles Using Laser

Desorption/Ionization Mass Spectrometry. *J. Am. Chem. Soc.* **2008,** *130* (43), 14139-14143.

39. Kim, C. K.; Ghosh, P.; Pagliuca, C.; Zhu, Z. J.; Menichetti, S.; Rotello, V. M., Entrapment of Hydrophobic Drugs in Nanoparticle Monolayers with Efficient Release into Cancer Cells. *J. Am. Chem. Soc.* **2009,** *131* (4), 1360-1361.
40. Montes-Navajas, P.; Gonzalez-Bejar, M.; Scaiano, J. C.; Garcia, H., Cucurbituril complexes cross the cell membrane. *Photoch. Photobio. Sci.* **2009,** *8* (12), 1743-1747.
41. Bulte, J. W. M.; Kraitchman, D. L., Iron oxide MR contrast agents for molecular and cellular imaging. *Nmr. Biomed.* **2004,** *17* (7), 484-499.
42. Roger, M.; Clavreul, A.; Venier-Julienne, M. C.; Passirani, C.; Montero-Menei, C.; Menei, P., The potential of combinations of drug-loaded nanoparticle systems and adult stem cells for glioma therapy. *Biomaterials* **2011,** *32* (8), 2106-2116.
43. Moyano, D. F.; Rotello, V. M., Nano Meets Biology: Structure and Function at the Nanoparticle Interface. *Langmuir* **2011,** *27* (17), 10376-10385.